NASA/TM-20210011787

Design Guidelines for Swirl-Venturi Fuel-Air Mixers for Lean Direct Injection Combustors

Yolanda R. Hicks and Kathleen M. Tacina
Glenn Research Center, Cleveland, Ohio

December 2021

NASA STI Program . . . in Profile

Since its founding, NASA has been dedicated to the advancement of aeronautics and space science. The NASA Scientific and Technical Information (STI) Program plays a key part in helping NASA maintain this important role.

The NASA STI Program operates under the auspices of the Agency Chief Information Officer. It collects, organizes, provides for archiving, and disseminates NASA's STI. The NASA STI Program provides access to the NASA Technical Report Server—Registered (NTRS Reg) and NASA Technical Report Server—Public (NTRS) thus providing one of the largest collections of aeronautical and space science STI in the world. Results are published in both non-NASA channels and by NASA in the NASA STI Report Series, which includes the following report types:

- TECHNICAL PUBLICATION. Reports of completed research or a major significant phase of research that present the results of NASA programs and include extensive data or theoretical analysis. Includes compilations of significant scientific and technical data and information deemed to be of continuing reference value. NASA counter-part of peer-reviewed formal professional papers, but has less stringent limitations on manuscript length and extent of graphic presentations.

- TECHNICAL MEMORANDUM. Scientific and technical findings that are preliminary or of specialized interest, e.g., "quick-release" reports, working papers, and bibliographies that contain minimal annotation. Does not contain extensive analysis.

- CONTRACTOR REPORT. Scientific and technical findings by NASA-sponsored contractors and grantees.

- CONFERENCE PUBLICATION. Collected papers from scientific and technical conferences, symposia, seminars, or other meetings sponsored or co-sponsored by NASA.

- SPECIAL PUBLICATION. Scientific, technical, or historical information from NASA programs, projects, and missions, often concerned with subjects having substantial public interest.

- TECHNICAL TRANSLATION. English-language translations of foreign scientific and technical material pertinent to NASA's mission.

For more information about the NASA STI program, see the following:

- Access the NASA STI program home page at http://www.sti.nasa.gov

- E-mail your question to help@sti.nasa.gov

- Fax your question to the NASA STI Information Desk at 757-864-6500

- Telephone the NASA STI Information Desk at 757-864-9658

- Write to:
  NASA STI Program
  Mail Stop 148
  NASA Langley Research Center
  Hampton, VA 23681-2199

NASA/TM-20210011787

Design Guidelines for Swirl-Venturi Fuel-Air Mixers for Lean Direct Injection Combustors

Yolanda R. Hicks and Kathleen M. Tacina
Glenn Research Center, Cleveland, Ohio

National Aeronautics and
Space Administration

Glenn Research Center
Cleveland, Ohio 44135

December 2021

This report is a formal draft or working paper, intended to solicit comments and ideas from a technical peer group.

This work was sponsored by the Transformative Aeronautics Concepts Program.

Level of Review: This material has been technically reviewed by technical management.

Available from

NASA STI Program
Mail Stop 148
NASA Langley Research Center
Hampton, VA 23681-2199

National Technical Information Service
5285 Port Royal Road
Springfield, VA 22161
703-605-6000

This report is available in electronic form at http://www.sti.nasa.gov/ and http://ntrs.nasa.gov/

Executive Summary

Design guidelines for aircraft gas turbine combustors are provided based on the swirl-venturi lean direct injection (SV–LDI) scheme. The guidelines are developed through a combination of literature review and internal research at NASA Glenn Research Center that sought to develop an understanding of how LDI geometry affects NO_x emissions, minimum stable fuel to air, and combustion dynamics. Key objectives are to improve low-power operability by reducing the fuel-to-air ratio achievable with the SV–LDI concept and to reduce NO_x emissions for both the subsonic landing-takeoff cycle and supersonic cruise conditions.

The design of any combustion system will be a set of compromises between flame stability and decreasing combustion emissions. This report is to serve as a guide for selecting the best options given the overall mission. Sections 1.0 to 3.0 serve as a general introduction and review of LDI and fuel-air mixer components for those who are unfamiliar with or new to LDI. Those with more fuel injection experience may choose to begin at Sections 4.0 and 5.0, which focus on the LDI array as a whole and the interactions between elements and how they affect mixing, combustion, and stability. Section 6.0 highlights guidelines for designing a combustor based on LDI. The appendixes provide fuller descriptions or references to NASA LDI geometries and test results from NASA programs and projects.

This report is organized as follows. In Section 1.0, the SV–LDI concept is introduced and described as a way to reduce NO_x emissions. Section 2.0 provides descriptions of the individual components that make up a single SV–LDI element—the venturi, swirler, and fuel injector—and their primary purposes. Considerable focus is applied to how changes on the air-side components affect the flow field. Section 3.0 examines variations within a single SV–LDI element swirler: blade thickness, presence of a diffuser section, position of fuel nozzle, etc. We include examples from the literature to emphasize key aspects of these changes. In Section 4.0, the interaction of a single element with the combustion chamber and with neighboring elements is considered. In Section 5.0, fuel staging effects on emissions, combustion efficiency, and combustion dynamics is reviewed. Throughout these sections, universal findings will be highlighted. Section 6.0 consolidates those findings to provide guidelines for use in SV–LDI designs.

Contents

Design Guidelines for Swirl-Venturi Fuel-Air Mixers for Lean Direct Injection Combustors

Yolanda R. Hicks and Kathleen M. Tacina
National Aeronautics and Space Administration
Glenn Research Center
Cleveland, Ohio 44135

1.0 Introduction

Gas turbine engines must meet both national and international environmental regulatory requirements for noise and emissions as part of the qualification process for entry into service. Among the emissions requirements is a regulation for oxides of nitrogen, NO_x. Figure 1 illustrates the three atmospheric regions that NO_x and other emissions affect. NO_x is regulated because at low altitudes, NO_x emissions contribute to ozone and smog production, and in the troposphere to smog and acid rain. For supersonic flight, NO_x may be responsible for destruction of the protective ozone layer in the stratosphere. Currently, landing and takeoff NO_x is regulated via the Federal Aviation Administration (FAA) and International Civil Aviation Organization (ICAO), and there may be regulation of cruise NO_x, especially for supersonic flight, at some time in the future.

A key factor in reducing NO_x is to keep the combustion temperatures as far as possible from stoichiometric mixtures because the NO_x formation rate is an exponential function of flame temperature, as illustrated in Figure 2.

Strategies to avoid high temperatures in aircraft engines are rich-quench-lean (RQL), lean-premixed-prevaporized (LPP), lean partially premixed (Hybrid), and lean direct injection (LDI). LPP is generally not used for aircraft engines because it is susceptible to flashback and lean blowout.

RQL is the traditional strategy to address NO_x and is shown conceptually in Figure 3. Examples of current engines using RQL are the Pratt & Whitney Talon combustor (Raytheon Technologies Corporation) and the Rolls-Royce plc Trent. RQL designs have a rich front end that keeps flame temperatures low. However, they must convert to overall fuel-lean operation quickly. This is done by introducing primary combustion air downstream in a way that minimizes the time the fuel-air mixture is near stoichiometric flame temperatures.

Lean partially premixed is best known as used in the GE Aviation Twin Annular Premixing Swirler (TAPS) combustor. TAPS introduces all the combustion air at the front of the combustor, but it uses a rich burn pilot along with fuel-lean main injection. ALECsys, currently being developed by Rolls-Royce plc, is also a lean partially premixed combustor.

LDI is shown conceptually in Figure 4. Like TAPS, LDI introduces all the combustion air at the front. Unlike TAPS, all LDI stages run fuel-lean most of the time. In fact, running fuel-lean is one of the two distinguishing features of LDI. The second distinguishing feature is the “direct injection” of the fuel into the flame zone, with no geometrically separated premixing region. Because there is no geometrically separated premixing region, rapid and uniform fuel-air mixing is critical to reducing NO_x and particulate emissions. To promote quick mixing, LDI designs replace a single traditionally sized fuel-air mixer with several small fuel-air mixers. By operating fuel lean, LDI produces many fewer particulates than does RQL or the Hybrid strategies. The smaller LDI injectors help promote faster fuel-air mixing, leading to a more uniform mixture in a shorter distance compared to traditional RQL. Arrays of smaller elements are also more easily scaled, so they can be applicable to both large- and small-core engines, and for both

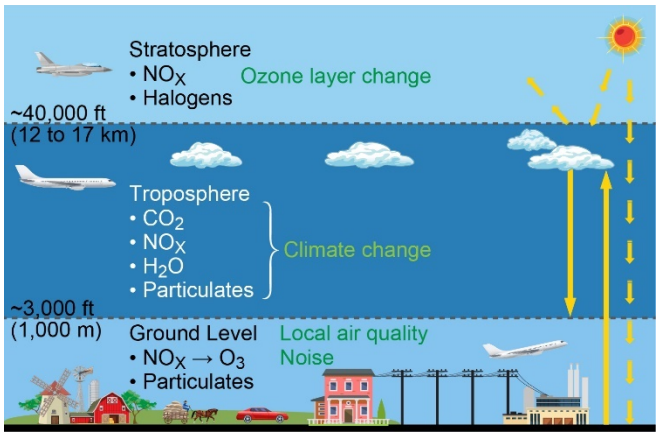

Figure 1.—Chemical emissions from aircraft engines. (Del Rosario, 2014).

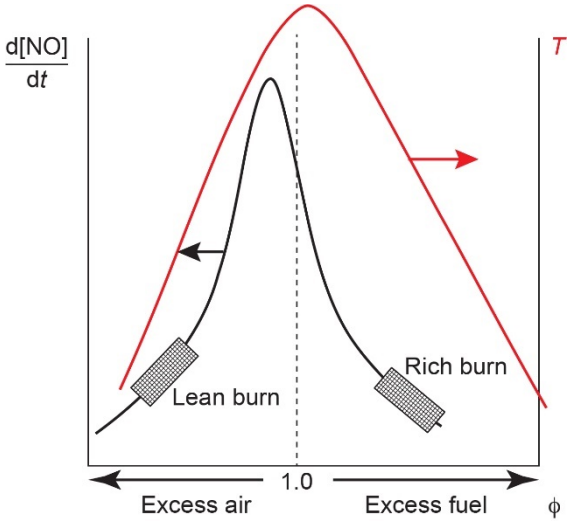

Figure 2.—Relation between NO formation rate and combustion temperature *T*, with respect to equivalence ratio ϕ.

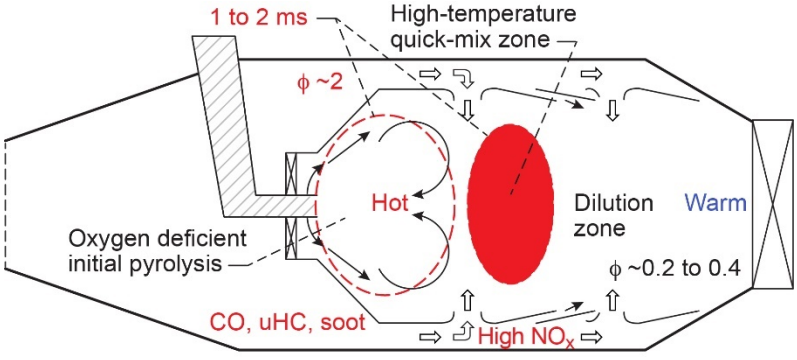

Figure 3.—Conceptual sketch of rich-quench-lean combustor. Equivalence ratio (ϕ).

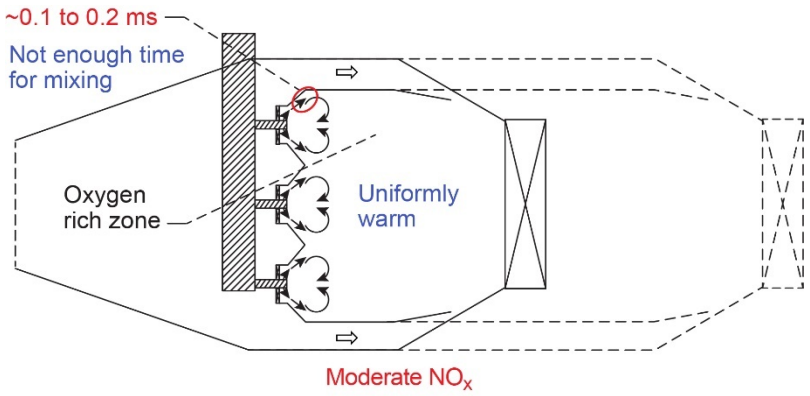

Figure 4.—Conceptual sketch of lean direct injection combustor.

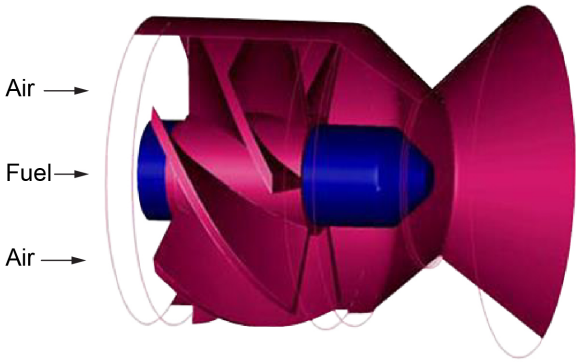

Figure 5.—Baseline swirl-venturi lean direct injection element consists of converging and diverging venturi, axial air swirler, and simplex fuel nozzle positioned at venturi throat.

subsonic and supersonic flight. The nine-point (9-pt) LDI has demonstrated success in reducing NO_x since its inception during the NASA High-Speed Research (HSR) and Ultra-Efficient Engine Technology (UEET) programs. One problem still to be solved for LDI is simultaneously maintaining the demonstrated low emissions while extending the operating range to low fuel-to-air ratios.

The baseline swirl-venturi LDI (SV–LDI) element is illustrated in Figure 5. The element is nominally 1 in. (25.4 mm) in diameter and consists of an axial swirler, converging-diverging venturi and simplex fuel nozzle atomizer. The simplex atomizer fits within the hub of the air swirler and its tip is positioned so that the fuel is injected at the venturi throat. The simplex nozzle produces a hollow cone spray with an angle nominally of 70°. The 9-pt mentioned previously (illustrated in Figure 6) is a 3 by 3 array of the baseline elements and has been used in testing from HSR in the 1990s through to the current Advanced Air Vehicle Technology (AAVT) Program. LDI can also be composed of radial swirlers and airblast and/or prefilming fuel nozzles. Section 2.0 will describe the individual components of SV–LDI and describe their effect on the flow field. Later sections will also include configurations of LDI that are not swirl-venturi, but have been studied by NASA and others, to add to our understanding.

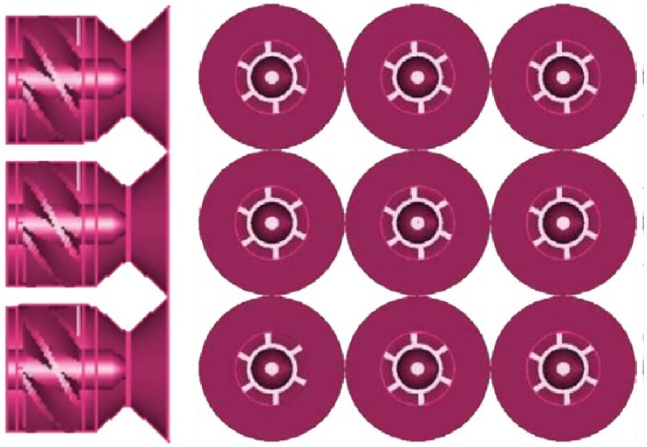

Figure 6.—Baseline configuration of nine-point swirl-venturi lean direct injection. (a) Side view. (b) Front view.

SV–LDI is distinguished by a converging-diverging venturi and air swirl, as shown in Figure 5. Presence of the venturi diffuser section is what defines this injector and mixer concept. There have been three generations of SV–LDI: SV–LDI–1 to SV–LDI–3. In first-generation SV–LDI–1, simplex fuel injectors were used with axial air swirlers and all elements were the same (Figure 5 and Figure 6). In second-generation SV–LDI–2, airblast fuel injectors were also used, and a dedicated pilot was incorporated. The third-generation SV–LDI–3 featured a more user-friendly fuel stem and prefilming fuel injectors. A full description of SV–LDI generations 1 to 3 and configurations used to date is in Appendix B.

2.0 Swirl-Venturi Lean Direct Injection Geometry: Regarding Fuel Injector, Air Swirler, and Venturi

This section provides general descriptions and functions of the individual components that make up a single SV–LDI element. It begins with brief descriptions of fuel injectors, typically pressure-swirl and airblast, then describes some of the work done to examine the two key elements on the air side—the venturi and the swirler—and to some extent, how they assist and support fuel atomization and stable flames.

2.1 Fuel Injectors

The process of liquid fuel injection is a key part of fuel-air mixing. For aeronautical gas turbine engines, as shown in Table I, the fuel flow varies by about an order of magnitude from idle to takeoff. Given the large range in fuel flow, fuel staging using several fuel injectors and/or fuel circuits are typically used. This fuel staging often takes the form of a pilot stage and one or two main stages.

To deliver fuel into a location in the most precise way to affect fuel atomization, vaporization, and mixing with the air for efficient combustion with minimal unwanted emissions, good fuel atomization is required at all conditions in the flight operating envelope. At high-power conditions such as takeoff, climb, and cruise, good atomization quality is critical to avoiding near-stoichiometric regions that produce high NO_x emissions. At low-power conditions, such as idle and approach, fuel vaporization is less rapid due to the (relatively) low combustor inlet temperatures and good atomization quality is needed to avoid the formation of soot and CO. In addition, although the overall fuel-to-air ratio is low at low-power

TABLE I.—INTERNATIONAL CIVIL AVIATION ORGANIZATION (ICAO) LANDING-TAKEOFF FUEL FLOW RATES FOR ADVANCED AIR TRANSPORT TECHNOLOGY (AATT) SMALL-CORE CYCLE

ICAO point, percent	Time, min	Fuel flow, kg/min
7 (idle)	26.0	3.68
30	4.00	11.3
85	2.20	38.1
100 (takeoff)	0.700	47.2

conditions, there may be significantly higher local fuel-to-air ratios because fuel staging typically puts more fuel to the pilot circuit to promote flame stability. Locally, high fuel-to-air ratios could lead to higher NO_x, so good atomization is also required to reduce NO_x emissions at low power.

To meet the requirements for good fuel atomization across the flight envelope, various fuel injection designs have been developed. Most commonly used in aircraft engines are pressure and airblast atomizers. Pressure atomizers work by forcing the fuel through a small exit orifice, which generates a high-velocity liquid stream into relatively quiescent ambient air, promoting jet breakup into droplets. The simplest pressure atomizer is a plain orifice and is more likely used in aircraft as a jet in crossflow. Plain orifice atomizers have narrow spray angles, however. Pressure-swirl atomizers (simplex or duplex) instill tangential momentum to the fuel by means of a swirler or swirl chamber, so that a conical sheet is formed upon exiting the nozzle. It is the swirl chamber geometry that determines the spray angle. Airblast injectors rely on high-velocity air impinging on a thin liquid sheet to break up the sheet into droplets. In addition, the fuel injector design might have some sort of prefilming, in which the fuel sprays onto a solid component of the injector, wicks off, and is blasted by the incoming swirling air. The prefilming type is common for aircraft airblast injectors.

Fuel atomization and fuel sprays are highly complex, with a journal and a textbook devoted to it. The latter, “Atomization and Sprays” (Lefebvre and McDonell, 2017), is a good reference, offering detail on fuel injector type, design, sprays, atomization, droplet size correlations, and applications. The book “Gas Turbine Combustion” (Lefebvre, 1999) provides general context for fuel injector effects on combustion instabilities and pollutant emissions.

The throughput capacity of pressure atomizers is often described by the flow number, FN, which gives the effective area of the nozzle. FN is defined as the liquid mass flow rate per the square root of (injection differential pressure × liquid density). Good atomization requires sufficient fuel pressure drop across the atomizer. Increasing the pressure drop also decreases the droplet size. Various experimentally and theoretically derived correlation equations (Lefebvre and McDonell, 2017) give the droplet size as Sauter mean diameter (SMD). Many of these equations relate SMD to FN^a and/or injector differential pressure ΔP^b, along with other exponentiated parameters such as viscosity or density. The exponents a and b are determined through correlation.

Simplex atomizers are typically designed to produce a solid- or hollow-cone spray. However, until the pressure drop is above a minimum value, the spray cone does not fully open. This minimum pressure varies with the details of the specific simplex design but is typically on the order of 50 to 700 kPa (15 to 100 psid). Therefore, if possible, one should identify the minimum pressure drop needed to operate any given atomizer design.

As an example, Figure 7 shows the effect of injector pressure drop on the spray pattern of two hollow-cone simplex fuel nozzles. For both of the nozzles, the hollow cone is not fully open at the lowest pressure drop(s) shown. However, as the pressure drop increases, the hollow cones open fully and the spray quality appears good. Note that the minimum pressure drop required for a good spray quality will depend on the internal design.

Since simplex nozzles can produce a good spray quality and fine droplets even at low airflow rates, they are often used for pilot and other low-power stages. However, because simplex nozzles rely on fuel pressure drop for atomization and because the fuel pressure drop increases with the square of the fuel flow rate, they often require a high-pressure fuel pump.

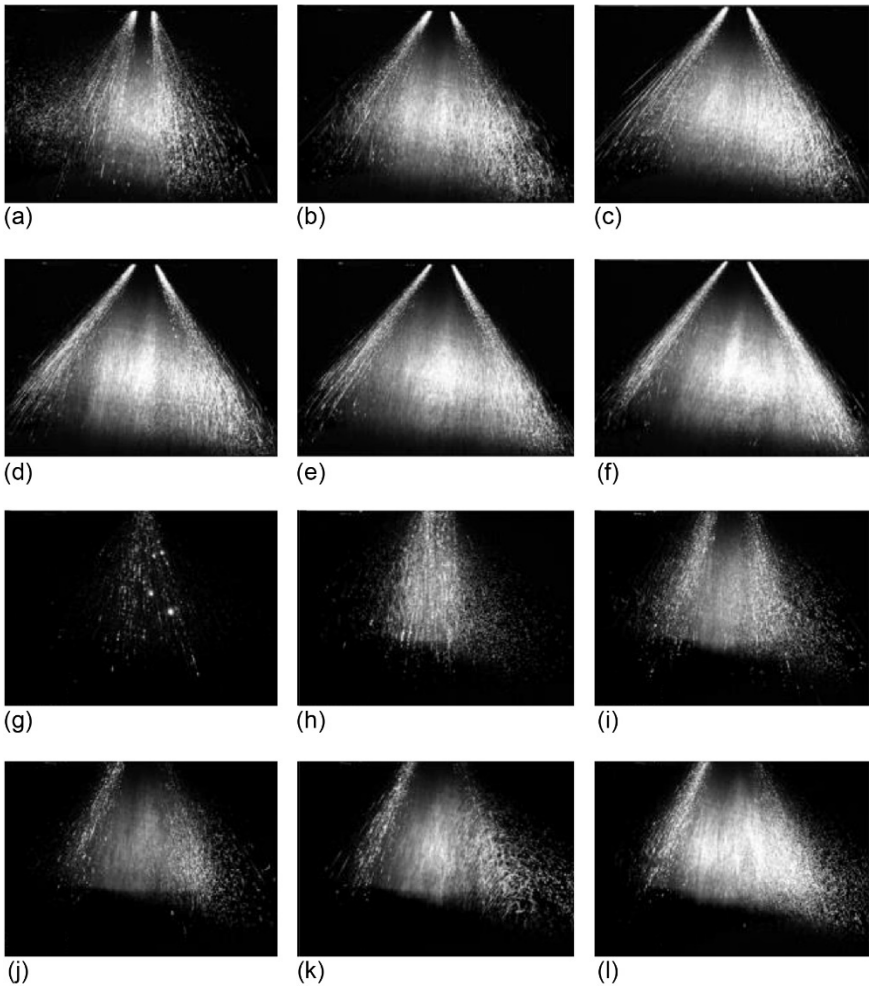

Figure 7.—Water spray pattern from two hollow-cone simplex atomizers into quiescent ambient air. Planar laser sheet was used to illuminate sprays. Both nozzles were used in lean direct injection (LDI) testing. Seven-point LDI–1 design at a flow number FN ≈ 0.7 for varying change in pressure drop ΔP. (a) 55 psid (344.7 kPa, 3.4 bar). (b) 100 psid (689.5 kPa, 6.9 bar). (c) 150 psid (1,034.2 kPa, 10.3 bar). (d) 200 psid (1379.0 kPa, 13.8 bar). (e) 250 psid (1,723.7 kPa, 17.2 bar). (f) 300 psid (2,068.4 kPa, 20.7 bar). LDI–3 design for FN ≈ 1.4 and varying ΔP. (g) 50 psid (344.7 kPa, 3.4 bar), 1 kHz. (h) 100 psid (689.5 kPa, 6.9 bar), 2 kHz. (i) 200 psid (1379.0 kPa, 13.8 bar), 2 kHz. (j) 300 psid (2,068.4 kPa, 20.7 bar), 5 kHz. (k) 400 psid (2,757.9 kPa, 27.6 bar), 5 kHz. (l) 400 psid (2,757.9 kPa, 27.6 bar), 3 kHz.

Unlike simplex and other pressure atomizing nozzles, airblast nozzles typically do not rely primarily on the fuel injection pressure drop to achieve good atomization. Instead, they rely on the airflow. For this reason, airblast nozzles can require a high air momentum flux and shear rate to achieve good atomization. Due to the airflow requirements, airblast nozzles tend to have poor low-power atomization and lean blowout performance. However, airblast nozzles often provide excellent atomization at high power. In addition, because atomization relies primarily on the airflow, the fuel injector tip can be a simple plain orifice, which is easier to manufacture than complex internal fuel flow paths required by pressure-swirl atomizers. Therefore, airblast nozzles are used for the main stage in some recent engines.

Since the mechanism for atomization of airblast injectors is different from pressure atomizers, correlations for SMD are more related to the fluid properties of both liquid and gas, their mass or volumetric flow rates and velocities.

To address concerns for flame stability and lightoff, aircraft engines often use a hybrid or compound fuel injector that is primarily airblast but also uses a simplex nozzle as the pilot. A common example is a piloted airblast atomizer, which uses a simplex pilot nozzle, especially at low power, and uses an airblast injector at high power. Another type, referred to as "airblast simplex," uses a simplex nozzle to inject fuel into a swirling, coflowing airstream. The simplest example of this is the baseline LDI described previously, but without the diffuser.

2.2 Air Swirlers

Next is arguably one of the most critical components, the air swirler. The most common types that have a physical structure (body and vanes) are axial and radial. Other swirlers may consist of passages made by drilled holes or slots. Predominantly, the swirlers used in NASA internal studies have been axial, and most of the discussion will be based on experience with those. Despite this, our findings should generally apply to all swirler types.

Air swirl serves two purposes. One purpose is to help promote fuel breakup, especially for plain jet and other atomizers that require air assist for good atomization and mixing. Most importantly, air swirl is used to help promote flame stability by creating a recirculation zone that anchors the flame in space. Within the recirculation zone, hot combustion products move upstream and provide additional heat for fuel vaporization. A disadvantage of recirculation zones is that the precessing vortex core that is created might lead to instability because of frequency coupling with heat release, that is, combustion dynamics. The second possible disadvantage of recirculation is the increased residence time, which can lead to increased thermal NO_x.

Examples of the benefit of swirl to promote the aerodynamic breakup of sprays include work by (Ingebo, 1983). In this study, Ingebo compared water drop sizes with and without air swirl for two styles of injection. First were four simplex atomizers injecting into a coflowing airstream. The second were four variants of splash plates, which injected radially, normal to the airflow direction. All eight fuel injectors had a different flow capacity or FN. The circular air duct had an inner diameter of 7.6 cm. The swirler had 10 flat vanes with a blade angle of 70°. Drop sizes were measured as a function of air mass velocity, $\rho_a V_a$. Table II shows results for air mass velocity of 10 g/cm^2·s. For every case, the drop size reduced significantly when the air swirler was used. Therefore, when swirl is used, one can reduce the air mass velocity and still achieve the same or smaller drop sizes compared to the nonswirl case.

As mentioned earlier, one key use of swirl is to promote a central recirculation zone (CRZ) to anchor the flame. There are typically two types of recirculation zones that may develop, depicted in Figure 8. Ideally, a CRZ develops directly downstream of the swirler element. In this way, the flame is anchored directly downstream from the swirler. The other type is sometimes referred to as a "corner (or edge)

recirculation zone" (CoRZ or ERZ). It has also been called an outer recirculation zone (ORZ). In this case, the recirculation develops on the borders of the swirler region(s) and possibly along the combustor walls. The CoRZ may be more likely to develop hot spots on dome hardware because hot gases more easily contact the dome or the combustor walls. Either sort of attachment can reduce fuel injector or combustor life.

TABLE II.—FUEL INJECTOR PARAMETERS USED BY INGEBO (1983) AND MEAN DROP DIAMETERS MEASURED

Fuel injector	Nozzle orifice, cm	Mean droplet diameter, μm	
		Without swirler	With swirler
Simplex atomizers			
45° spray angle, flow number (FN) = 0.014	0.090	5.9	4.1
45° spray angle, FN = 0.034	0.130	6.9	3.4
80° spray angle, FN = 0.091	0.230	6.3	3.1
80° spray angle, FN = 0.301	0.340	6.7	3.1
Splash plate atomizers			
Disk 1	0.0102	5.0	2.8
Disk 2	0.216	6.9	3.0
Cone	0.157	---	3.1
Groove	0.015	7.1	2.9

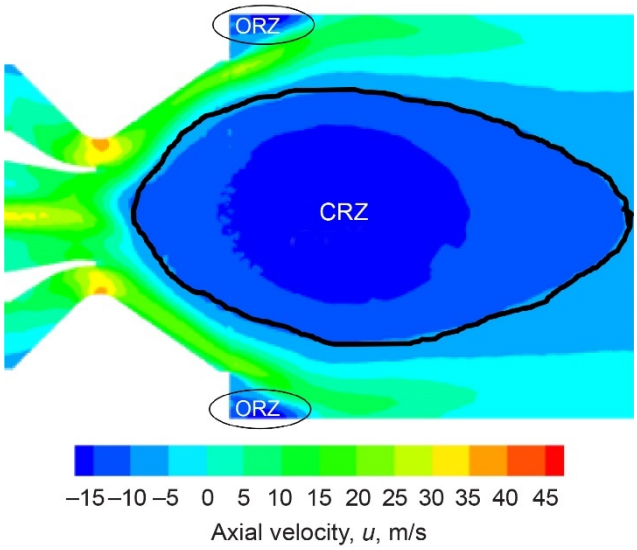

Figure 8.—Typical recirculation zones created by swirl, showing one central recirculation zone (CRZ) and two outer recirculation zones (ORZs).

Swirl number (SN) is defined (Beer and Chigier, 1972; Gupta, Lilley, and Syred, 1984) as the ratio of the tangential momentum flux in the axial direction to the axial momentum flux in the axial direction with respect to the swirl chamber size (typically the radius). Velocities are typically designated with *u* as the axial velocity and *w* as the tangential velocity. Nearly all reported values of SN are estimates based on the swirler geometry and might not be the actual value in the system. The actual SN can be determined by measuring the fluxes using a two- or three-component measurement tool, such as phase Doppler interferometry (PDI), or by calculating the ratio of the measurements of maximum (or average) *w* to maximum (average) *u*. PDI and particle image velocimetry (PIV) might be used for determinations based on velocity. Typically, the higher the swirler blade angle with respect to the central axis of flow, the higher the SN. For most of the examples described here, comparisons are based on a common swirler style. For example, all NASA one-point (1-pt), seven-point (7-pt), and 9-pt SV–LDI tests since 1999 use the same design for their axial swirlers. This way, even though we do not necessarily know the true SNs, we will know which in any given grouping will produce the highest swirl. In general, a recirculation zone will form when SN is greater than 0.6 (Syred and Beer, 1974).

Section 3.0 discusses the variations of swirl: angle or SN, CRZ size and location, and how swirl affects the flow and NO_x.

2.3 Venturi

The converging-diverging venturi in SV–LDI has two main purposes:

1. Convergence to provide a region of high-velocity air to aid in fuel atomization.
2. Divergence to help with pressure recovery and to promote a recirculation zone.

Examples from prior NASA work that show the benefits of having a converging-diverging venturi include Ercegovic (1979) and Johnson (1982).

Incorporating a converging-diverging venturi into the fuel-air mixer has been shown to reduce droplet size, which in turn might help to reduce NO_x emissions. Ercegovic (1979) conducted tests burning jet-A fuel using three different fuel injector modules, with and without a swirler-venturi. One used a simplex atomizer. Two used different versions of an airblast atomizer, splash groove and splash plate. For all three injector modules, those that used the venturi reduced NO_2 emissions by roughly 50 percent over a wide range of equivalence ratio. Figure 9 shows the effect seen for the simplex injector module and plots the NO_2 emissions index (EI) as a function of equivalence ratio. EI for a specie is defined as measured grams of that specie in the product gases per kilogram of fuel burned. To determine if the NO_2 reduction could be attributable to reduced droplet sizes, Johnson conducted further studies using the simplex atomizer modules to gain insight on the Ercegovic results. In that work, Johnson measured the SMD of water spray with and without the venturi (Figure 10), finding that the venturi module significantly decreased the droplet size by about 30 percent. The results supported the hypothesis that the confinement of the swirling air and acceleration through the throat helps atomize the fluid. Johnson correlated the SMD against the NO_2 emissions using a power of –2, directly relating NO_x to droplet size. We find that correcting the SMD to the –1.5 power rather than the –2 power collapses NO_2 emissions with and without the venturi onto each other, as shown in Figure 11. Based on this correlation, adding a venturi appears to reduce NO_x emissions by reducing the droplet size and not by improving the fuel-air mixing.

The converging-diverging venturi helps support and enhance a recirculation zone. Chigier and Beer (1964) measured velocity and static-pressure distributions from swirling air jets with and without diverging nozzles. Swirl was instilled using four tangential jets into an axial airstream. Its linear physical scale was about 10 times the baseline SV–LDI. The flow chamber had a 24.5-cm-diameter passage and a

6-cm-diameter central hub. At the end of the tube was placed either a convergent or convergent-divergent nozzle with a 24.5-cm outer diameter and a 12.5-cm throat diameter. The divergence had a smooth transition from the throat at a full angle of approximately 75° and final diameter of 22 cm.

For the same flow rates and SN, the addition of the divergence to the nozzle resulted in an increased reverse flow velocity and enlarged size (radius) of the recirculation region, as indicated in Figure 12.

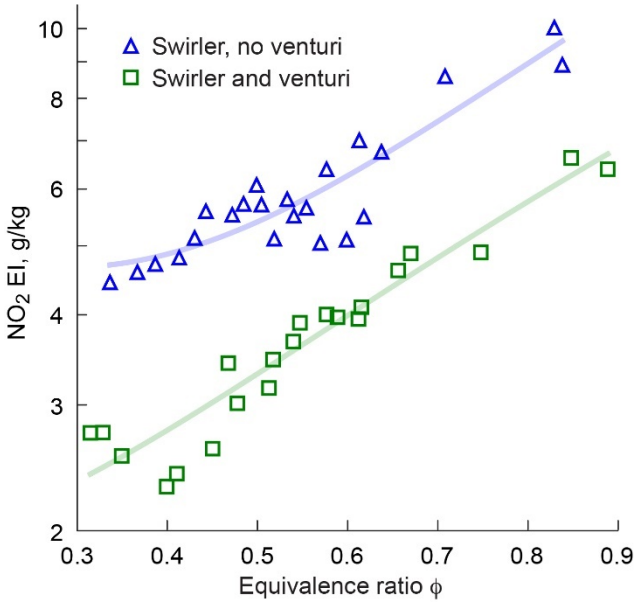

Figure 9.—Effect of converging-diverging venturi on NO_x emissions. Emissions index (EI). (Data from Ercegovic, 1979).

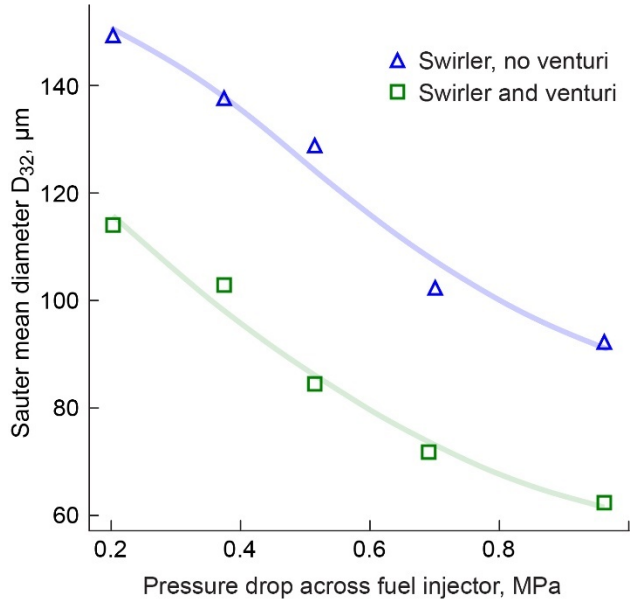

Figure 10.—Effect of converging-diverging venturi on droplet size. (Data from Johnson, 1982).

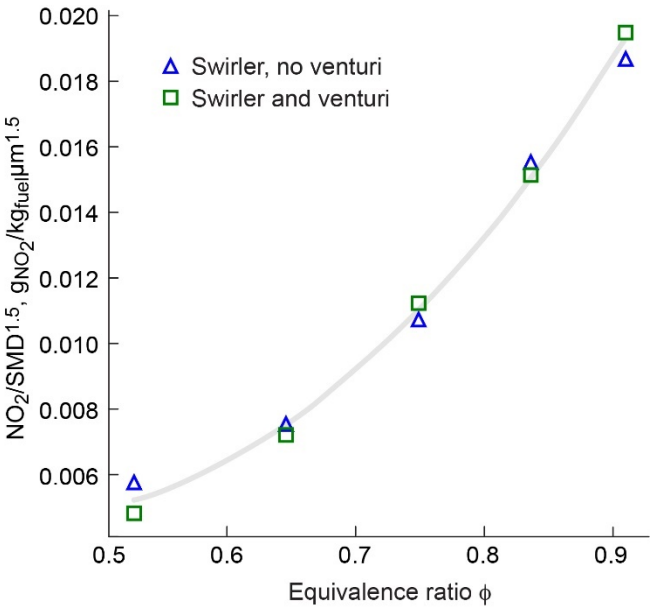

Figure 11.—NO_2 adjusted for droplet size by dividing by Sauter mean diameter (SMD) to the 3/2 power, $SMD^{1.5}$. (Data from Johnson, 1982).

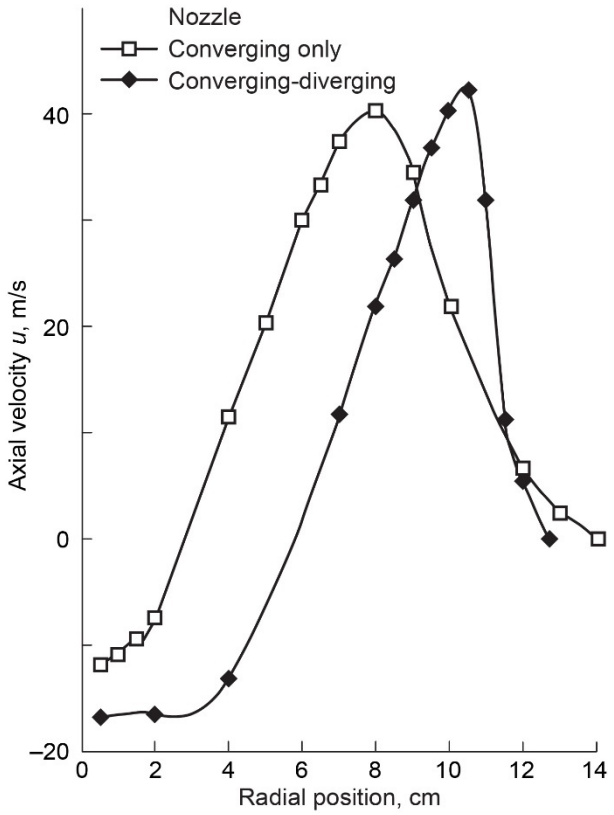

Figure 12.—Comparison showing effect of exit nozzle type on axial velocity. (Adapted from Chigier and Beer, 1964).

In other work that has the same scale (1 in. or 25.4 mm) as the baseline SV–LDI, Ren et al. (2016; 2018) compared the flow structure that develops downstream from an airblast injector having an axial-axial swirler to the same injector with a diffuser. The diffuser angle was 70°. A 60° inner air swirler was used in conjunction with a 60° counterrotating outer swirler. Without the diverging section, a CRZ did not form; instead a central jet issued, and CoRZs formed. With the diffuser, a CRZ was produced.

These last two examples show that the presence of the diffuser helps conserve the azimuthal velocity developed by the injector. Without the diffuser, the swirling component quickly dissipates, but the axial component is preserved. In their review paper, Syred and Beer (1974) noted that for a fixed 35° divergence half-angle, a short divergence length (L) seven-tenths of the exit diameter (D) ($L/D = 0.7$) more than doubled the CRZ diameter. When the length was increased to about 3 times the exit diameter, the CRZ diameter more than trebled. They also noted that the divergent outlet typically reduces the coefficient of pressure loss by 10 to 20 percent.

Given that increased diffuser length will increase weight, a shorter diffuser will likely be better for aircraft engine applications.

The baseline SV–LDI has a diffuser half-angle of about 40° and an L/D ratio of ~0.22. These values were chosen based on the guidelines given in Beer and Chigier (1972). In particular, the diffuser half-angle was chosen to be large enough to promote a stable recirculation zone but not so large as to promote wall flow.

3.0 Variations on the Basic Swirl-Venturi Lean Direct Injection Elements

This section extends the previous descriptions to practical considerations of use for SV–LDI elements by looking at some variations and their effect on the flow field and emissions. It reviews the air swirler blade thickness, fuel nozzle axial position relative to the venturi throat, and swirler angle.

3.1 Swirler Blade Thickness

One finding is that the swirler blade thickness does not affect NO_x emissions, however, the thicker blades result in a higher pressure drop, which reduces overall engine efficiency. Supporting this finding is work conducted by R. Tacina using a 7-pt LDI (Tacina, 2018). This study analyzed the data, and the results are shown in Figure 13. At an airmass flow rate of 0.5 kg/s, the cold flow area × coefficient of discharge and pressure drops were 575 mm^2 and 7.5 percent for the thin blades and 485 mm^2 and 9.5 percent for the thick swirler blades. Although increasing the swirler blade thickness would be expected to promote recirculation by increasing blockage, it did not seem to have a significant effect for this configuration. NO_x emissions were the same regardless of swirler blade thickness

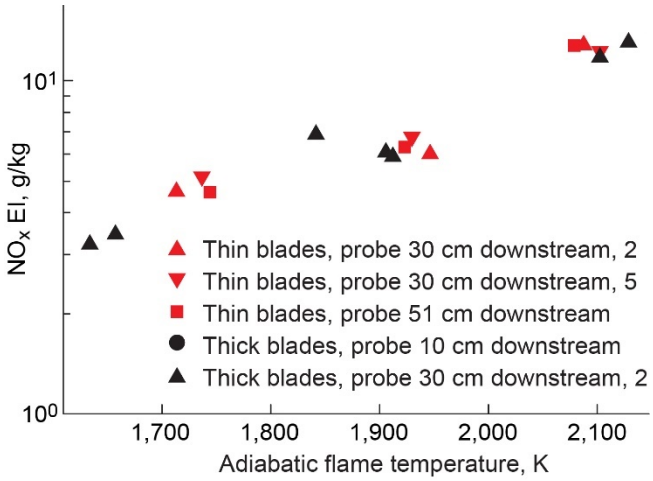

Figure 13.—Effect of swirler blade thickness on NO_x emissions. Inlet temperature T_3 = 838 to 844 K, inlet pressure P_3 = 10.3 bar, airflow = 0.5 kg/s. Emissions index (EI) (Tacina, 2018).

3.2 Fuel Injector Tip Axial Position Relative to Venturi Throat

Another finding is that fuel injector tip position has little effect on the flow structure and little to no effect on NO_x emissions. Two studies illustrate this finding.

Tedder et al. (2014) conducted studies in nonreacting flow using single LDI (see Figure 14 to Figure 16). For three different axial swirler angles, the tip was located either at the throat or 0.18 or 0.31 throat diameters upstream of the venturi throat. Water was injected through the simplex nozzle. Two-dimensional (2D) PIV was used to determine the axial and radial velocity profile and shadowgraphy was used to measure droplet sizes in the combustor.

The injector tip location appeared to only shift the flow without changing the structure for most flows. The CRZ location downstream (based on its widest dimension) was linearly related to the distance from the throat. The recirculation zone had the largest width when the tip was located at the throat. There was an effect on the droplet size distribution across the combustor diameter that decreased with increasing swirler blade angle. At an axial location of 11 mm from the dome, the 60° swirler produced a smoother radial droplet size distribution than did the 52° swirler. For both blade angles used, the radial distribution of droplet sizes was most uniform when the fuel nozzle was located at the throat and less uniform upstream of the throat. For the 52° swirler, distributions were more uniform.

Tacina (2018) explored 7-pt hardware test data acquired in the 1990s that varied tip locations. The test considered four tip locations, including one position with the nozzle downstream of the venturi throat. The results, shown in Figure 17, show that injector tip location did not affect NO_x emissions. This finding corresponds with there being minimal differences in the nonreacting flow study.

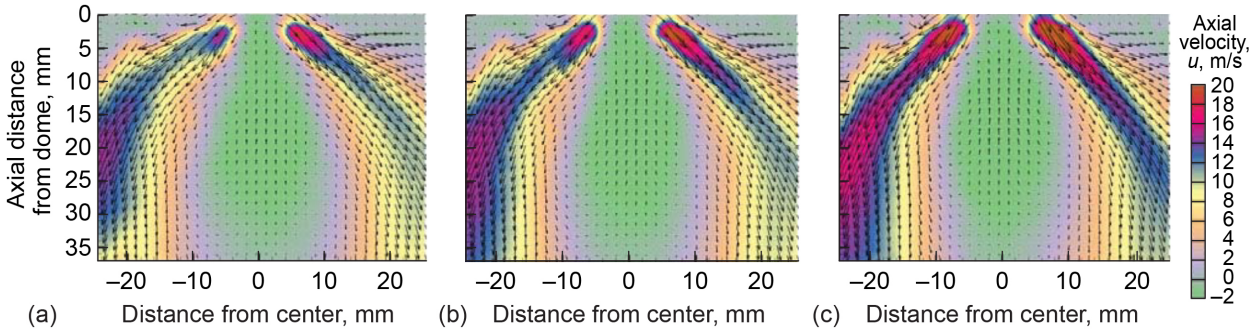

Figure 14.—Average particle image velocimetry-measured velocity fields for one-point lean direct injection with 60° swirler using nozzle water spray. Injector tip distances upstream of throat, measured in throat diameters are (a) 0, (b) 0.16, and (c) 0.31 (Tedder et al., 2014).

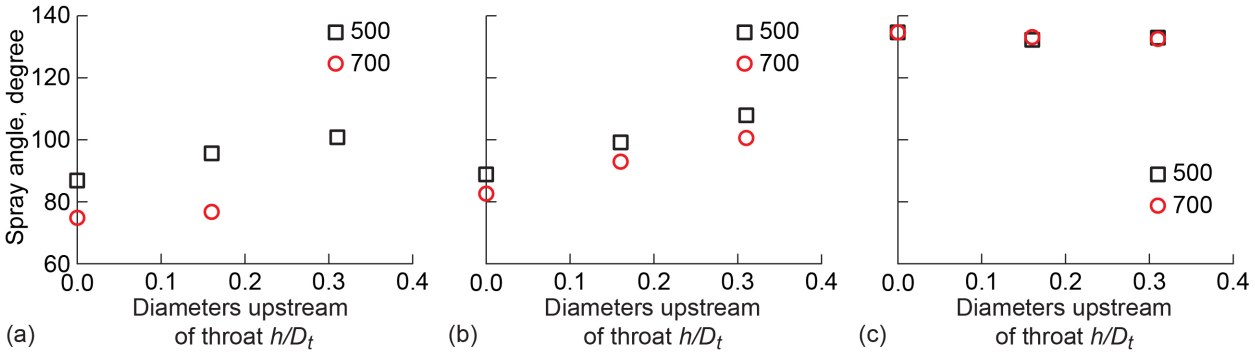

Figure 15.—Effect of injector tip location on spray angle. Plots of spray angle versus location of injector tip measured in throat diameters, h/D_t. Plots are for swirler angles of (a) 45°, (b) 52°, and (c) 60° (Tedder et al., 2014).

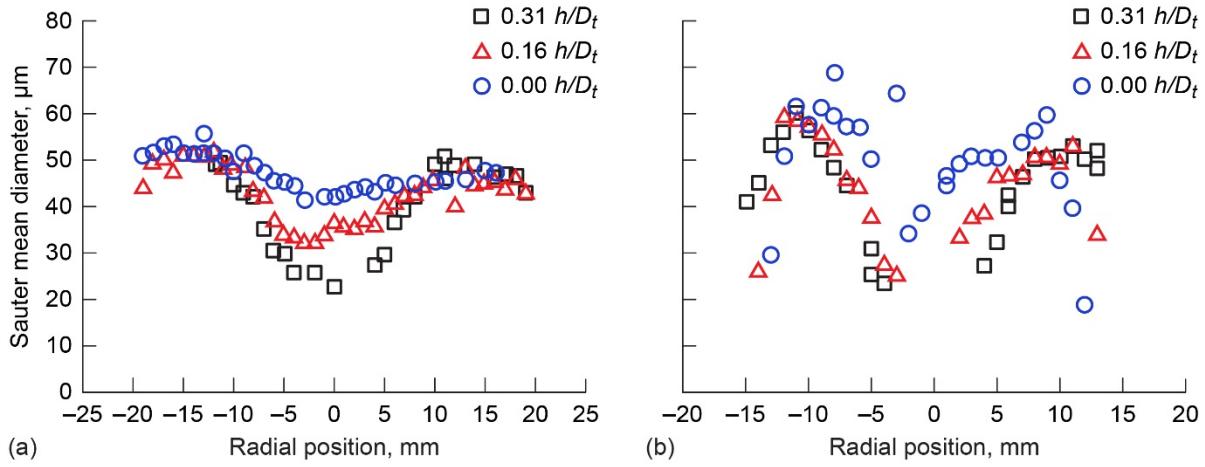

Figure 16.—Droplet size distribution effect on injector tip. Plots of droplet size versus radial location for range of injector tip locations. (a) Swirler angle = 60°. (b) Swirler angle = 52°. Nondimensional distance of injector tip relative to throat diameter (h/D_t). (Tedder et al., 2014).

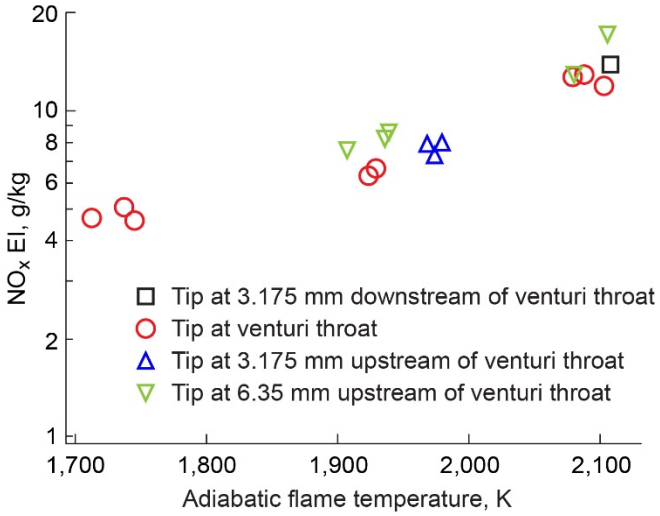

Figure 17.—Effect of fuel tip position relative on NO_x emissions, from Tacina (2018). Seven-point lean direct injection air inlet conditions: temperature T_3 = 838 to 844 K, pressure P_3 = 10.3 bar, mass flow rate = 0.5 kg/s. Emissions index (EI).

3.3 Air Swirler Variation Effects

As noted in Section 2.0, the air swirler is used to help with droplet breakup and also used to help stabilize the flame, often through the creation of a CRZ. The Chigier and Beer (1964) work noted that as the swirl increases, "the size and strength progressively increase."

The size and strength of the CRZ depend not only on the swirl strength but also on combustor geometry (Alekseenko, Kuibin, and Okulov, 2007). For example, although the guidelines from Beer and Chigier (1972) indicate that a recirculation will form above a SN of 0.6, Syred and Beer (1974) later described SN ≈ 0.6 to produce weak swirl. This fits in with the study by Fu et al. (2005), who did not observe a CRZ until the SN approached 1. Syred and Beer also noted that although axial and radial swirlers with similar SNs move similar mass, tangential entry swirlers produce more compact CRZs with higher reverse flow velocities, gradients, and turbulence levels. Thus, instead of recommending numerical values for SN that may be highly specific to one combustor geometry, the guidelines on swirler design will focus on how changes to the SN affect the flow field and flame zone. To aid the reader in applying these guidelines to their particular combustor geometry, these guidelines will be illustrated with specific examples from the literature.

In addition to the determination that swirling flow enhances atomization, there are four additional findings related to swirler strength. For a fixed airflow rate:

1. As the swirl angle and SN increases, the magnitude of CRZ reverse flow velocity typically increases.
2. As the SN increases, the flame zone shifts upstream.
3. As the SN decreases, the likelihood of corner recirculation size increases.
4. Beyond the point of there being no CRZ, the flame zone also expands and becomes thicker.

Four single-swirler studies highlight these findings. Durox et al. (2013) used radial air swirlers. Ren et al. (2016; 2018; 2020) used axial air swirlers. The final studies used SV–LDI–1 (first generation) with axial swirlers: first, Fu et al. (2005) and second, NASA Glenn Research Center (Hicks et al. 2016; 2019). Table III lists parameters of the hardware used in these studies.

TABLE III.—RELEVANT HARDWARE PROPERTIES OF SINGLE ELEMENT SWIRLERS TO DESCRIBE SWIRLER ANGLE VARIATION EFFECTS

[Swirler-venturi lean direct injection (SV–LDI).]

Group	Brief description	Swirler angles	Venturi	Injector
Durox et al. 2013 isothermal, combusting	Radial swirler: 8 blades, contour based on NACA 0030 profile. Blade centers on 25-mm diameter (*D)*; combustor: *D* = 50 mm length (*L*) = 200 or 300 mm	Variable, 23° to 61°	None	Plain jet, 12 into 50 mm sudden expansion
Ren et al. 2016, 2018, 2019, and 2020 isothermal, combusting	SV–LDI–2 nominal 25 mm; axial swirlers: inner (IAS) outer (OAS); combustor: 50 by 50 mm *L* = 305 mm	IAS: – 60° OAS: helical, ±45°, ±60°	Converge-diverge (C-D) throat *D*: 12.7 mm diffuser angle: 70°	Airblast
Fu et al. 2005 isothermal	SV–LDI–1, nominal 25 mm; axial swirler: 6 helical blades; combustor: 50 by 50 mm *L* = 305 mm	40°, 45°, 50°, 55°, 60°, 65°	C-D throat *D*: 12.7 mm diffuser angle: 80°	Simplex
Tedder et al. 2014 isothermal, Hicks et al. 2014 isothermal, combusting	SV–LDI–1, nominal 25 mm; axial swirler: 6 helical blades; combustor: *D* = 76 mm with annular screen *L* = 107 mm	45°, 52°, 60°		Simplex

Durox et al. (2013) considered the effect of air swirler angle in a premixed methane-air combustion system, using a radial swirler in which the blade angle could be varied. The swirler exit and combustion chamber diameters were 12 and 50 mm. They held equivalence ratio and reference velocity fixed. Nonreacting measurements were conducted using laser Doppler velocimetry (LDV). Durox et al. noted that a CRZ was observed when the SN in their system was greater than 0.45, which corresponded with blade angles of 48° and above. The measurements of *u* showed a radially symmetric flow with a local minimum on the centerline for all swirler angles considered. As the SN increased from its minimum value, the centerline velocity continually decreased. Once SN = 0.45 was reached, a CRZ formed. The CRZ became larger and had increasing negative velocity as the SN increased. During combustion, as the SN increased, the primary flame region (luminous zone) moved closer to the burner exit and became more compact. For the cases when the SN was well below 0.45 (i.e., not CRZ), the flame zone became much thicker and was farther from the burner exit.

Using two single-point SV–LDI–2-style designs, Ren et al. (2016; 2018; 2020) studied the effect of swirl strength on the *u* and the flame location. In the high-swirl variation, a recirculation zone formed; in the low-swirl variation, a CoRZ formed instead. For both configurations, the flame location was farther downstream in the low-swirl variations than in the high-swirl variations.

The Fu et al. (2005) work was a nonreacting flow study. In the Fu study, six swirler blade angles were considered, providing SNs from 0.48 to 1.23. Fu et al. used 2D LDV to determine velocity field up to 8 in. (200 mm) downstream from the dump plane. With respect to CRZ formation, Fu divided the swirlers into three groups: no CRZ, transitional, or strong CRZ:

- No CRZ: 40° and 45° swirlers (SN = 0.48 and 0.58, respectively). These display CoRZ. Higher swirl reduces the size of the CoRZ. These have highest levels of turbulence.
- Transitional: 50° and 55° swirlers (SN = 0.69 and 0.83, respectively). The 50° swirler produces a weak, unstable CRZ. The 55° swirler has a larger CRZ, which moves up and down axially, and is not stable.
- Strong CRZ: 60° and 65° swirlers (SN = 1.0 and 1.23, respectively). They have almost no CoRZ. These have lowest turbulence levels.

In a study similar to that of Fu et al. (2005), NASA used three swirlers with angles of 45°, 52°, and 60° (SN = 0.59, 0.77, and 1.02, respectively). 2D PIV measurements provided the axial (vertical) and

horizontal velocities up to roughly 40 mm downstream. Figure 18 shows the noncombusting results, which are qualitatively similar to those of Fu et al. The NASA high-swirl case was the only one observed to produce a CRZ. In the low- and intermediate-swirl cases, we did not observe a CRZ but did find a CoRZ. As with Fu et al., the CoRZ size increased as the SN decreased.

Referring to Figure 18, the 45° and 52° swirler flow fields use green coloring to indicate the locations of the CoRZs and their reverse flow. For all swirlers, airflow that passed through the screen (beyond radial position ±20 mm) is unaffected. Comparing the flow structures that develop in the vicinity of the swirler, the cone of high-velocity air passing through the 45° swirler has a narrow angle of spread, with radii approximately ±10 mm at the x-axis line. The corresponding cone of high-velocity air through the 52° swirler is slightly wider than for the 45° swirler, but neither show a CRZ. The structure through the 60° swirler is significantly different. The CRZ is large and wide, and the air that passes through the swirler opens to an angle of roughly 150°.

Although the NASA results were similar, they were slightly different from the Fu et al. (2005) results in that NASA did not observe a CRZ with the 52° swirler. However, chamber sizes, inlet conditions, and boundary conditions were different. In the NASA study, the swirler was surrounded by the zero-swirl coflow that came through the screen surrounding the fuel-air mixer, whereas the Fu study had no coflow. Thus, even though the Fu study had a nearly identical fuel-air mixer size and smaller test section size, it effectively had a higher expansion ratio. Confinement and blockage also affect the flow structure. For

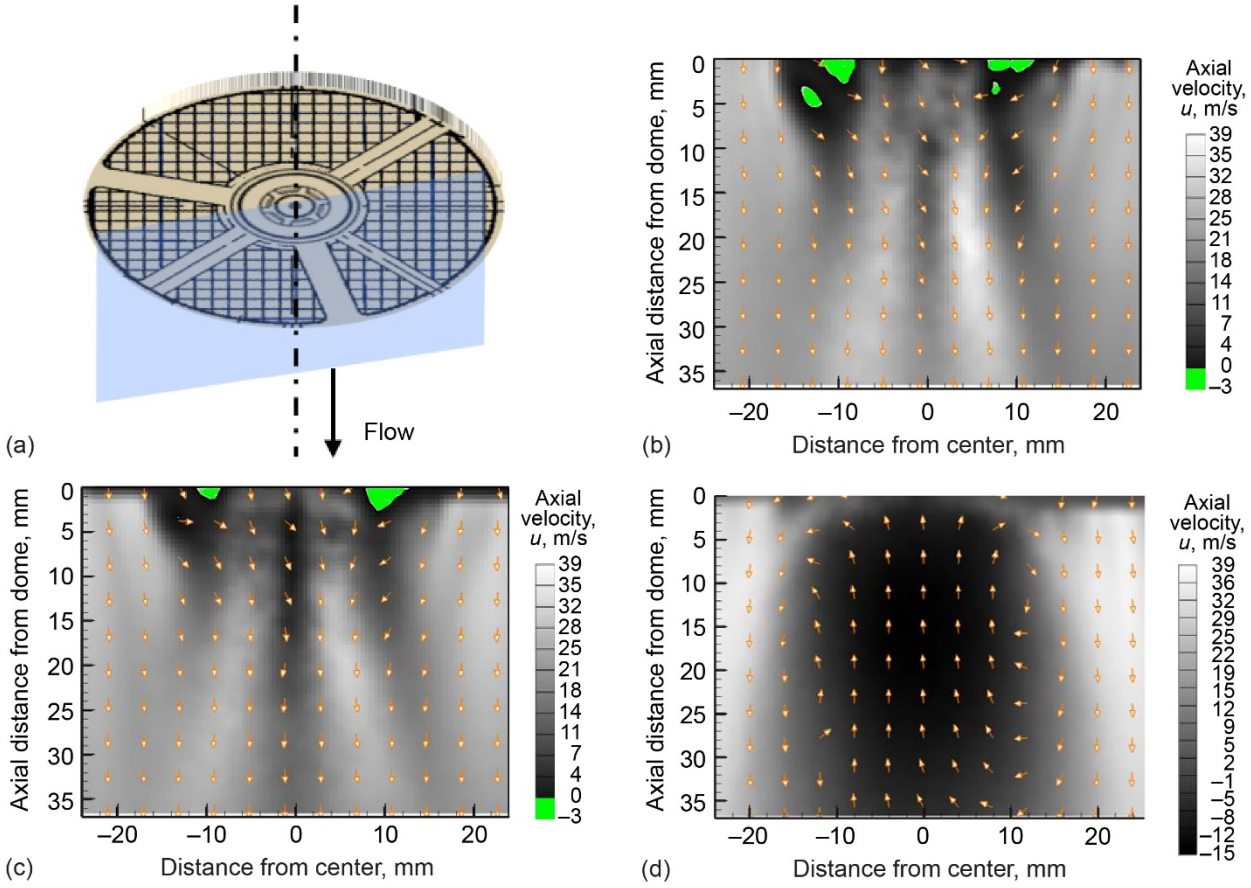

Figure 18.—One-lean direct injection results. Cold flow velocity with contour showing average axial velocity magnitude and vectors showing direction. Flow passes from top to bottom. Oil-seeded air, with air flowing at cold flow reference velocity = 15.24 m/s (50 ft/s). Air inlet pressure P_3 = 310.2 kPa (45 psia) and temperature T_3 = 422 K. Areas near dome for 52° and 45° swirlers are colored green to indicate locations of corner recirculation. (a) Cross section of screen. Swirlers (b) 45°. (c) 52°. (d) 60°.

example, as shown by the time-filtered Navier-Stokes (very large eddy simulation) (TFNS (VLES)) computational fluid dynamics (CFD) simulations of Ajmani, Mongia, and Lee (2015), the high-expansion-ratio second-generation SV–LDI designs have a CRZ downstream of the 45° swirlers.

Beer and Chigier (1972) noted that a CRZ will typically form for SN > 0.6. Neither the Fu nor NASA experimental studies noted here revealed stable CRZs until SN ≥ 1. Many NASA computational studies have shown CRZs at lower SNs. A particular example is from Ajmani, Mongia, and Lee (2013a), who modeled the Fu et al. experimental conditions using Reynolds' Averaged Navier Stokes (RANS) and saw that both the 45° and 60° swirlers generated CRZs. The CFD results are shown on the right side of Figure 19(b). These show two orthogonal slices through the centerline, with flow from left to right, up to a distance of 150 mm from the dump plane. Despite measuring to 200 mm downstream, Fu saw no CRZ for the 45° swirler. A possible reason might be because the spatial density of the measurements was 2 mm. More on the 45° swirler comparison follows, in a comparison with the NASA results.

NASA experimental results with the Ajmani, Mongia, and Lee (2013a) computational study are also compared. In addition to a different chamber size and shape, the experiment also did not match in airflow conditions. Furthermore, NASA experimental results were obtained using PIV in the near field (near the dump plane), and the computational results extend to the far field. The comparison is shown in Figure 19.

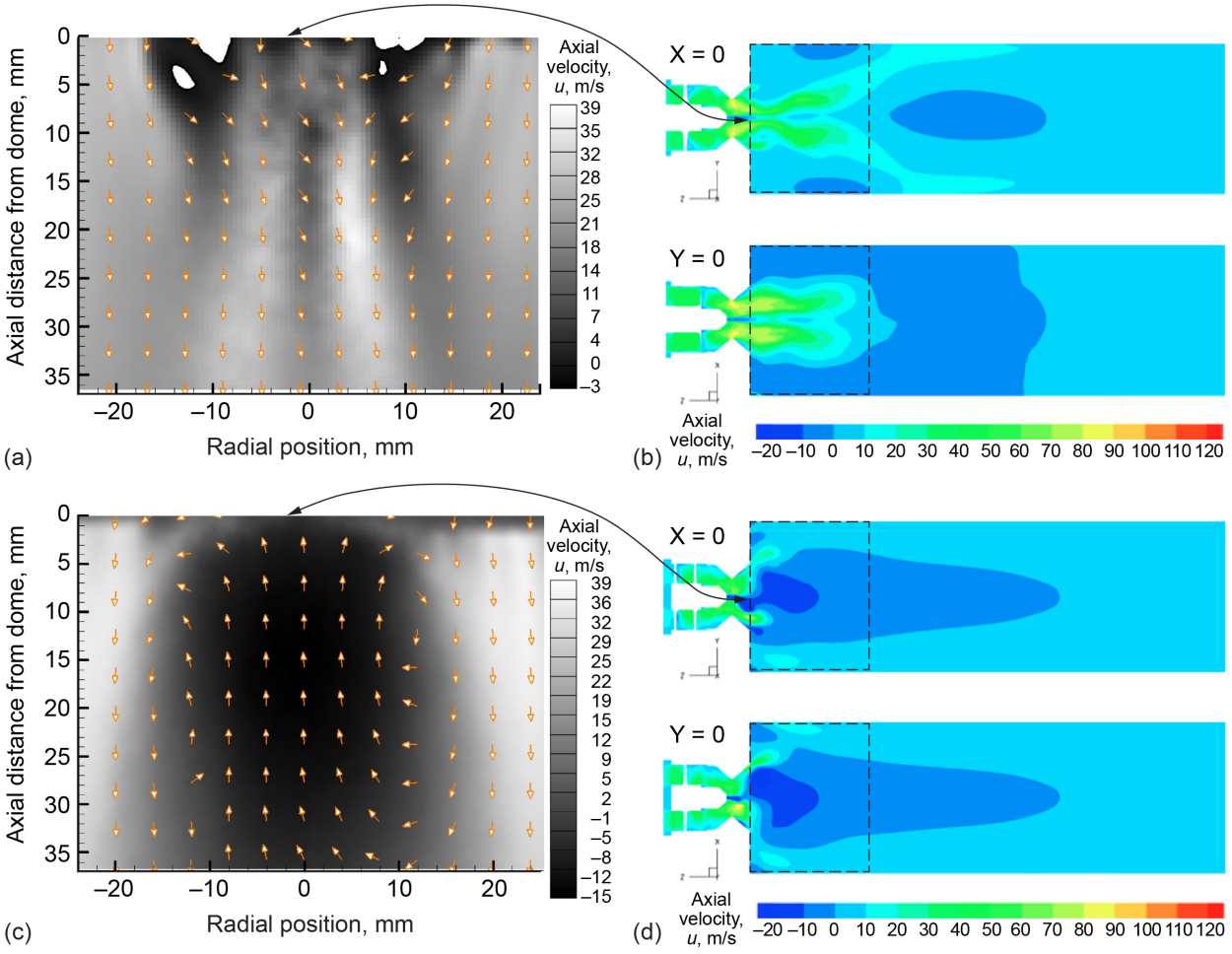

Figure 19.—Comparing nonreacting experimental and Reynolds' Averaged Navier Stokes- (RANS-) predicted flow fields of two swirler angles for single lean direct injection element. 45° swirler: (a) nonreacting experimental and (b) RANS predicted. 60° swirler (c) nonreacting experimental and (d) RANS predicted. Experimental conditions were inlet pressure P_3 = 303 kPa, temperature T_3 = 422 K, and cold flow reference velocity = 15.24 m/s. Computational parameters: P_3 = 101 kPa, $\Delta P/P_3$ = 4 percent, and T_3 = 296 K.

Figure 19(a) shows the PIV results, using *u* contours and flow passing top to bottom; as noted earlier, the CFD results are in (b). In the near field (dashed box in the CFD results), there were remarkably similar results for the 45° swirlers: an expanding free jet that has a thin area along the centerline with much slower velocity than the expanding downstream field. The CFD result shows that a CRZ forms downstream of the field of view of the experimental results. Given the similarity, it may be the case that a CRZ does form outside the field of view. One other feature of note in the 45° swirler CFD result is an asymmetry; X = 0 slice shows a CRZ, but the Y = 0 slice does not. This might indicate that the field downstream from the 45° swirler is metastable and that a CRZ does not always form. (The Fu et al. (2005) study indicated no CRZ for 45° swirlers and a metastable CRZ for the 52° swirler.)

For the 60° swirler, both results show a large CRZ that begins at the dome and extends beyond the experimental field of view. NASA did not observe a CRZ form downstream of the 52° swirler, but it is likely that if there is one, it is positioned farther downstream than for the 60° swirler CRZ. Supporting the downstream displacement are combusting results from the 7-pt that compare the average luminous flames between two coswirling configurations, shown in Figure 20. One uses all 52° swirlers, the other has a 60° swirler in the center. When all swirlers are 52°, the flame is farther from the dome, but with a center 60° swirler, the flame is closer to the dome.

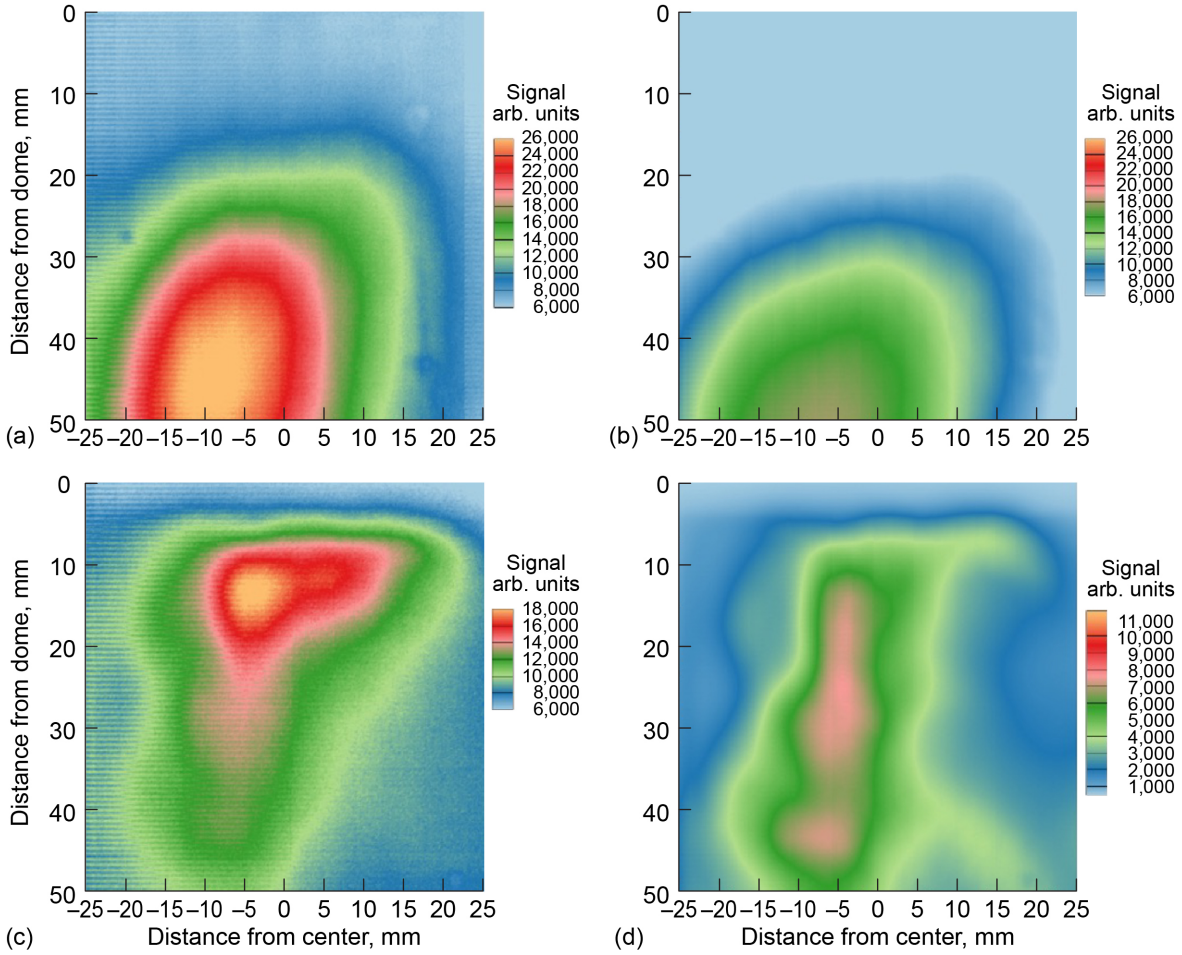

Figure 20.—Comparing flame standoff for configurations RH52all and RH60cRH52o. RH52o for mean signal intensity and signal standard deviation. Flow is top to bottom. (a) RH52all mean. (b) RH52all standard deviation. (c) RH60cRH52o mean. (d) RH60cRH52o standard deviation.

In addition, combusting results from a 7-pt LDI array supports finding 2.

We noted in Section 2.2 that a key concern of introducing swirl is the possible instability due to combustion dynamics brought about by coupling of the precessing vortex core frequency to the heat release rate. As demonstrated by Durox et al. (2013), this may possibly be mitigated through adjusting the chamber length and/or by slight adjustments of swirl strength.

There are many mitigation strategies to address combustion dynamic instabilities, which include both passive and active techniques. These are beyond the scope of this report. The reader is referred to Lieuwen and Yang (2005); Richards, Straub, and Robey (2003); Banaszuk et al. (2002); and Li (2004), among others.

4.0 Considerations of Swirler Array Element Confinement, Spacing, Size Offset From Dome for Pilot, Coswirl and Counterswirl on NO_x Emissions and Flame Stability

This section looks at SV–LDI from more of a systems perspective, to consider what happens when multiple elements are integrated into flame tubes and sectors. It can be used as a guide to implementation in a full annular combustor.

4.1 Confinement Ratio Effects

This section shows that differences in the flow field downstream of a swirler are affected by its confinement and through interactions with adjacent swirlers.

Confinement ratio (CFR) and area ratio (AR) are reciprocal terms (CFR = 1/AR) that compare the area of the burner to the area of the injector elements. We define CFR as the ratio of the cross-sectional area of the total flow path to the total cross-sectional area of the swirlers at the dome exit. Note that this definition of CFR gives an inverted relationship to actual confinement. That is, the greater the CFR, the less confined the system. Thus, AR is perhaps a more intuitive comparison, but CFR is more similar to expansion ratio in its definition.

Two nonreacting flow studies that used single elements to determine the effect of CFR are Fu, Jeng, and Tacina (2006) and Kao (2014). The Fu, Jeng, and Tacina study used the SV–LDI mentioned in Section 2.0, with a 60° axial swirler, and some results are reproduced in Figure 21. The Kao study used a counterrotating radial-radial swirler. The reported geometric SNs of the two swirlers were the same at 1. Different confinements were used. Fu, Jeng, and Tacina used CFRs of 1.7, 3.8, 6.8, and 10.6. Kao used CFRs of 5.1, 8.0, and 11.5. The key results of both studies were the same:

- Confined systems have a closed CRZ.
- Greater confinement (smaller CFR) leads to a smaller, more compact CRZ.
- The average upstream speed within the CRZ typically increases with decreasing CFR.
- As the CFR increases, the CRZ physical size increases, both radially and axially.

The smallest CFR of the Fu, Jeng, and Tacina study (CFR = 1.7) matches the CFR of the baseline NASA 9-pt. A comparison of PIV results between the NASA 9-pt and 1-pt is shown in Figure 22. Figure 22(a) is a slice through the 9-pt combustor centerline, showing axial-radial vectors along with an u contour. The center CRZ has comparable size and shape to that observed by Fu, Jeng, and Tacina (2006), as shown in Figure 21(a). The NASA 1-pt results described in Section 2.0, Tedder et al. (2014), had a CFR of 4. The 1-pt result is in Figure 21(c) for a side-by-side comparison. The less-confined 1-pt CRZ is much wider and extends farther downstream—beyond the field of view—compared to the more confined 9-pt.

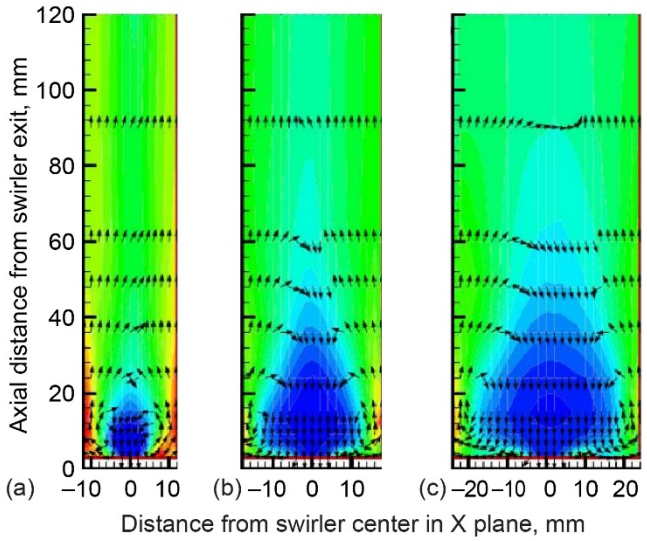

Figure 21.—Confinement effect on flow field downstream of single axial swirler. Flow is bottom to top. Axial velocity contours and two-dimensional vector field at Y = 0. Confinement ratios are (a) 1.7, (b) 3.8, and (c) 6.8 (Fu, Jeng, and Tacina, 2006).

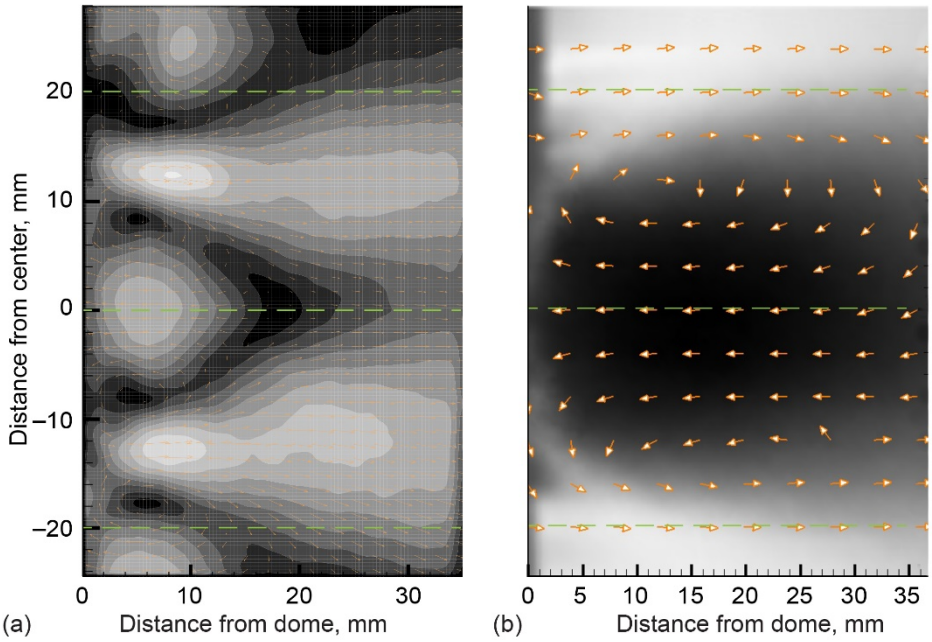

Figure 22.—Two-dimensional (2D) particle image velocimetry results showing axial velocity contours and 2D vector fields in plane containing centerline. Flow is left to right. (a) From nine-point with inlet conditions 10.3 bar, 828 K. (b) From one-point with inlet conditions 3 bar, 422 K.

The confinement studies show that an array with similar confinement to a single element can produce similar flow structures downstream of the individual array elements. The cases of element spacing in arrays of like elements is explored next.

4.2 Element Spacing and Interactions Between Elements

In this section, whether single swirler performance will be consistent when surrounded by neighbors, first with all like elements, then by different elements is considered.

There is no doubt that interactions occur between swirler elements. The key concern is whether the interactions are helpful, neutral, or harmful with respect to combustor stability, durability, and emissions reduction.

4.2.1 Interactions Between Coswirling Cups of Same Type

Examples in the literature that compare single element aerodynamics and combustion to multiple elements used linear arrays (Kao, 2014; Kao, Tambe, and Jeng, 2013; Dolan, Villalva Gomez, and Gutmark, 2017) or single annular combustors (Fanaca et al., 2010; Durox et al., 2016). Swirl cup spacing ranged from 1.1 to 6.9 diameters, with an average distance of 2.5. All groups reported changes to adjacent injectors that changed the size and/or strength of the recirculation zones and that also affected flame stability, heat release, and pattern factor. Under certain circumstances of element spacing, diffuser flare angle, or other change that might affect the CFR, every other swirler produced stronger (weaker) flames than its neighbor, with one generating a “V” flame, and its neighbor producing an “M” flame. These effects are sufficient enough that one should consider them when designing an LDI system, especially since the Kao and Dolan examples were designed for use with liquid jet fuels. Kao used a radial-radial dual swirler and Dolan used a slotted diffuser swirler similar to the multizone, multistage LDI concept designed and tested under Environmentally Responsible Aviation (ERA) (Chang et al., 2013). Please refer to the papers cited here or see Appendix C for more detail on these interaction effects.

On the other hand, work conducted using a mesoscale burner by Rajasegar et al. (2019) has the intent to promote flame to flame interactions between neighboring elements so as to enhance combustion stability. This study uses element spacing similar to that used in NASA LDI concepts. It shows that whether in the “V,” transitional, “M,” or merged flame regime depends on equivalence ratio and Reynolds number.

Because the objective of LDI is to use multiple elements that replace a single swirler (swirl cup), the spacing of elements will be smaller than would be between swirl cups in a modern annular combustor. The spacing between adjacent LDI swirlers is typically on the order of a swirler diameter. The range for the NASA in-house designs is between 1 to 1.2 swirler diameters. For first generation LDI (LDI–1), that work used elements that are of similar size, and the CFR is between 1 and 2. Additionally, via optical probes isothermal results were found to be a fairly good indicator of the combusting results with regard to symmetry.

The flow field produced by like LDI elements is fairly uniform or symmetric, as shown in the examples of Figure 23 and Figure 24, which have element spacing of 1.1 diameters. All use axial swirlers with six helical blades. These figures show flame visualization and CH* from the 9-pt and fuel planar laser-induced fluorescence (PLIF) from the 49-point (49-pt).

Figure 23 shows a series of chemiluminescence images obtained during combustion, from a standard color video (30 Hz, Figure 23(a)), an intensified charge-coupled device (ICCD) camera (10 Hz, Figure 23(b)), and a high-speed camera (10 kHz, Figure 23(c) and (d)). For the ICCD and high-speed cameras only the center row is fully optically accessible; part of the lower top row and upper bottom row structure can be seen. Each row is the line-of-sight integrated luminescent intensity. The averaged chemiluminescence images (Figure 23(b) and (c)) suggest some possible interaction in the upper part of the center row seems to not extend as far downstream as the lower part of the upper row, but the gaps between swirlers observed near the dome for all the images reveal separation exists between the elements. This is especially evident in Figure 23(d), which shows a high degree of symmetry for the three rows. The

image was obtained by tracking the light emission from frame-to-frame of 9,000 successive high-speed image pairs using PIV processing.

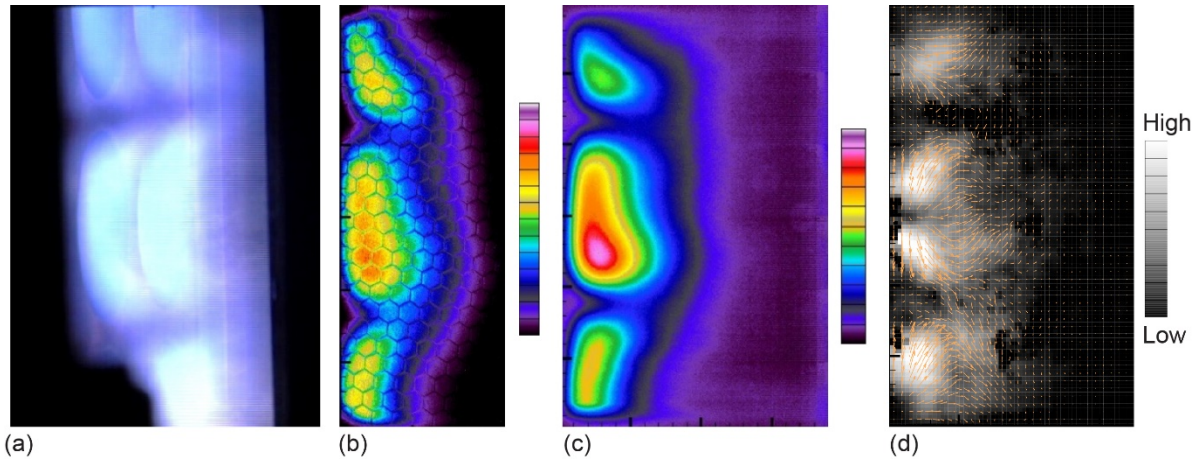

Figure 23.—Examples from nine-point swirl-venturi lean direct injection tests. Equivalence ratio (ϕ) = 0.45. (a) Color video. (b) 600 shot integrated on-chip average of CH*. ϕ = 0.35. (c) Flame emission average from 9,000 high-speed camera images. (d) Resultant mean image derived from tracking emissions from high-speed camera images. Flow was left to right.

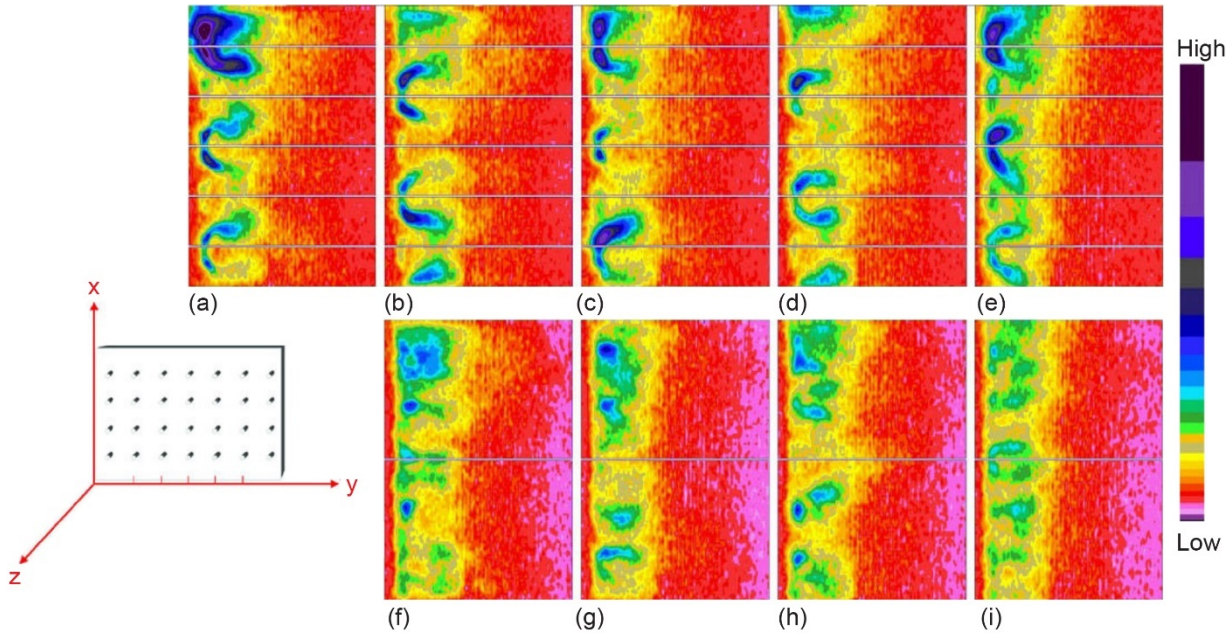

Figure 24.—Average fuel distribution from 49-point multiplex lean direct injection with 45° axial swirlers, by planar laser-induced fluorescence at inlet temperature T_3 = 715 K, inlet pressure P_3 = 1,380 kPa, $\Delta P/P$ = 3 percent, equivalence ratio ϕ = 0.5, and every other injector flowing. Y-planes are indicated above or below image. Top row images use horizontal lines to indicate spatial locations of element centerlines. Flow is left to right. Field of view limited to rows 2 to 6 of 7 by 7 array. Y = (a) –20 mm, (b) –10 mm, (c) 0 mm, (d) 10 mm, (e) 19 mm, (f) 15 mm, (g) 5 mm, (h) 5 mm, and (i) 15 mm. (Tacina, Mao, and Wey, 2003).

Images of average fuel distribution via fuel PLIF from the 49-pt multiplex LDI (Tacina, Mao, and Wey 2003) are shown in Figure 24. The 49-pt is a 7 by 7 array. The visible field is limited to array rows 2 to 6. In this case, every other fuel nozzle was active, and the laser sheet was aligned with nozzle centers roughly every 10 mm (top row). Although there are some differences in fuel spray appearance, they all have a similar "C" or crescent shape (it was noted by Tacina, Mao, and Wey (2003) that the variation in flow number for the injectors was ±6 percent). The very center element at Y = 0 appears smaller, so it might be affected by its surrounding swirlers.

Although these examples show very symmetric isothermal and combusting flows, there is interaction between adjacent swirlers, which is demonstrated most clearly in the 7-pt SV–LDI. For example, Figure 25 shows isothermal PIV results using all clockwise 60° swirlers. Figure 25(a) and (b) shows a composite slice at approximately 10 mm downstream from the dome. Blue represents reverse flow. There is clearly a CRZ downstream from the outer swirlers, but just a small area of reverse flow downstream from the center swirler. Figure 25(c) shows the isocontours that show where $u = 0$ and indicates a very small CRZ behind the center swirler. Interactions between the center swirler with the surrounding outer swirlers eliminated nearly all of the w component generated by the center swirler, while the outer wall helped to preserve the w for the outer swirlers.

Finally, the bulk flow in the intermediate and far fields for 2D arrays, rectangular or circular, is discussed. Measurements using PIV in isothermal flow for the 9-pt (Hicks, Locke, and Anderson, 2007) and 7-pt SV–LDI–1 (Hicks and Tacina, 2017) arrays have shown that when all elements of the same type are coswirling, the individual element streams begin to merge together. By midfield, a central core

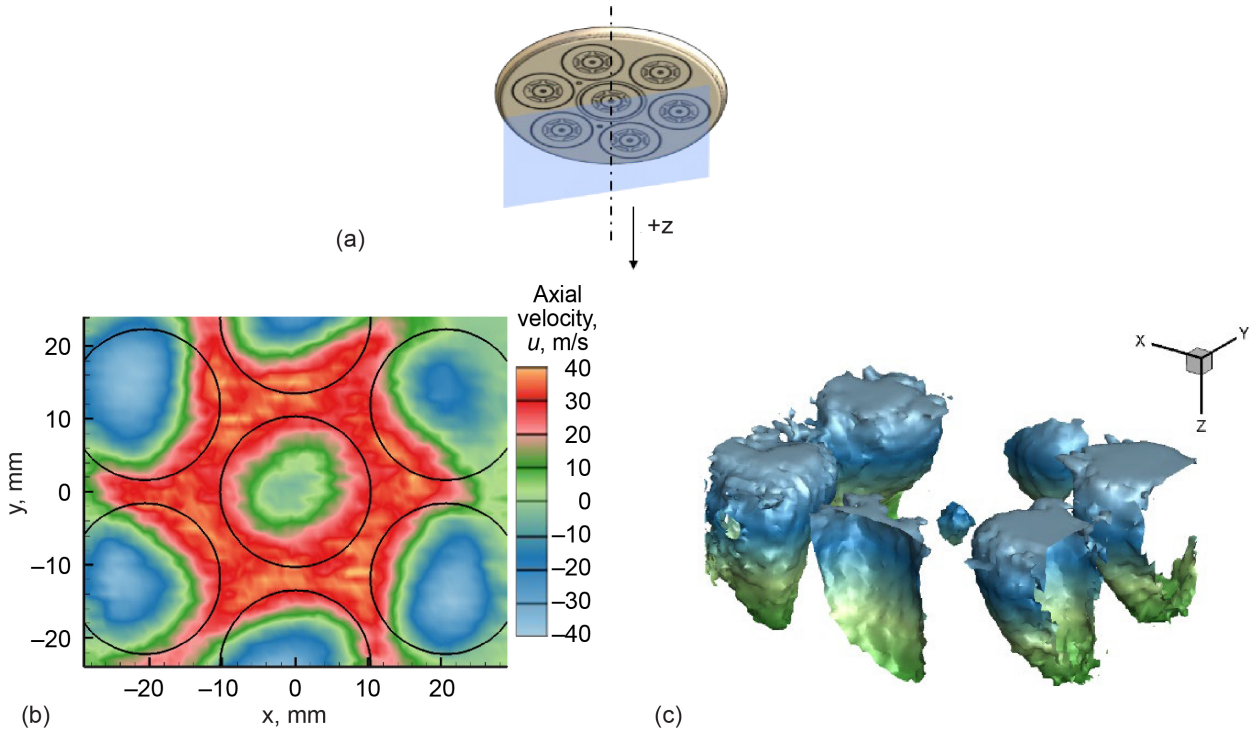

Figure 25.—Nonreacting particle image velocimetry results for seven-point swirl-venturi lean direct injection with all coswirling 60° swirlers. (a) Cross-sectional cut. (b) Contour of axial velocity at z ~10 mm from dome. (c) Isovelocity contours of $Vz = 0$ that show central recirculation zone volumes, colored by distance from dome.

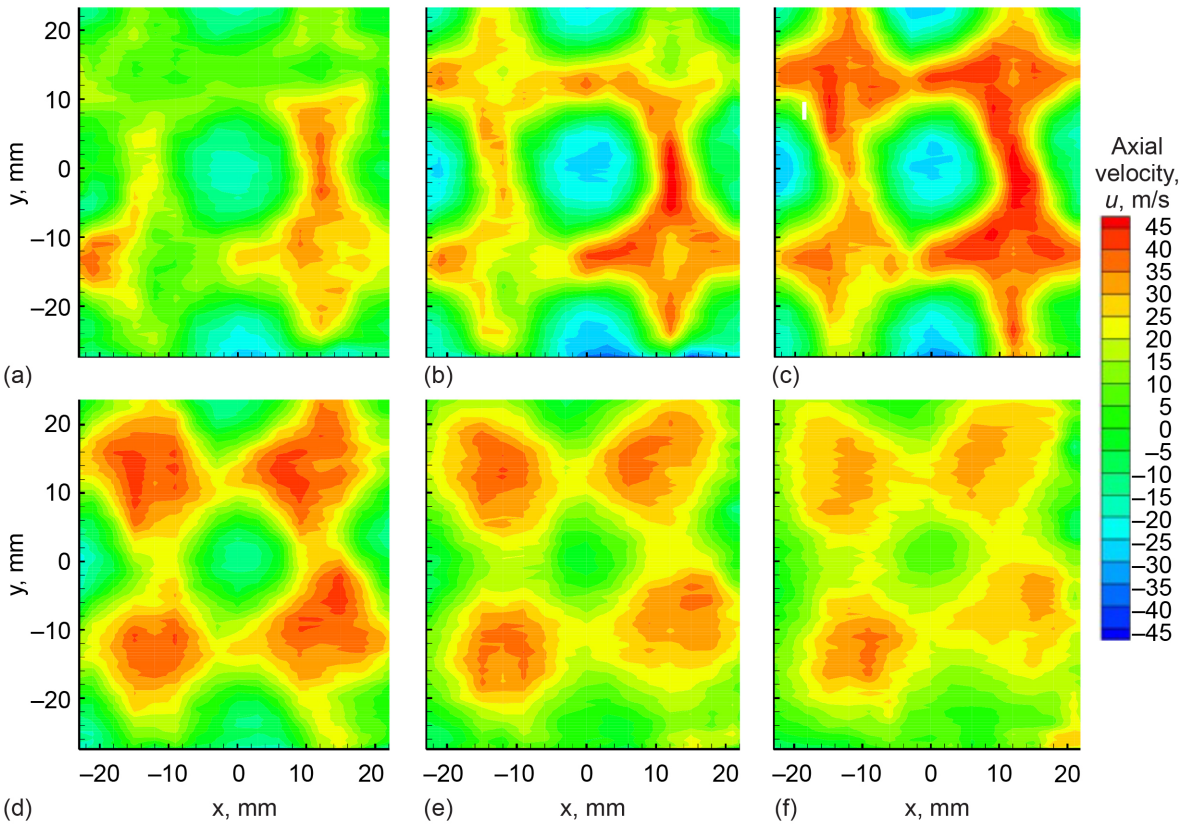

Figure 26.—Aft-looking forward views of axial velocity contours from 3 to 25 mm downstream from injector exit plane. Inlet conditions: temperature T_3 = 617 K, pressure P_3 = 1,030 kPa. (a) 3 mm. (b) 6 mm. (c) 9 mm. (d) 15 mm. (e) 20 mm. (f) 25 mm (Hicks et al., 2007).

rotation in the bulk flow is evident, with a swirl direction the same orientation as an individual element. Figure 26 illustrates this for the 9-pt LDI. The figure shows *u* contours viewed from downstream looking upstream (aft looking forward), at axial distances from 3 to 25 mm downstream from the dome. All swirlers are 60° clockwise swirlers in the streamwise sense, so the apparent motion of flow based on the images should be counterclockwise. The downstream flow has not completely merged by 25 mm downstream; however, the distance is far enough to identify the overall rotation. Focusing on the high-velocity yellow and red features between swirlers, the position at the 25-mm position has shifted in a counterclockwise sense compared to the structure at 15 mm. This consolidated core rotation of the bulk flow was also observed by (Samarasinghe et al., 2016) in a five-element circular array.

4.2.2 On Swirler Number Density and Mixer Size

Element spacing per diameter tended to be very similar for different LDI designs. This is also true for the CFRs in the square arrays, with values ranging from 1.3 to 2 or 2.6. In this section, size and number density of swirler elements and the effect on NO_x emissions is reviewed.

Several sizes of fuel-air mixers were tested. Typically, the change in fuel-air mixer size was accompanied by a change in fuel-air mixer design, making it difficult to determine if changes in NO_x emissions were caused by the change in design or size. However, for the SV–LDI–1 venturi flats configuration (see Appendix B), the fuel-air mixer size was changed while keeping the fuel-air mixer design constant.

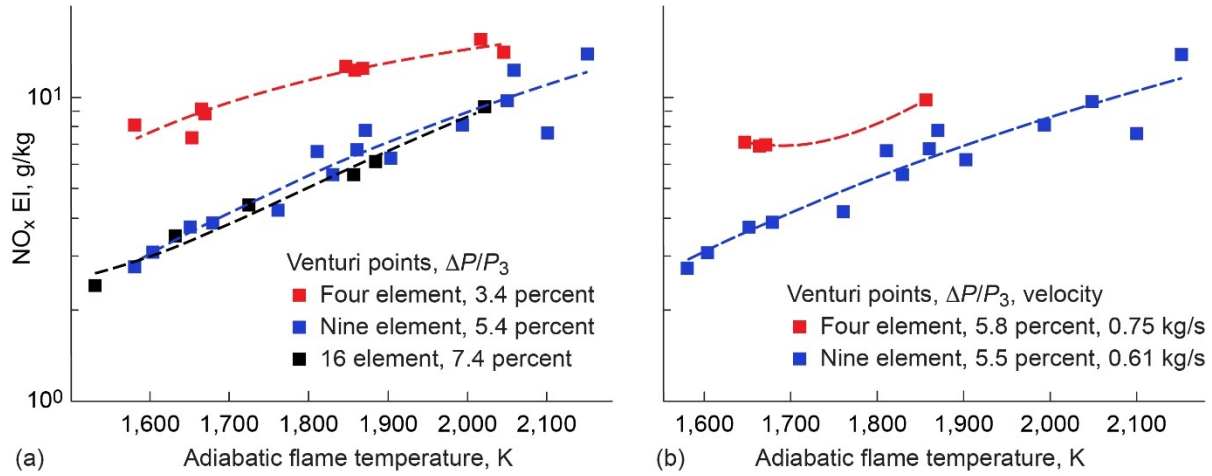

Figure 27.—Comparison of NO_x emissions from 4-element venturi flats, 9-element venturi flats, and 16-element venturi flats configurations. (a) Mass flow of air (thus reference velocity) is kept constant at 0.60 kg/s. (b) Pressure drop $\Delta P/P_3$ across dome is kept (approximately) constant at 5.5 percent. Emissions index (EI).

NO_x emissions for three SV–LDI–1 fuel-air mixer sizes are shown in Figure 27. Figure 27(a) shows the effect of fuel-air mixer size when the mass flow rate of air is kept constant, and Figure 27(b) shows the effect when the pressure drop of air is kept constant. Decreasing the fuel-air mixer size from 38.1 (four-element) to 25.4 mm (nine-element) decreases NO_x emissions. However, further decreasing the fuel-air mixer size to 17.8 mm (16-element) does not further decrease NO_x emissions.

This effect cannot be explained by changes in expected fuel drop size. According to Lefebvre and McDonell (2017), the drop size (SMD) depends on pressure drop to the –0.28 to –0.44 power. Mean drop size also depends on the fuel mass flow rate per injector to the 0.25 power. The 4-element and 16-element configurations have approximately the same total FN (FN per injector × number of injectors) but the 4-element has 4 times as much mass flow per injector. Therefore, Lefebvre's correlations estimate that the drop size for the 4-element will be approximately 40 percent higher than the drop size for the 16-element. The nine-element configuration has both a higher total FN and a higher per injector mass flow rate than the 16-point. Its drop size should be between 35 and 48 percent higher than the drop size for the 16-element and about the same as the drop size for the 4-element.

It could be argued that decreasing the fuel drop size will decrease NO_x emissions because smaller fuel drops will vaporize more quickly. However, in this case, although the 16-element is expected to have a smaller drop size than the 9-element, the NO_x emissions were similar for both of these configurations. Thus, fuel-air mixer size also seems to be important.

Some previous publications (Tacina et al., 2002; Tacina, Lee, and Wey, 2005) have figures that seem to show reducing the fuel-air mixer size below 2.54 cm continues to reduce NO_x emissions. One of these figures is reproduced as Figure 28. Note that although the naming scheme suggests similarity, the airflow passages for all five configurations are significantly different. The three macrolaminate LDI (MPIM) designs had significantly different air paths, so the reduction in NO_x in the 36-point MPIM design (nominal size: 1.27 cm) as compared to the two 25-point MPIM (nominal size: 1.52 cm) designs could have been caused by either the size reduction or the difference in swirler design. Similarly, the lack of NO_x reduction between the two discrete-jet or multiplex LDI (MPX LDI) designs cannot be used to make any conclusions about the optimal fuel-air mixer size: the 25-point MPX LDI design (nominal size: 1.52 cm) used discrete-jet swirlers, whereas, the 49-point MPX LDI design (nominal size: 1.09 cm) used axial swirlers. Currently, there is no consistent evidence to support decreasing the fuel-air mixer size below 2.54 cm.

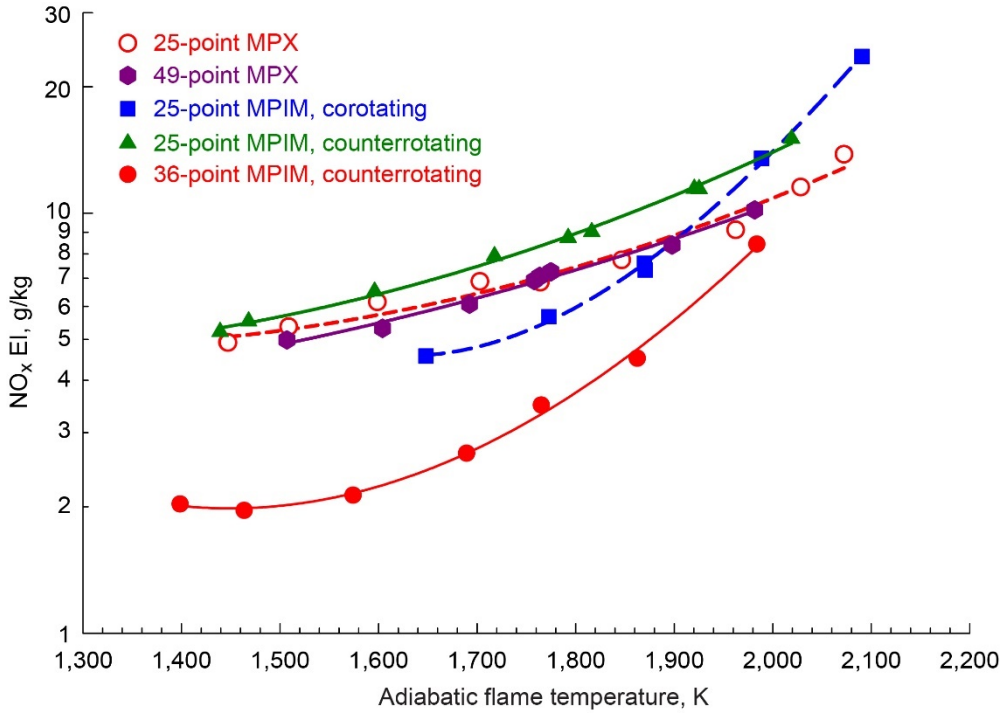

Figure 28.—Comparison of several lean direct injection (LDI) configurations at inlet temperature of 810 K, inlet pressure of 2,760 kPa, and pressure drop of 4 percent. Emissions index (EI). Discrete-jet or multiplex LDI (MPX LDI). Macrolaminate LDI (MPIM). (Tacina, Mao, and Wey, 2004).

4.3 Effect of Swirl Direction of Adjacent Swirlers

There are primarily two ways of introducing counterswirl to a SV–LDI array. One is for the center element of an array to swirl in a different direction from the surrounding swirlers. The other is that every other element alters its swirl direction in a checkerboard pattern. We saw a bit of this method in the previous discussion.

The following discussion supports two conclusions. First, comparing LDI configurations with adjacent fuel-air mixers corotating to those with counterrotating fuel-air mixers, the difference in NO_x emissions is typically small. Swirl strength is a more important parameter. Second, flow structure differences between coswirl and counterswirl should be considered for application in an annular array. For multielement configurations with corotating elements of the same type, the flow from the individual fuel-air mixers combines into one swirling structure. For multielement configurations with counterrotating elements of the same type, the flow from the individual fuel-air mixers combine farther downstream (compared to coswirling) into a large central swirling structure, surrounded by smaller counterswirling structures in the corners (for rectangular arrays).

4.3.1 Alternating Swirl Direction of Adjacent Swirlers

Two counterswirl configurations of the 9-pt SV–LDI were tested, one each using all 45° swirlers (Figure 29(a)) and all 60° swirlers (Figure 29(b)). The counterrotating cases consistently produced higher NO_x for both the 45° and 60° swirlers. (The only exception to this is for the 60° swirlers at inlet conditions around 620 K and 17 bars.) Overall, NO_x is lower for the 45° swirlers; however, its range for operability is lower than for the 60° swirlers. For the 45° swirlers, operability was much better for the

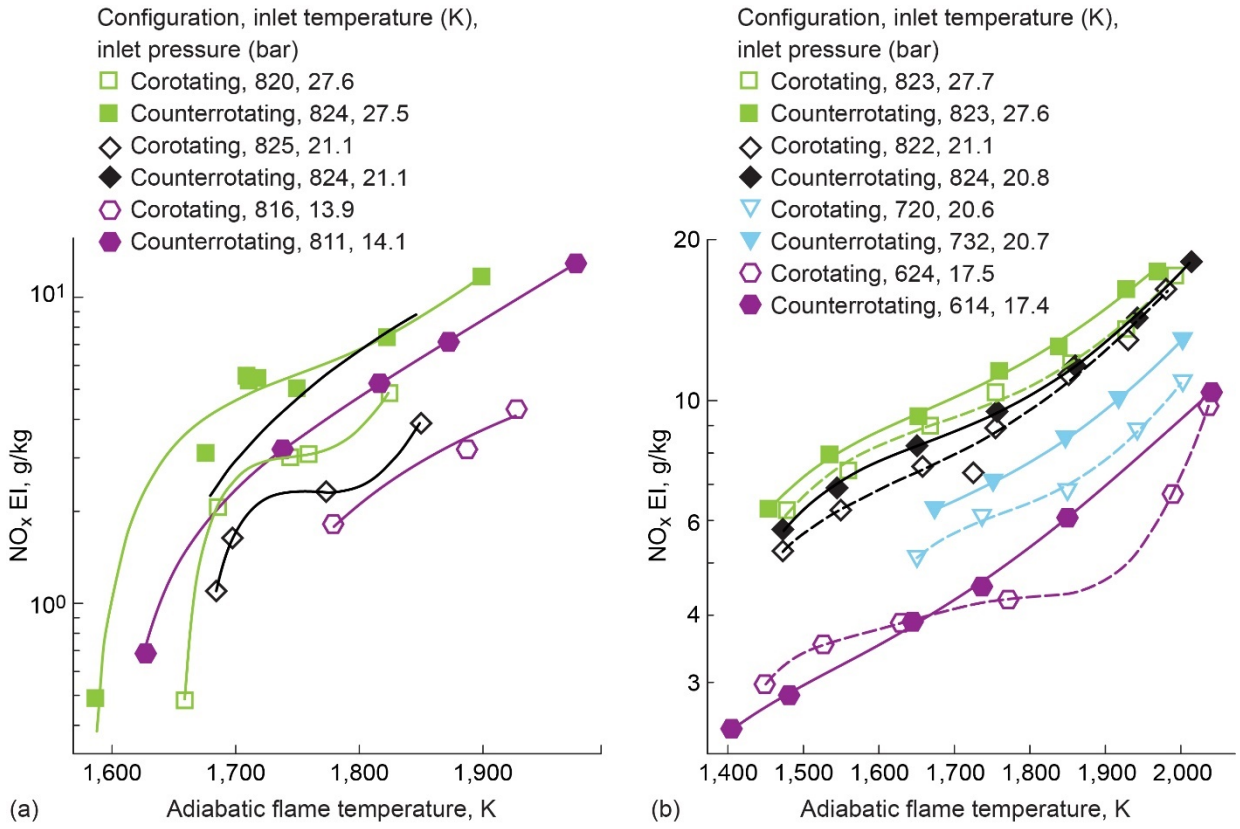

Figure 29.—Nine-point swirl-venturi lean direct injection injector results from gas sample analysis. NO_x emissions index (EI) as function of adiabatic flame temperature that compare coswirling and counterswirling configurations using all (a) 45° and (b) 60° swirlers at various inlet conditions. Pressure drop of 4 percent.

counterswirl configuration. Operability was arguably only slightly improved with counterswirling 60° swirlers, so increased swirl strength might be a mitigating factor for decreased operability.

Using LDV applied to a 9-pt discrete-jet configuration, Cai, Jeng, and Tacina (2002) compared the flow structures between an all coswirling array and one with alternating counterswirlers. As with the SV–LDI 7- and 9-pt coswirling configurations discussed earlier, within an element diameter, the flow field had merged enough to have one large swirling mass. On the other hand, the counterswirling configuration maintained separation between the elements for a longer distance; farther downstream, a large central core rotation was formed that had small counterswirling regions in the corners.

4.3.2 Alternating Swirl Direction of Center Swirler Relative to Surrounding Swirlers

In addition to the all 60° coswirling configuration (LH60all or RH60all), tests using the 7-pt SV–LDI included comparing coswirl and counterswirl of the 60° center swirler with 52° outer swirlers (RH60c_RH52o, LH60c_RH52o) and a counterswirling center offset configuration (RH60coff_RH52). Data were acquired at inlet temperature T_3 = 700 K and inlet pressure P_3 = 5 bar. Gas samples and OH* chemiluminescence images were acquired. Figure 30 shows the NO_x gas analysis results. These tests used a single-hole, fixed sample probe at the centerline position. In Figure 30(a), NO_x EI is plotted as a function of the equivalence ratio determined based on gas analysis. The reference velocity was 10.7 m/s. Figure 30(b) shows NO_x EI as a function of reference velocity with a nominal metered equivalence ratio of 0.45.

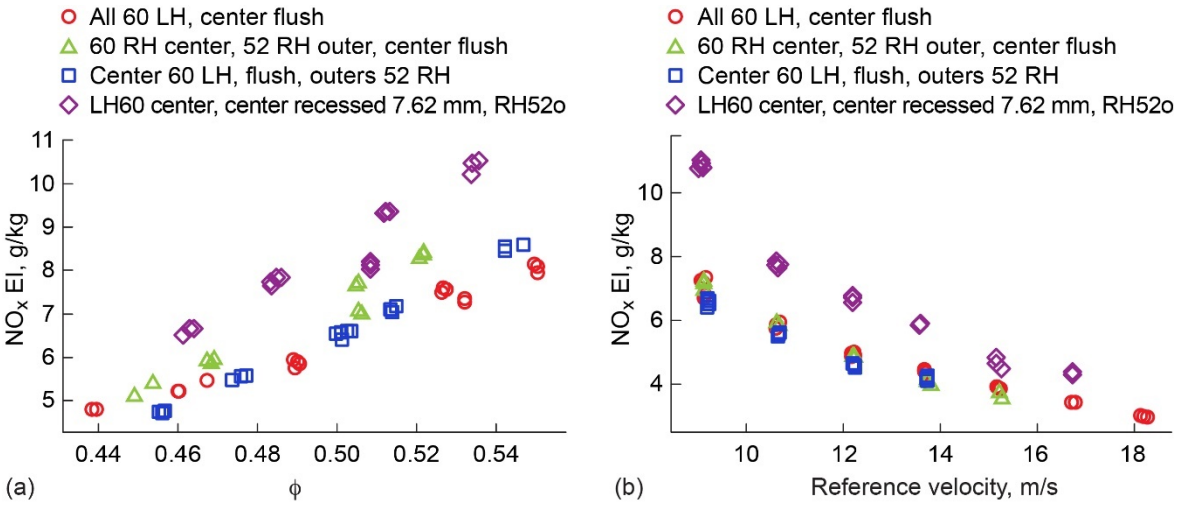

Figure 30.—Comparison of NO_x results from gas analysis for four seven-point swirl-venturi lean direct injection configurations. Combustor inlet conditions were 800 °F (700 K) and 517.1 kPa (75 psia). (a) Reference velocity kept constant at 10.7 m/s and the equivalence ratio (ϕ) is varied. (b) Equivalence ratio kept constant at 0.45 and the reference velocity is varied. Emissions index (EI). Left hand (LH). Right hand (RH).

Note two results. First, recessing the center element increased NO_x, but probably because the fuel spray wetted the recessed cylindrical area, resulting in poor atomization. Second, for the other configurations, there was not much difference in NO_x. This could be because the sampling occurred in the center only, and the flow from the outer swirlers had not yet mixed out by the probe location. On the other hand, the original 7-pt configuration tests indicated NO_x emissions did not depend strongly on swirler angle, since the 45° and 60° swirlers had similar NO_x emissions. During the UEET program, tests of the 9-pt showed that NO_x emissions converged at the highest equivalence ratios for the 45°, 52°, and 60° swirlers.

Figure 31 and Figure 32 show OH* chemiluminescence images. These figures show the differences in flame structure that result from using different equivalence ratios while holding the cold-flow reference velocity constant; and by holding equivalence ratio fixed while varying the reference velocity. These parametric tests were conducted to gain insight into the effect of swirler configuration on flame structure and combustion stability.

From most to least stable for combustion, the order of configurations is LH60all, LH60coff–RH52o, RH60c–RH52o, and LH60c–RH52o. The most stable configuration was the LH60all because it could sustain the lowest equivalence ratio on the matrix ($\phi = 0.4$) and also could sustain the highest reference velocity (60 ft/s or 18.3 m/s). In nonreacting measurements of velocity, LH60all had a CRZ downstream of every swirler, which helped to support the flame. LH60coff–RH52o had a more isolated center, to act as a pilot; and when compared to its counterpart without the center recess (and poorest performer), could sustain an additional 10-ft/s (3.05 m/s) reference velocity. RH60c–RH52o could sustain a reference velocity of 50 ft/s (15.24 m/s). If the offset effect is comparable, it would be expected that RH60coff–RH52 matches LH60all for reference velocity.

It is notable that these results agree with the findings presented in Section 3.3, on air swirler variation effects.

The chemiluminescence images show that higher flame symmetry also corresponds with stability. The most symmetric flame was LH60all, followed by LH60coff–RH52o. Least symmetric was LH60c–RH52o, which had the least stable flame.

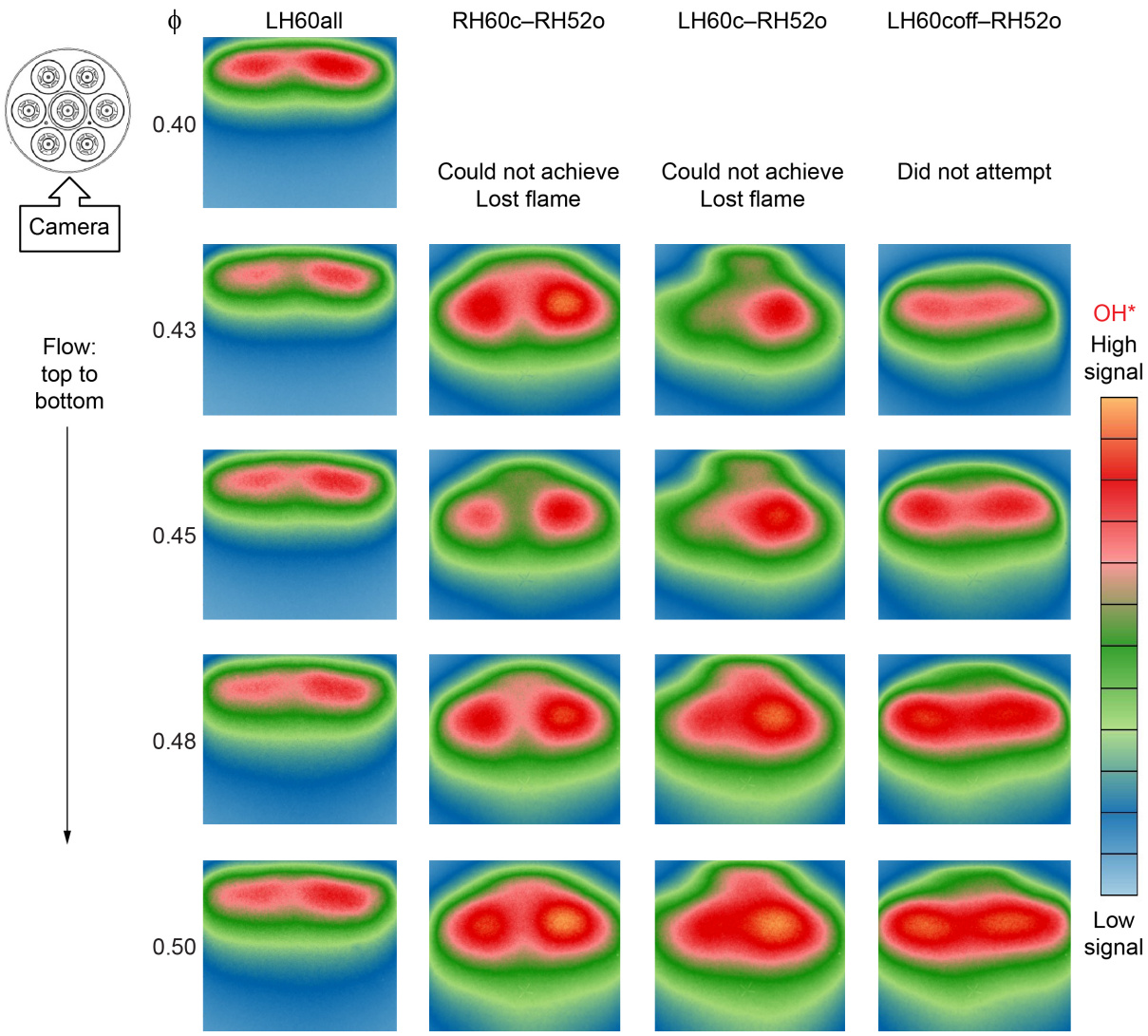

Figure 31.—Four seven-point swirl-venturi lean direct injection swirler configurations that reveal OH* structure for equivalence ratios (ϕ) shown with reference velocity of 10.7 m/s (35 ft/s). Images within each configuration (column) are scaled together. Flow passes from top (nominally z = 0) to bottom. Combustor inlet temperature is 700 K and inlet pressure is 517.1 kPa (75 psia).

In examining the PIV results from these and other configurations, it was difficult to determine a bulk flow direction for any configuration that did not have the same swirler elements at all positions. In the cases with a 60° swirler in the center and 52° or 45° swirlers in outer positions, it was possible to occasionally decipher the near-field direction behind the center swirler, but it was not possible to determine an overall swirling motion.

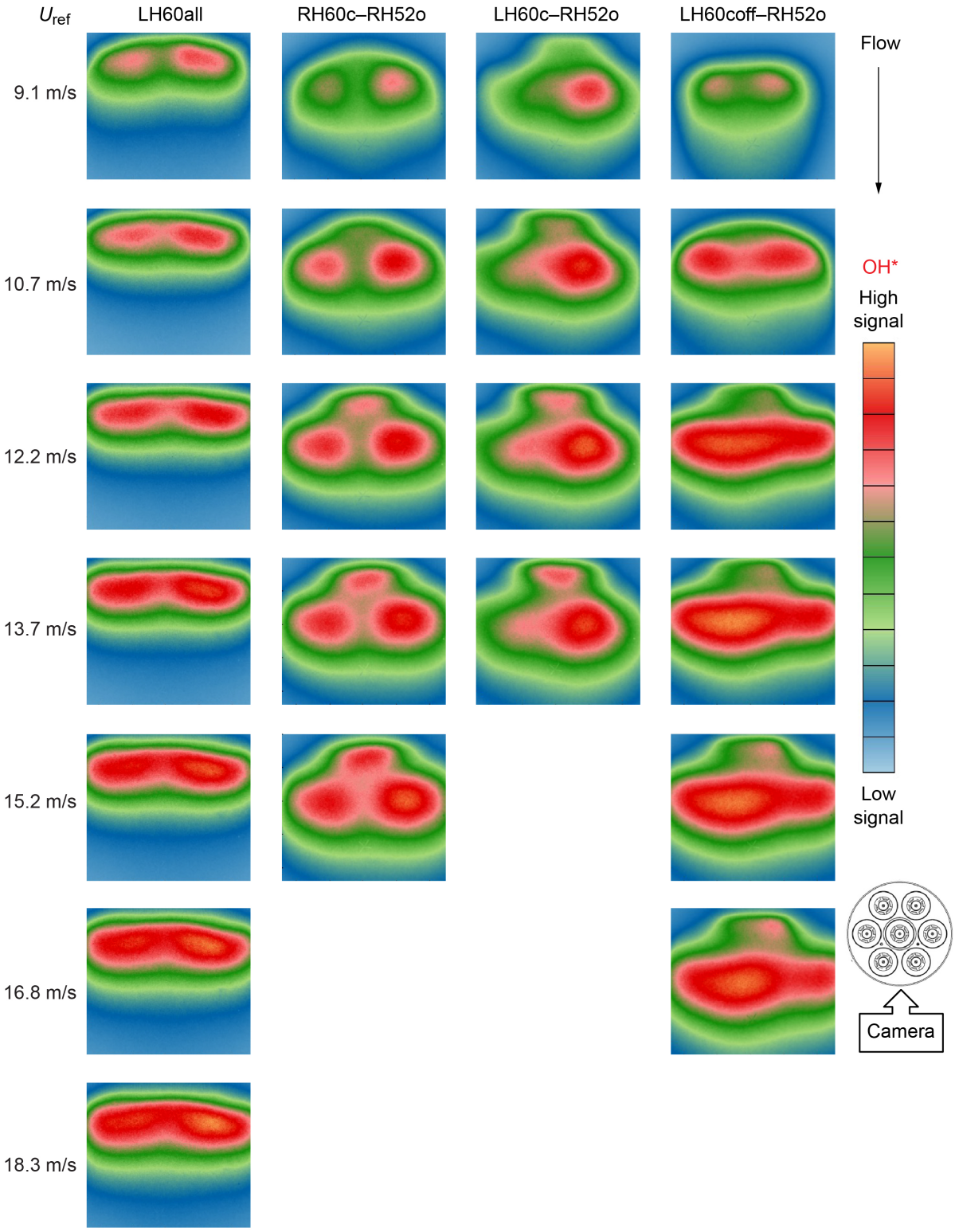

Figure 32.—Four seven-point swirl-venturi lean direct injection swirler configurations that reveal OH* structure for reference velocities (U_{ref}) shown. Images within each configuration (column) are scaled together. Flow passes from top (nominally z = 0) to bottom. Inlet temperature T_3 = 700 K. Inlet pressure P_3 = 517.1 kPa (75 psia). Equivalence ratio ϕ = 0.45.

5.0 Considerations of Fuel Injector Type and Fuel Staging

5.1 Comparing Airblast and Simplex Injectors

In SV–LDI, simplex fuel injectors tend to produce more intense flames that are more closely attached to the dome than comparable airblast atomizers. This can be seen in a RANS CFD simulation of a SV–LDI–2 configuration. This was a staged LDI configuration with one pilot stage and three main stages. The first two main stages—main 1 and main 2—each consisted of four fuel-air mixers and these stages were identical except for the type of fuel injector. The main 1 stage had simplex fuel injectors and 45° air swirlers with a counterclockwise orientation. The main 2 stage had airblast fuel injectors and 45° clockwise inner and outer air swirlers. As shown in Figure 33, the main 1 and main 2 stages alternate around the pilot cup (main 3 stage are the four corner injectors). Thus, the main 1 and main 2 stages give a direct comparison of simplex and airblast fuel injectors. Figure 33(a) also shows the position at which the dome is "sliced" so that one simplex and one airblast injector can be compared. Those slices are shown in Figure 33(b) to (d). The simplex main 1 stage has a strong CRZ and an attached, intense flame zone that produces higher NO_x emissions. In contrast, the airblast main 2 stage has no CRZ, a less intense flame, and lower NO_x emissions. Flame imaging confirmed that the flames behind the airblast fuel injectors were less intense. Standard video showed an apparently steady blue flame behind each simplex injector and a barely visible flame behind each airblast injector.

Another direct comparison of simplex and airblast fuel injectors is shown in Figure 34. This comparison was done using the SV–LDI–2 nine-recess (pilot, main 1, and main 2 are recessed from the dome exit) configurations. Except for the recess, the main 1 and main 2 stages were identical to the corresponding stages for the flat dome configuration. For this comparison, the temperature and pressure were set to be representative of an idle point for an advanced cycle and the pilot fuel flow rate kept constant. The main 1 simplex stage was turned on and fuel was increased until combustion dynamics became significant (0.7 psi peak-to-peak); this led to a flame zone equivalence ratio of 0.35, triple the equivalence ratio of an idle point for this cycle. Then, keeping the total fuel flow constant, the fuel was shifted from the simplex main 1 stage to the airblast main 2 stage. Shifting the fuel from the simplex stage to the airblast stage decreased the combustor pressure fluctuations and NO_x emissions, as shown in Figure 34. The decreased NO_x emissions might indicate better fuel-air mixing leading to a less intense flame zone, at least on average. This is consistent with the flat dome CFD simulations.

However, shifting the fuel from the simplex main 1 stage to the airblast main 2 stage also increased the CO and unburned hydrocarbon emissions and so decreased the combustion efficiency. It is possible the combustion efficiency could be improved by changes to the airblast design. Videos of the flame show liquid sheets intermittently passing through the airblast tip; the lack of primary breakup is indicative of poor atomization. Poor atomization might also indicate poor mixing, or delayed mixing at the dome; this might explain the lower NO_x emissions. Adding a prefilmer might eliminate these liquid sheets. This was done in the third-generation SV–LDI configurations; video showed no evidence of liquid sheets from the prefilming surface. In addition, according to the literature, changing the orientation of the concentric air swirlers could improve atomization. For those prefilming airblast that use double swirl in conjunction with fuel film rotation, Chin, Rizk and Razdan (2000) found that a corotating inner swirler, with a counterrotating outer swirler produced the smallest SMD, and that the worst atomization was when both airstreams were opposite to the liquid swirl direction.

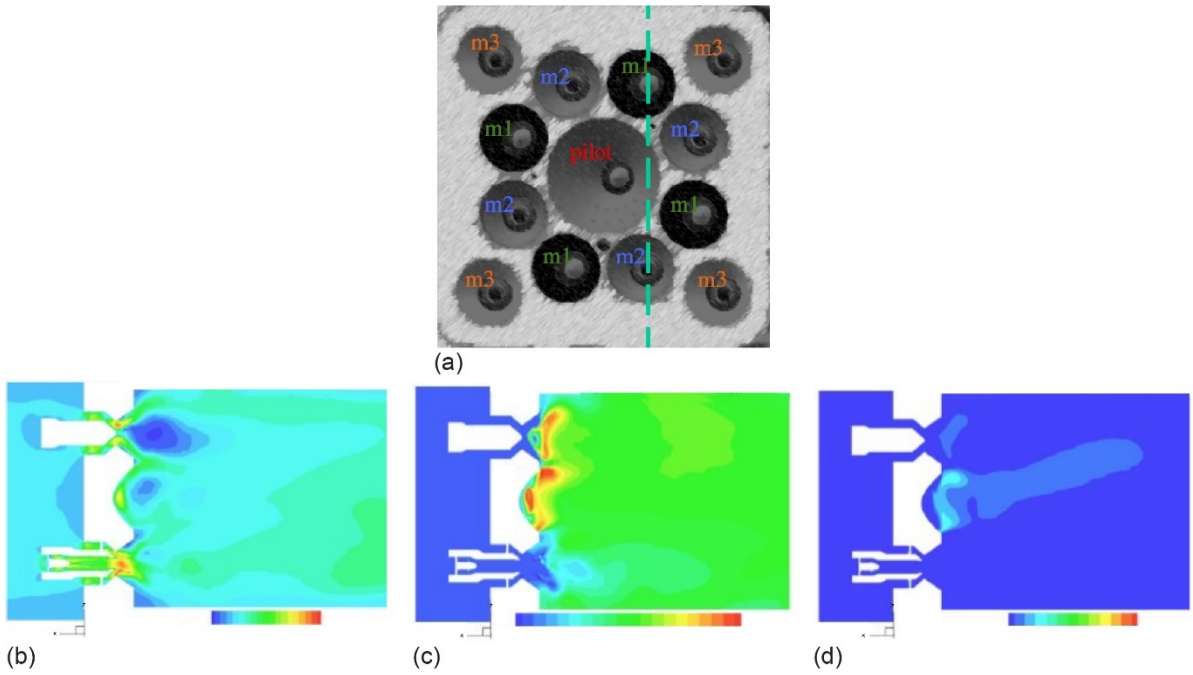

Figure 33.—Swirl-venturi lean direct injection (SV–LDI) SV–LDI–2. (a) Flat dome configuration. Main 1 (m1). Main 2 (m2). Main 3 (m3). Reynolds' Averaged Navier Stokes- (RANS) simulations show slices that bisect one simplex m1 and one airblast m2 fuel injector as indicated in (a). Color contours showing: (b) Axial velocity. (c) Flame temperature. (d) NO_x emissions.

5.2 Fuel Staging at Low-Power Conditions

First-generation LDI designs almost exclusively used pressure-atomizing simplex tips. Fuel staging was attempted by fueling only some of the injector tips. However, this fuel staging was not successful because the pilot fuel-air mixers were not isolated. Instead, the air from adjacent fuel-air mixers mixed with the pilot air, lowering the actual equivalence ratio in the flame zone and preventing first-generation designs from operating well at idle conditions. The current version of the NASA 7-pt can isolate the pilot by recessing the center fuel-air mixer, but without changing the venturi geometry; instead, the venturi was followed by a constant-diameter cylindrical section. This venturi offset was not successful because the fuel wetted the cylindrical walls, resulting in poor atomization and increased NO_x in the flame zone. Second- and third-generation SV–LDI designs were more successful. In these designs, the throat of the pilot venturi was moved upstream and the overall length (and thus the venturi diameter at the dome) was increased. These designs were able to operate successfully at idle and had reasonable lean blowout performance, although the combustion efficiency was still below the desired value. (Combustion efficiency was typically 97 to 98 percent instead of the desired 99+ percent. This lower-than-desired combustion efficiency was also partially due to the very low overall combustor equivalence ratio at the idle-like conditions, e.g., 0.103 at the 7 percent ICAO point.). The second-generation MPX LDI design took a different approach to isolating the pilot (Villalva et al., 2015). Instead of clustering the individual fuel-air mixers into nominal 5-, 7-, 9-, or 13-pt cups with the main stages surrounding a central pilot stage, the second-generation MPX LDI designs arranged the individual fuel-air mixers into five staggered rows, with the center row being the pilot stage, the rows just above and below the pilot being the intermediate stage, and the top and bottom rows being the outer stage used at the highest power conditions. At idle conditions, the pilot performance was similar to that of second- and third-generation SV–LDI.

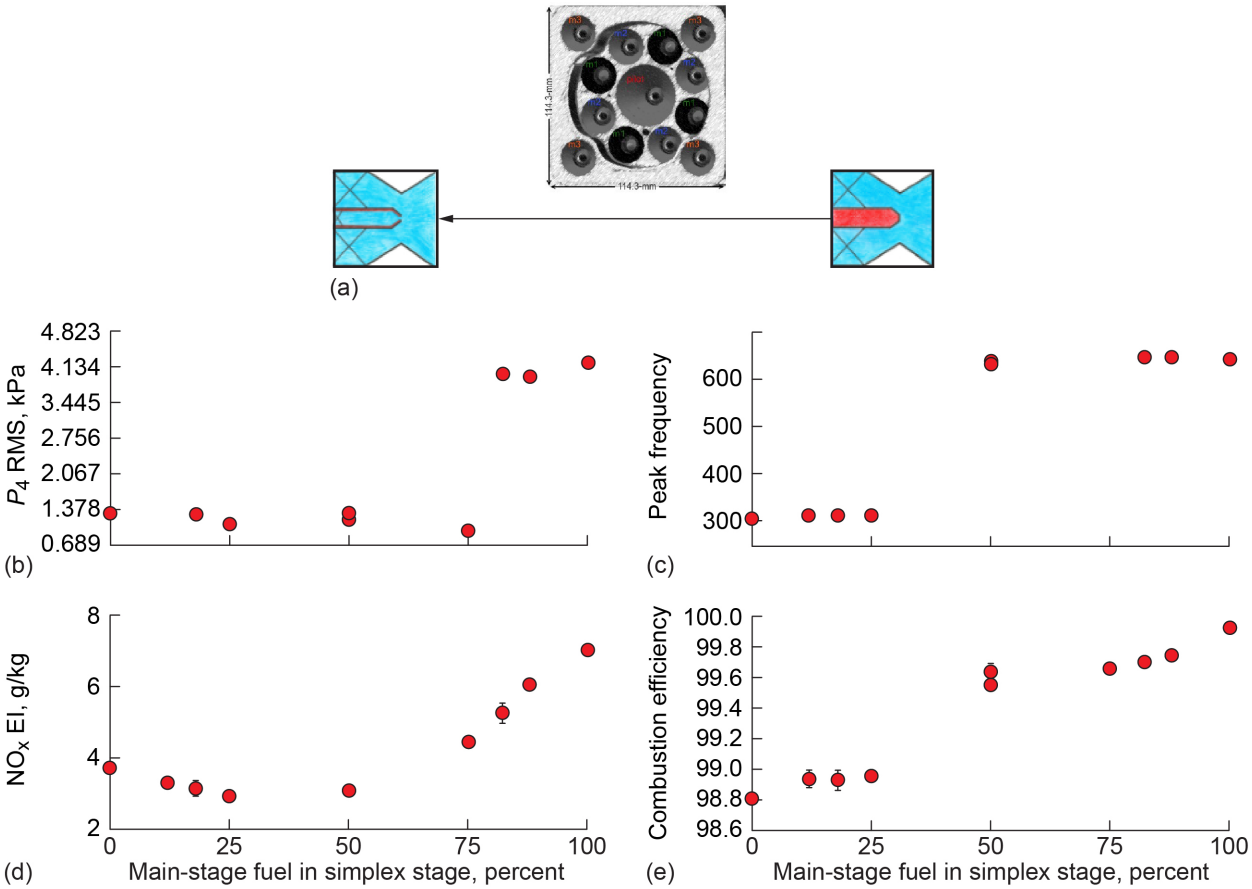

Figure 34.—Effect of fuel staging on gaseous emissions and combustion dynamics at 505 K and 0.7 MPa and an overall equivalence ratio of 0.35 for the swirl-venturi lean direct injection (SV–LDI) SV–LDI–2 nine-recess configuration. Temperature and pressure are representative of 7 percent International Civil Aviation Organization (ICAO) conditions, but equivalence ratio is much higher than typical 7 percent ICAO conditions. Pilot fuel flow is kept fixed and main fuel is split between simplex main 1 stage and airblast main 2 stage. (a) Nine-recess configuration. (b) Combustor pressure fluctuations (P_4) in psi. Root mean square (RMS). (c) Peak frequency of fluctuations. (d) NO_x emissions index (EI). (e) Combustion efficiency. (Reproduced from Tacina et al., 2015).

5.3 Fuel Staging at High-Power Conditions

The pilot fuel stage of the second- and third-generation SV–LDI designs was designed to achieve high combustion efficiency and stability at low-power conditions instead of to minimize NO_x emissions. Consistent with this design strategy, when all fuel-air mixers have the same local fuel-air ratio, CFD simulations consistently show higher NO_x emissions for the pilot stage. This is most pronounced with third-generation SV–LDI designs and can be clearly seen in Figure 35 (Ajmani, Mongia, and Lee, 2017). Due to the higher NO_x emissions from the pilot stage, reducing the pilot-stage equivalence ratio could be reasonably expected to reduce the overall NO_x emissions. However, experiments have consistently shown that changing the equivalence ratio for the pilot has only a small effect on NO_x emissions. There are two possible explanations for this lack of effect. First, the pilot stage is small, with only an order of 8 to 15 percent of the airflow going through the pilot. Thus, even if the pilot produces twice as much NO_x per kilogram of fuel as the LDI design overall, it will still produce a relatively small percentage of the total NO_x emissions (on the order of 16 to 30 percent). Second, decreasing the equivalence ratio for the pilot stage requires increasing it for the main stage. This increases the flame temperature for the main stage.

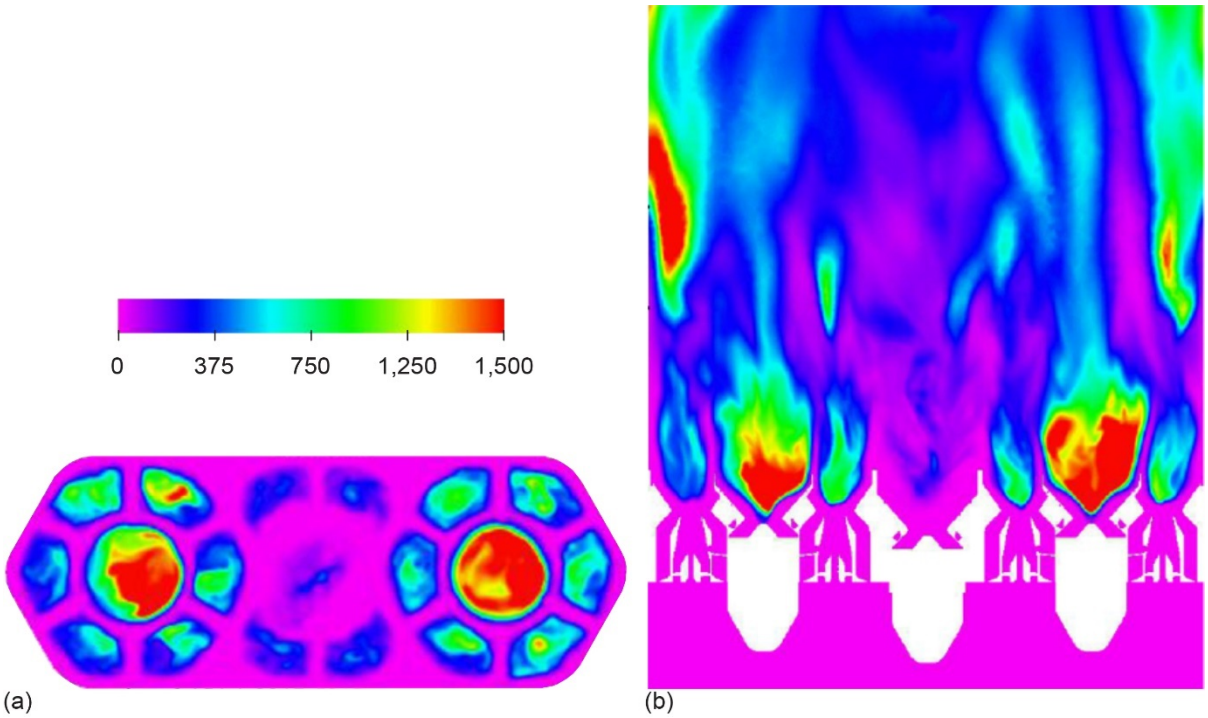

Figure 35.—Predicted NO_x emissions from swirl-venturi lean direct injection (SV–LDI) SV–LDI–3. (a) At dome exit plane. (b) Axial distribution in center plane that bisects pilot swirlers (Ajmani, Mongia, and Lee, 2017).

Since NO_x increases exponentially with flame temperature, the additional NO_x emissions from the main stages may more than compensate for the decreased pilot-stage NO_x.

As a practical matter, this simplifies LDI testing and fuel staging. High-power NO_x emissions can be estimated by testing with the local equivalence ratio equal to the overall equivalence ratio for all stages. The staging can be adjusted if necessary (e.g., to reduce combustion dynamics, if needed) without a large penalty in NO_x emissions.

6.0 Design Guidelines

As seen, there are many tradeoffs in considering an overall combustor design based on SV–LDI. In previous sections, the effect on flow field and/or NO_x emissions of swirl strength, venturi characteristics, element confinement, adjacent swirl direction, fuel injector type, and staging, among others was reviewed. The interaction between air swirl and fuel nozzle is especially important.

Twelve guidelines specifically for SV–LDI are identified and enumerated in the following information. There may be some differences for other designs such as multilaminate or discrete jet. Differences may be especially pertinent with regard to swirl strength. Please refer to the relevant references and Appendix C for more insight.

6.1 Air Path

6.1.1 Air Swirler

1. Thin swirler blades are to be preferred so long as structural integrity is maintained. Increasing the swirler blade thickness does not decrease the NO_x emissions but does increase the combustor pressure drop.

2. Decreasing the swirl tends to decrease NO_x emissions but also tends to increase flame length and decrease combustor stability.
   a. The higher the swirler blade angle, thus the SN, the more compact the CRZ.
   b. As the SN decreases, the flame zone shifts downstream.
   c. As the SN decreases, the likelihood of a CoRZ increases.
   d. Beyond the point of there being no CRZ, the flame zone also expands and becomes thicker.

Note that this particular guideline has strong caveats with respect to an actual design, as briefly discussed in Appendix C, which provides flame tube and sector test results for NO_x emissions over a wide range of inlet temperatures and pressures. Selecting the best swirl strategy is highly complex.

6.1.2 Venturi

1. The diverging section of the venturi stabilizes and promotes the recirculation zone.
2. A converging-diverging venturi assists in atomizing fuel.

6.2 Fuel Injection

1. The location of the fuel injector tip relative to the venturi throat has at most a small effect on NO_x emissions.
2. Simplex fuel injectors produce higher NO_x than similar airblast fuel injectors (i.e., they have the same physical envelope).

6.3 Regarding Lean Direct Injection Element: Confinement, Size, Spacing, and Interactions

1. Small changes in confinement and element spacing can cause a qualitative difference in the flow field.
2. There will be an optimal number density of fuel-air mixer elements in any given design space. For a fixed cross-sectional area (dome size), increasing the number (thus decreasing the size) of fuel-air mixers may initially decrease NO_x emissions. However, as the fuel-air mixer size continues to decrease, NO_x emissions plateau.
3. Regarding coswirl versus counterswirl for NO_x: Comparing LDI configurations with adjacent fuel-air mixers corotating to those with counterrotating fuel-air mixers, the difference in NO_x emissions is typically small. Swirl strength is a more important parameter.
4. Regarding coswirl versus counterswirl for flow field (nonreacting): Flow structure differences between coswirl and counterswirl should be considered for application in an annular array.
   a. For multielement configurations with corotating elements of the same type, the flow from the individual fuel-air mixers combines into one swirling structure.
   b. For multielement configurations with counterrotating elements of the same type, the flow from the individual fuel-air mixers combine farther downstream (compared to coswirling) into a large central swirling structure, surrounded by smaller counterswirling structures in the corners (for rectangular arrays).

6.4 Staging Strategies

1. To minimize NO_x emissions at high-power conditions, keep the local fuel-air ratio approximately equal for all stages.

2. The pilot stage can be isolated by extending the diverging section of the venturi, allowing for improved low-power operation.

6.5 Final Thoughts

Pay attention to pattern and profile factor. This is increasingly important as engine cores go to higher density to improve thermodynamic efficiency.

There is reference to several computational modeling studies in this report, especially for LDI–2 and LDI–3. However, the focus of this report has been on experimental work rather than CFD. Additional modeling references are compiled in Table IV for review.

TABLE IV.—SOME SWIRL-VENTURI LEAN DIRECT INJECTION (SV–LDI) MODELING REFERENCE PAPERS

SV–LDI generation	References
One-point LDI–1	Knudsen and Pitsch, 2010 Patel et al., 2007 Patel and Menon, 2008 Kirtas et al., 2006 Kim, Menon, and Darin, 2014 El-Asrag, Iannetti, and Apte, 2014 Dewanji, 2012 Iannetti, Liu, and Davoudzadeh, 2008 Ajmani, Kundu, and Yungster, 2014 Ajmani, Mongia, and Lee, 2013a Liu, Shih, and Wey, 2011
Three-point LDI–1	Heath, 2014
Nine-point LDI–1	Dewanji, 2012 Ajmani, Mongia, and Lee, 2013a Ajmani, Mongia, and Lee, 2013b
LDI–2	Ajmani, Mongia, and Lee, 2014a Ajmani, Mongia, and Lee, 2014b Heath, 2016
LDI–3	Ajmani, 2015 Ajmani et al., 2019a Ajmani et al., 2019b Ajmani et al., 2018a Ajmani et al., 2018b Ajmani, Mongia, and Lee, 2015 Ajmani, Mongia, and Lee, 2016 Ajmani, Mongia, and Lee, 2017

Appendix A.—Nomenclature

1-pt	one point
2D	two dimensional
7-pt	seven point
9-pt	nine point
49-pt	49 point
AATT	Advanced Air Transport Technology
AAVP	Advanced Aviation Vehicles Program
AAVT	Advanced Air Vehicle Technology
ACC	burner in annular array
AR	area ratio
ARMD	Aeronautics Research Mission Directorate (NASA)
AST	Advanced Subsonic Technology
c	center (swirler)
CFD	computational fluid dynamics
CFR	confinement ratio
CH*	CH radical
CoRZ	corner recirculation zone
CRZ	central recirculation zone
CST	Commercial Supersonic Technology
D	exit diameter
ΔP	pressure drop, differential pressure
EI	emissions index, emitted grams of species per kilogram of fuel burned
ERA	Environmentally Responsible Aviation (NASA ARMD Program)
ERZ	edge recirculation zone
FA	Fundamental Aeronautics
FAA	Federal Aviation Administration
FN	flow number
HSR	High-Speed Research
IAS	inner air swirler
ICAO	International Civil Aviation Organization
ICCD	intensified charge-coupled device
L	divergence length
L/D	length to diameter ratio
LDI	lean direct injection/injector
LDV	laser Doppler velocimetry
LH	left-hand, counterclockwise (swirl, swirlers)
LPP	lean-premixed-prevaporized
MPIM	macrolaminate LDI
MPX LDI	discrete-jet or multiplex LDI
NO_x	oxides of nitrogen
OAS	outer air swirler
ORZ	outer recirculation zone
o	outer (swirlers(s))
P, p	pressure

PDI	phase Doppler interferometry
PICS	Pilot-in-Can Swirler
PIV	particle image velocimetry
PLIF	planar laser-induced fluorescence
RANS	Reynolds' Averaged Navier Stokes
RH	right-hand, clockwise (swirl, swirlers)
RMS	root mean square
RQL	rich-quench-lean
S	space between adjacent swirlers
SCC	Alstom EV–5 premixed gas burner
SMD	Sauter mean diameter
SN	swirl number
SV–LDI	swirl-venturi lean direct injection
T	temperature
TAPS	Twin Annular Premixing Swirler
TFNS	time-filtered Navier-Stokes
TTT	Transformational Tools and Technology (Project in NASA ARMD)
u	axial velocity
U_{ref}	cold flow reference velocity
UEET	Ultra-Efficient Engine Technology
UTAS	United Technologies Aerospace Systems
UTRC	United Technologies Research Center
V	velocity
VLES	very large eddy simulation
w	tangential velocity
3	combustor inlet
4	combustor exit

Symbols

ϕ	equivalence ratio, fuel-to-air, mass basis
$\rho_a V_a$	air mass velocity

Subscripts

3	combustor inlet
4	combustor exit
comb	combusted gas
eng	engine
ref	reference

Appendix B.—NASA Lean Direct Injection Geometries and History

Three broad classes of multielement lean direct injection (LDI) configurations have seen the most sustained development. The classes are called swirl-venturi LDI (SV–LDI), macrolaminate LDI (MPIM), and discrete-jet LDI (MPX LDI). They are distinguished by the type of fuel-air mixer used. Although some parametric experiments have been done on all three classes of LDI, most of the in-house NASA research and much of the research done in collaboration with universities has used SV–LDI.

The design guidelines in this report were developed using SV–LDI fuel-air mixer configurations, MPIM, and MPX LDI. The configurations and selected references are enumerated in Table V and described in order of configuration number in more detail in the following sections.

TABLE V.—LISTING OF PRIMARY CONFIGURATIONS USED TO DEVELOP DESIGN GUIDELINES, ALONG WITH SELECTED REFERENCES
[Lean direct injection (LDI). Swirl-venturi LDI (SV–LDI).]

Configuration number	Configuration name	LDI class	Swirler type	Injector type	Figure	References
1	Single element with screen	SV–LDI–1	Axial	Simplex	37(a) and (b)	Tedder et al., 2014; Hicks et al., 2014
2	Single element with 2-in. (50.8-mm) square duct	SV–LDI–1	Axial	Simplex	37(c) and (d)	Fu, Jeng, and Tacina, 2006; Ajmani, Mongia, and Lee, 2013a; Ajmani, Mongia, and Lee, 2013c
3	Original seven-element	SV–LDI–1	Axial	Simplex	38(a) and (b)	Tacina, 2018
4	New seven-element	SV–LDI–1	Axial	Simplex	38(c) and (d)	Tacina et al., 2015; Hicks et al., 2019
5	Four-element venturi points	SV–LDI–1	Axial	Simplex	39(a)	Tacina, 2018
6	Nine-element venturi points	SV–LDI–1	Axial	Simplex	39(b)	Tacina, 2018
7	16-element venturi points	SV–LDI–1	Axial	Simplex	39(c)	Tacina, 2018
8	Nine-element venturi flats	SV–LDI–1	Axial	Simplex	40	Tacina, 2018; Tacina, Lee, and Wey, 2005; Heath et al., 2010; Hicks et al., 2011; Ajmani, Mongia, and Lee, 2013b
9	Single LDI airblast	SV–LDI–2	Axial	Airblast	41	Ren et al., 2016; 2018; 2020
10	Single airblast injector (converging only)	SV–LDI–2	Axial	Airblast	41(b)	Ren et al., 2016; 2018; 2020
11	Flat dome	SV–LDI–2	Axial	Simplex, airblast	42(a)	Tacina et al., 2015; Ajmani, Mongia, and Lee, 2014a; Ajmani, Mongia, and Lee, 2014b; Tacina et al., 2014; Tacina et al., 2016
12	Nine-recess	SV–LDI–2	Axial	Simplex, airblast	42(b)	Tacina et al., 2015; Tacina et al., 2016
13	Five-recess	SV–LDI–2	Axial	Simplex, airblast	42(c)	Tacina et al., 2014; 2015; 2016
14	Single-stem, LDI–3	SV–LDI–3	Axial, radial	Simplex, prefilming	43	Ajmani, Mongia, and Lee, 2016; 2017; Tacina et al., 2017; Ajmani et al., 2018a; 2018b; Tacina et al., 2019
16	Macrolaminate LDI, MPIM	Macrolaminate	Radial	Plain jet	44	Tacina et al., 2002; Mansour, 2015
17	Discrete-jet or Multiplex LDI, MPX LDI	Discrete jet	Discrete jet	Simplex, airblast	45	Tacina, Mao, and Wey, 2004; Goeke et al., 2014; Zink, Ryon, and Pack, 2014

B.1 Swirl-Venturi Lean Direct Injection

SV–LDI is distinguished by a converging-diverging venturi downstream of the air swirler, as shown in Figure 36. There have been three generations of SV–LDI: SV–LDI–1 to SV–LDI–3. In the first-generation SV–LDI–1, simplex fuel injectors were used with axial air swirlers, as shown in Figure 36(a) and (b). In the second-generation SV–LDI–2, airblast fuel injectors were also used. These are shown schematically in Figure 36(c). In the third-generation SV–LDI–3, prefilming fuel injectors were incorporated. Axial air swirlers were used on the main stages and simplex or prefilming-simplex fuel injectors were used with radial air swirlers for the pilot stage.

B.1.1 Swirl-Venturi Lean Direct Injection (SV–LDI–1)

This is the first-generation SV–LDI, and baseline LDI design. Each SV–LDI–1 fuel-air mixer uses a single axial air swirler with helical blades and a simplex fuel injector. For multielement SV–LDI–1 designs, all fuel-air mixers are the same size.

Configurations 1 and 2 are single-element designs used to better understand the LDI mixer. The elements are nominally the same size, but the flame tubes are different. Configuration 1 is referred to as "single element with screen" and issues into a 3-in. (76.2-mm) circular tube. Since the test section diameter is much larger than that of the fuel-air mixer, coflow is used to avoid a large expansion that would be unrepresentative of multielement SV–LDI configurations. This is accomplished by surrounding the element with a screen chosen to roughly match the pressure drop across the fuel-air mixer, as shown in Figure 37. Three six-bladed swirlers are used with this configuration: a low-swirl 45° swirler with a swirl number (SN) of 0.59; a medium-swirl 52° swirler with SN = 0.77, and a high-swirl 60° swirler with SN = 1.02. The venturi has a finite-length throat with a throat diameter of 0.51 in. (13 mm). In this configuration, the fuel injector tip can be moved to three positions with respect to the venturi throat: at the throat, 0.16 throat diameters upstream of the throat, and 0.31 throat diameters upstream of the throat. However, unless otherwise noted, the fuel injector tip is located at the venturi throat. More details on this configuration can be found in Hicks et al. (2014).

Configurations 3 and 4 are seven-point designs, shown in Figure 38. Configuration 3 is the "original seven element," while the "new seven element" is configuration 4. Each has a center element surrounded by six outer elements. All elements are nominally 1 in. in diameter. The seven-element configurations are nominally 3 in. in overall diameter.

Configuration 3, the original seven element, is shown in Figure 38(a). It used five-bladed axial air swirlers. Two swirler angles were used with this configuration, 45° and 60°. The effects of swirler blade thickness; swirler blade angle and orientation; and fuel injector tip position relative to the venturi throat were examined using this configuration. See Tacina (2018) for more details.

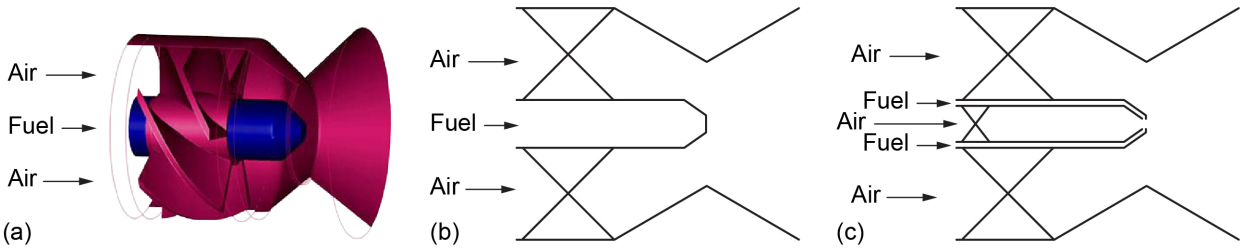

Figure 36.—Swirl-venturi lean direct injection (SV–LDI). (a) Single SV–LDI mixer element with simplex fuel injector. (b) Simplex fuel injector. (c) Airblast fuel injector.

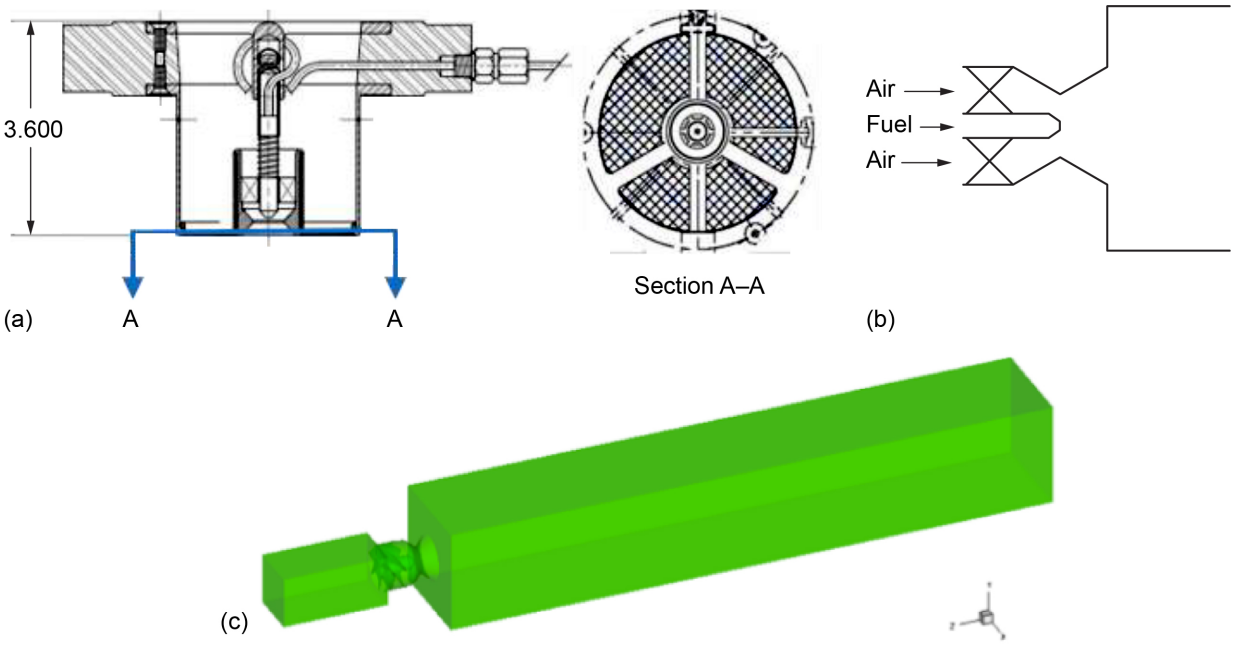

Figure 37.—Swirl-venturi lean direct injection (SV–LDI) SV–LDI–1 single-point research designs, configurations 1 and 2. (a) Configuration 1 is shown in plan view that illustrates airflow path. Cross-sectional slice A–A shows screen and its relation to LDI element. (b) Plan view of configuration 2 into square duct flow path. (c) Geometric model of configuration 2 from Ajmani et al. (2013a).

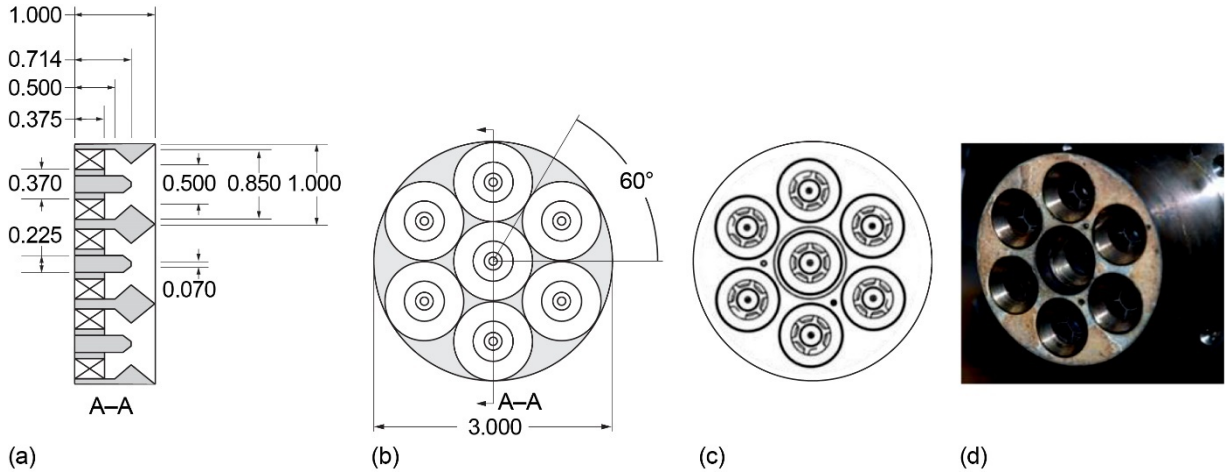

Figure 38.—Swirl-venturi lean direct injection (SV–LDI) SV–LDI–1 seven-element configurations 3 (original) and 4 (new). (a) Configuration 3 cross-sectional A–A view. (b) Configuration 3 cross section. (c) Configuration 4 cross section. (d) Configuration 4 showing that center (pilot) element can be recessed. All dimensions are in inches.

Configuration 4, the new seven-element configuration, is shown in Figure 38(c). The swirlers used with this configuration are identical to the ones used in configuration 1. However, since this is a multielement configuration, swirler orientation matters. Thus, both left-handed (LH) and right-handed (RH) swirlers are used. This gives two low-swirl swirlers, 45° (SN = 0.59) LH and RH; two medium-swirl swirlers, 52.5° (SN = 0.77) LH and RH; and two high-swirl swirlers, 60° (SN = 1.02) LH and RH. For some nonreacting flow testing, the swirlers and fuel-air mixers were replaced by screens. Finally, the center (pilot) fuel-air mixer could be slid axially upstream in a cylindrical channel to recess it from the dome, as shown in Figure 38(c).

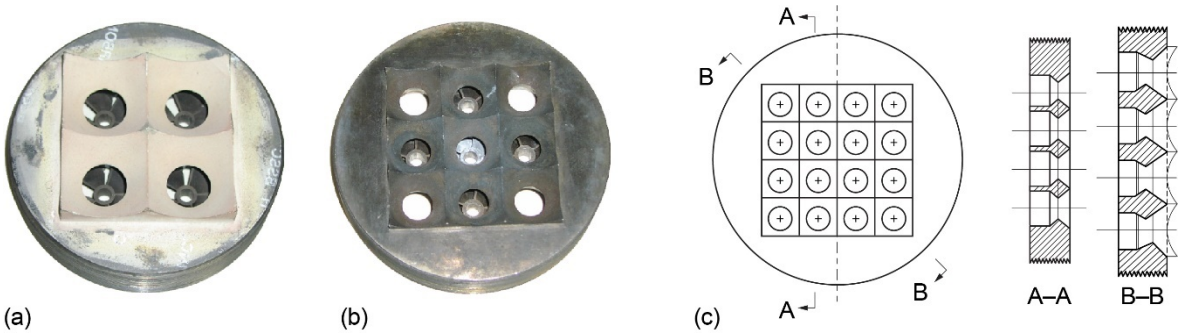

Figure 39.—Three swirl-venturi lean direct injection (SV–LDI) SV–LDI–1 venturi points configuration. (a) Four-element venturi points, configuration 5. (b) Nine-element venturi points, configuration 6. (c) Sixteen-element venturi points, configuration 7.

The following is information on SV–LDI–1 venturi points configurations 5 to 7. The three venturi points configurations are the only LDI configurations where the size of the fuel-air mixer was changed without also changing the design of the air path. For these three configurations, the total cross section was also kept constant, 3- by 3-in. square. The number of fuel-air mixers and the size of each fuel-air mixer was changed. Configuration 5, the four-element venturi points, had four nominally 1.5-in.-diameter fuel-air mixers arranged in a 2 by 2 array; configuration 6, the nine-element venturi points, had nine nominally 1-in.-diameter fuel-air mixers arranged in a 3 by 3 array; and configuration 7, the 16-element venturi points, had 16 nominally 4/3-in.-diameter fuel-air mixers arranged in a 4 by 4 array. Unlike the other SV–LDI–1 configurations, the dome of the venturi points configurations is not flat. Instead, it is contoured to partially match the diverging venturi. This can be seen most clearly in the photograph in Figure 39(a) and in Section B–B in the drawing in Figure 39(c). The venturi points configurations had five-bladed axial air swirlers; only results for a swirler angle of 60° are reported here. See Tacina (2018) for more details.

SV–LDI–1 nine-element venturi flats configuration 8 is described here. The nine-element venturi flats configuration is the baseline SV–LDI configuration. It has nine fuel injectors arranged in a 3 by 3 array. Like the venturi points configurations, it has a 3- by 3-in. square cross section. It has six-bladed axial swirlers. In fact, it uses the same six swirlers as configuration 4, the new seven-point configuration: two low-swirl swirlers, 45° (SN = 0.59) LH and RH; two medium-swirl swirlers, 52° (SN = 0.77) LH and RH; and two high-swirl swirlers, 60° (SN = 1.02) LH and RH. There are also two minor variations on the venturi. In the version used exclusively for gaseous emissions measurements, the length of the diverging section of the venturis was set so that neighboring venturis just intersected so that each diameter at the dome measured just less than 1 in. This version is shown in Figure 40(a). The version used for optical diagnostics used an extended air box to reach the windows, and the length of the diverging section was (inadvertently) slightly less, 0.875-in. diameter, so there was a small gap between neighboring fuel-air mixers, as shown in Figure 40(b). More details on this configuration can be found in references Tacina, Lee, and Wey (2005); Heath et al. (2010); and Hicks et al. (2011).

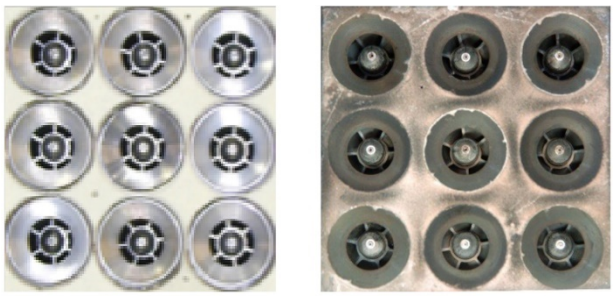

(a) (b)

Figure 40.—Configuration 8, nine-element venturi flats configuration. (a) Version shown here was used exclusively for gaseous emissions and in flame tubes that could provide pressures greater than 18 atm. (b) Version shown here was used also with laser-based and optical measurements below 18 atm. Gaseous emissions were also taken with this version.

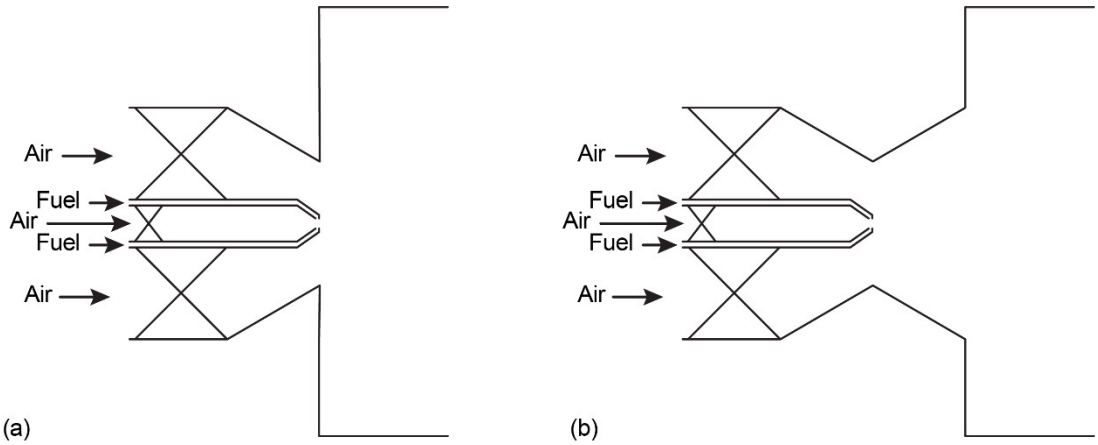

Figure 41.—Single lean direct injector (LDI) and swirl-venturi LDI (SV–LDI) configurations that use airblast fuel nozzles: (a) Airblast LDI (converging only). (b) SV–LDI (converging-diverging) with airblast fuel injector.

B.1.2 Swirl-Venturi Lean Direct Injection (SV–LDI–2)

Like SV–LDI–1, SV–LDI–2 has axial air swirlers. However, in SV–LDI–2, both airblast and simplex fuel injectors are used. In addition, in multielement SV–LDI–2 configurations, not all fuel-air mixers have the same venturi exit area (i.e., they do not all appear to be the same size). The venturi exit area of the pilot fuel-air mixers is significantly larger than that of the main-stage fuel-air mixers.

SV–LDI–2 single element research configurations include single LDI airblast. Two research configurations were used to examine the importance of the diverging section of the venturi. As shown in Figure 41, both configurations had airblast fuel injectors with two axial air swirlers, an outer air swirler (OAS) and an inner air swirler (IAS). Configuration 9 is the airblast nozzle which, like many single fuel nozzles, exits with either a convergence (as in this case), or has a cylindrical orifice. There was no diverging/diffuser section before exiting into the combustion chamber. Configuration 10 added the diverging section before exiting into the combustion chamber. These configurations can also be thought of as being comparable to the baseline SV–LDI. In this case, the airblast nozzle replaces the simplex nozzle. The airblast nozzle has only the IAS, and the airblast nozzle fits through the OAS with the nozzle tip at the venturi throat. Again, configuration 9 has no diffuser, and configuration 10 had a converging-diverging venturi downstream of the air swirler, thus rendering it an LDI fuel-air mixer.

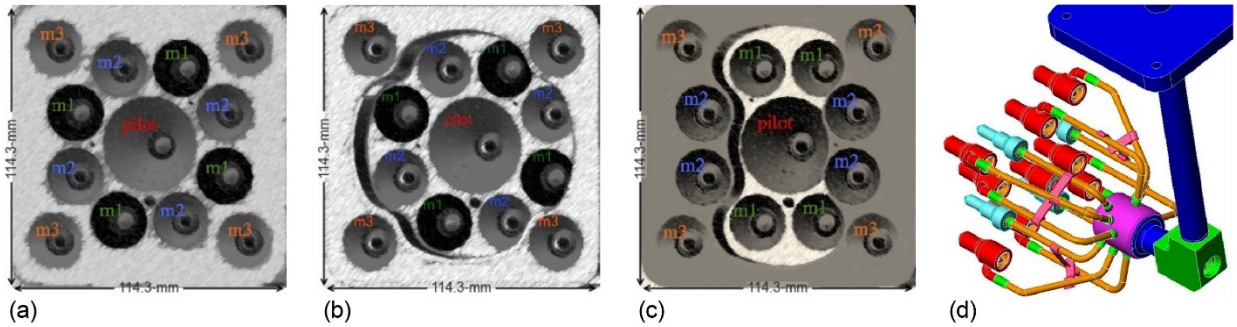

Figure 42.—Swirl-venturi lean direct injection (SV–LDI) SV–LDI–2 configurations. Main stage 1 (m1). Main stage 2 (m2). Main stage 3 (m3). Dimensions are millimeter. (a) Flat dome configuration, configuration 11. (b) Nine-recess configuration, configuration 12. (c) Five-recess configuration, configuration 13. (d) Fuel stem used to feed 13 individual SV–LDI–2 fuel injectors.

Both configurations had low- and high-swirl variations. In the low-swirl variant, the IAS had a 45° blade angle (SN ≈ 0.6), whereas in the high-swirl variant, the IAS had a 60° blade angle (SN ≈ 1). The blade angle for the outer air swirler was always 60°.

SV–LDI–2 multielement configurations are the flat dome, configuration 11; the nine-recess, configuration 12; and the five-recess, configuration 13. Second-generation SV–LDI–2 configurations are shown in Figure 42. Like SV–LDI–1, SV–LDI–2 configurations use axial air swirlers. In all SV–LDI–2 configurations, the fuel-air mixers are grouped into four stages, the center pilot and three main stages (labeled m1, m2, and m3 in the figure). Each of the main stages is composed of four fuel-air mixers. For the main 1 stage, each fuel-air mixer has a simplex fuel injector with a single 45° air swirler (SN ≈ 0.6). The other two main stages have airblast fuel injectors with 45° IAS and OAS. For configuration 11, the flat dome configuration, the pilot has a simplex fuel injector with a single 45° air swirler. For the other two configurations, the pilot has an airblast fuel injector with 57° IAS and OAS.

Except for the pilot stage, all fuel-air mixers are the same size. The venturi exit diameter of the pilot is much larger than the venturi exit diameter of the main stages. However, as can be seen in Ajmani, Mongia, and Lee (2014b), the venturi throat diameter of the pilot fuel-air mixer is about the same as the venturi throat diameter for the main fuel-air mixers. The venturi exit diameter is much larger for the pilot because the venturi throat for the pilot is moved upstream; this was done to isolate the pilot to limit mixing with the neighboring main fuel-air mixers at low-power conditions.

As their names imply, in the nine-recess and five-recess configurations, configurations 12 and 13, respectively, some fuel-air mixers are set back from the dome. As shown in Figure 42(b), in the nine-recess configuration, configuration 12, the pilot fuel-air mixer, the four main 1 stage fuel-air mixers, and the four main 2 stage fuel-air mixers are set back. In the five-recess configuration, configuration 13, only the pilot and main 1 stage fuel-air mixers are set back.

B.1.3 Swirl-Venturi Lean Direct Injection (SV–LDI–3)

Third-generation SV–LDI–3, configuration 14, replaces the complex, multibranched fuel stem found in SV–LDI–1 and SV–LDI–2 configurations with a single, multi-injection-point fuel stem. Each fuel stem supplies one pilot and either four or six main mixers. This both simplifies fuel stem design and improves the thermal management of the fuel.

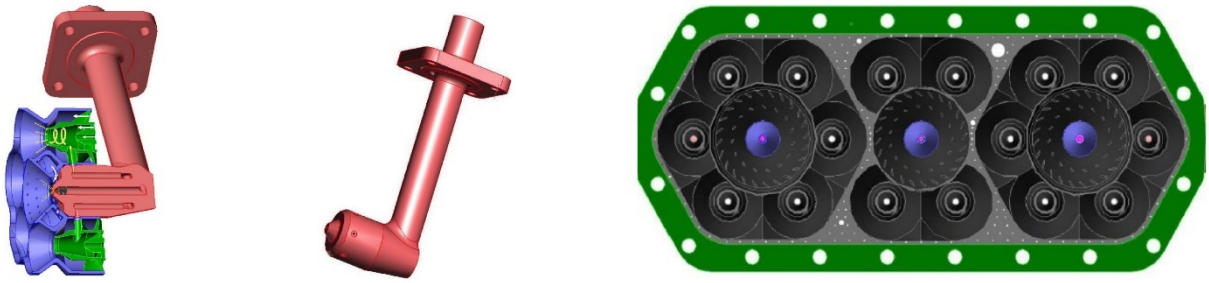

Figure 43.—Swirl-venturi lean direct injection (SV–LDI) SV–LDI–3 hardware. (a) Seven-point cup. (b) Fuel stem for single cup. (c) Three-cup rectangular sector consisting of two seven-point cups and one five-point cup.

A single “cup” of a SV–LDI–3 combustor consists of a pilot fuel-air mixer surrounded by multiple main fuel-air mixers. In particular, the pilot is surrounded either by six main fuel-air mixers (a “7-point” cup, see Figure 43) or four main fuel-air mixers (a “5-point” cup). Since third-generation SV–LDI targets a small-core engine, the fuel-air mixers must be tightly packed. To accomplish the tight packing, 7-point and 5-point cups alternate.

Since each cup is not identical, the flame tube tests were done with multiple cups instead of a single cup. Therefore, a three-cup sector was tested in the CE–5 medium pressure flame tube. The three-cup sector is composed of two 7-point cups and one 5-point cup.

Each cup is fed by a single, multi-injection-point fuel stem. Each of these fuel stems contain three fuel lines that can be controlled separately. For the 5-point cup, one fuel line feeds the pilot, the second feeds the two top mains, and the third feeds the two bottom mains. For the 7-point cup, one fuel line feeds the pilot, the second feeds the three inner mains, and the third feeds the three outer mains.

The fuel-air mixers are grouped into four stages. The first stage is made up of all the pilots. The second stage, called main 1, is made up of the four mains in the 5-point cup. The third stage comprises three inner mains in each of the 7-point cups. The fourth stage comprises three outer mains in each of the 7-point cups.

B.2 Discrete-Jet or Multiplex Lean Direct Injection

The second class of LDI designs is discrete-jet LDI, configuration 17. Discrete-jet LDI has also been called multipoint or multiplex LDI, abbreviated as MPX LDI. As shown in Figure 44, the distinguishing feature of this class is discrete-jet air swirlers. There is no converging nozzle. Instead there is a diverging venturi through which the swirling air is introduced in a series of slots integrated into the venturi. These air passages provide the “discrete” jets of air to help atomize the fuel. As with SV–LDI, all fuel-air mixers were identical in the first MPX LDI configurations. In later MPX LDI, the fuel-air mixers are split into a pilot stage and two main stages, which differ in the design of the discrete jets and the type of fuel injector (pressure atomizer or airblast).

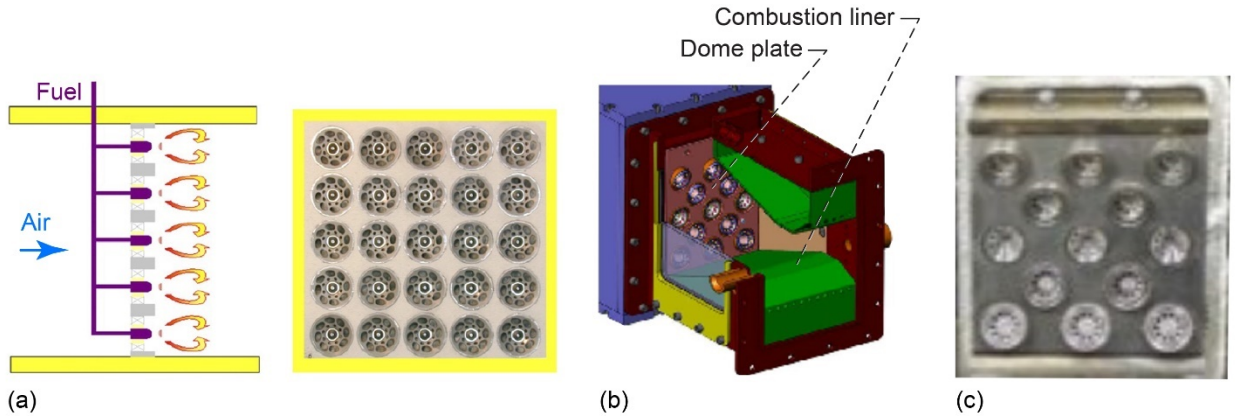

Figure 44.—Discrete-jet lean direct injection (MPX LDI), configuration 17. (a) First MPX LDI configuration, with 25 injectors arranged in 5 by 5 array in a 76.2- by 76.2-mm array. (b) Schematic of later design. (c) Later design configuration; this later configuration has dome area of more than 12 times that of first design.

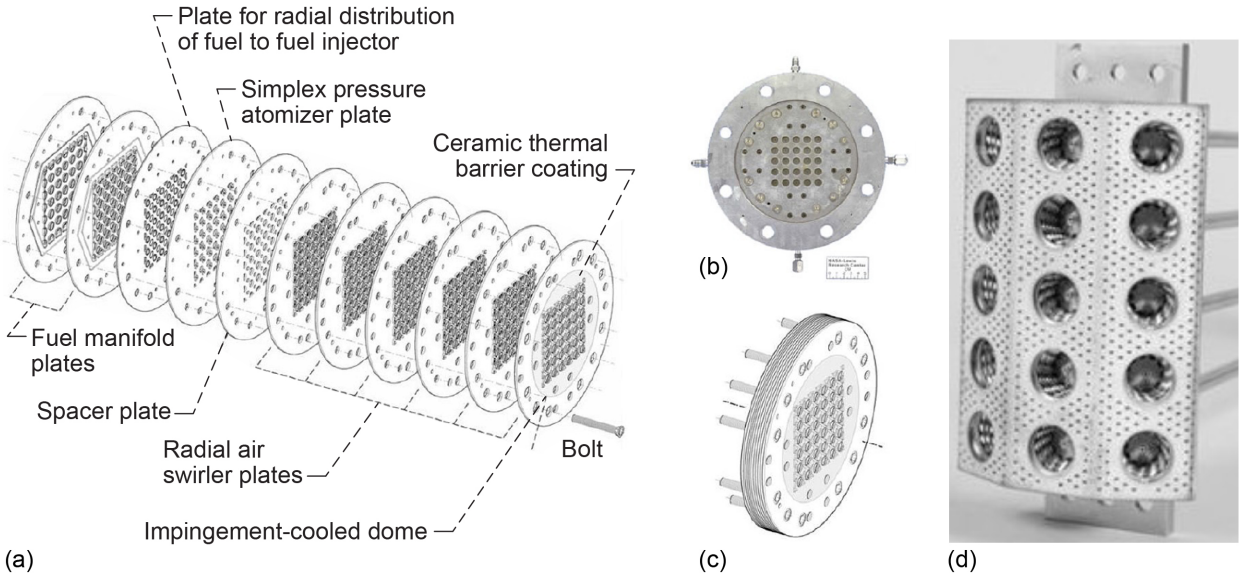

Figure 45.—Macrolaminate lean direct injection (MPIM), configuration 16. (a) First MPIM configurations developed under Ultra-Efficient Engine Technology (UEET) program. (b) MPIM 76.2- by 76.2-mm cross-sectional area containing 25 injectors in 5 by 5 array. (c) MPIM with 36 injectors in 6 by 6 array. (d) Later (Environmentally Responsible Aviation (ERA) program) three-zone, 15-cup macrolaminate configuration.

B.3 Macrolaminate Lean Direct Injection

The third class of LDI designs is MPIM, configuration 16, highlighted in Figure 45. Distinguishing features of this class are diverging radial air swirlers, fuel injection upstream of the air swirlers, and the macrolamination fabrication method. Figure 45(a) shows individual laminate sheets that build up to the 36-element MPIM module. Note that even though the 25- and 36-element variations appear similar, there are major differences in the air swirler design: the number of swirler blades changed dramatically. In addition, for the 25-point MPIM, two SN were used: 0.5 and 0.8 and four variations of swirler plate, all

coswirling. Thus, the low-swirl plates were either all clockwise or all counterclockwise, likewise, for the high-swirl plates. Using these plates, four stacks were bonded:

1. A stack with all SN = 0.5 corotating swirler plates
2. A stack with all SN = 0.8 corotating swirler plates
3. A stack that alternated SN = 0.5 and 0.8 corotating swirler plates
4. A stack that alternated SN = 0.5 and 0.8 counterrotating swirler plates

Note that the stacks composed of alternating plate type did not produce a checkerboard swirler pattern with respect to the dome.

Figure 45(b) shows a newer MPIM 15-cup module developed under the Environmentally Responsible Aviation (ERA) program. MPIM is discussed in more detail in Tacina et al. (2002) and Mansour (2015).

Appendix C.—Short Synopsis of Tests and Analyses From NASA Programs and Projects

This section includes synopsis of tests and analyses of NASA programs and projects including the High-Speed Research (HSR), Advanced Subsonic Technology (AST), Fundamental Aeronautics (FA), Ultra-Efficient Engine Technology (UEET), Environmentally Responsible Aviation (ERA), and Advanced Aviation Vehicles Program (AAVP).

Adiabatic flame temperature is a key variable for NO_x reduction, so this discussion will concentrate on how NO_x varies with combustion zone flame temperature for low NO_x concepts and configurations tested at NASA Glenn Research Center. This appendix also serves to summarize that work through the NASA programs and projects that focused on NO_x reduction from aircraft engines and offer thoughts about the more recent efforts (small core and supersonics) that are challenging to manage temperature T_4.

Table VI and Table VII along with Figure 46 show that the best design depends on the combustor condition for that high-power cycle. For the subsonic cruise Advanced Air Transport Technology (AATT) small-core engine cycle (Table VI), the key conditions are the two high-power International Civil Aviation Organization (ICAO) points and the subsonic cruise condition; for these, the combustion zone flame temperature ranges from 1,680 to 1,887 K. For the supersonic cruise conditions given in Table VII, the combustion zone flame temperature ranges from 1,945 to 2,071 K for the nearer term derivative engine cycle, and from 2,064 to 2,214 K for the farther term advanced cycle.

Figure 46 shows NO_x emissions as a function of adiabatic flame temperature for multiple lean direct injection (LDI) combustor concepts (swirl-venturi lean direct injection (SV–LDI), macrolaminate LDI (MPIM), and discrete-jet LDI (MPX LDI)) at many inlet conditions. The focus of the graph is on supersonic emissions goals, and symbol shape and color are chosen to enable comparison across injector configurations and show overall trends. LDI combustor concepts are designated by symbol color. Gray symbols noted as “other” include newer SV–LDI–2 and SV–LDI–3 concepts. Symbol shape and style indicate the inlet condition. Two horizontal lines are shown on the graph to indicate the HSR and Commercial Supersonic Technology (CST) NO_x goals, at 5 and 10 emissions index (EI) NO_x. Also highlighted on the graph are regions for the derivative and advanced supersonic cruise cycles.

TABLE VI.—NASA ADVANCED AIR TRANSPORT TECHNOLOGY (AATT) N+3 SMALL-CORE CYCLE FOR ENGINE WITH 30,000-LBF- (133-KN-) RATED THRUST

[Giving combustor inlet pressure P_3, combustor inlet temperature T_3, and combustor equivalence ratio ϕ_{eng}. Flame tube combusted gas temperatures T_{comb} assume 15 or 20 percent combustor liner cooling (lc).]

Condition	P_3, bar	T_3, K	ϕ_{eng}	$T_{comb,15lc}$, K	$T_{comb,20lc}$, K
International Civil Aviation Organization (ICAO), 7 percent	7.1	553	0.103	872	890
ICAO, 30 percent	14.1	661	0.186	1,199	1,231
ICAO, 85 percent	32.8	835	0.321	1,680	1,727
ICAO, 100 percent	38.1	870	0.354	1,784	1,832
Cruise	18.3	827	0.392	1,833	1,887
Top of climb	19.4	834	0.377	1,806	1,858
Rolling takeoff	44.3	957	0.446	2,050	2,107

TABLE VII.—SUPERSONIC CLIMB AND CRUISE CONDITIONS

[Given are supersonic cycle (derivative (Deriv) or advanced (Adv)), altitude, Mach number, engine power setting, combustor inlet pressure P_3 and temperature T_3, combustor equivalence ratio (ϕ_{eng}), and combusted gas temperature T_{comb} in flame zone when adjusted for 15 and 20 percent liner cooling (lc). Supersonic climb points are at altitudes of 12.2 to 14.6 km, shown in bold font; all other points are supersonic cruise points.]

Cycle	Altitude, km	Mach no.	Power setting, percent	P_3, bar	T_3, K	ϕ_{eng}	$T_{comb,15lc}$, K	$T_{comb,20lc}$, K
Deriv	15.2	1.4	100	8.1	805	0.484	2,010	2,071
Deriv	15.2	1.4	90	7.5	785	0.459	1,945	2,004
Adv	**12.2**	**1.1**	**100**	**15.2**	**833**	**0.405**	**1,866**	**1,921**
Adv	**12.8**	**1.2**	**100**	**15.6**	**860**	**0.423**	**1,926**	**1,981**
Adv	**13.4**	**1.3**	**100**	**16.1**	**890**	**0.442**	**1,989**	**2,046**
Adv	**14.0**	**1.4**	**100**	**16.5**	**922**	**0.462**	**2,056**	**2,113**
Adv	**14.6**	**1.5**	**100**	**17.1**	**956**	**0.484**	**2,125**	**2,184**
Adv	15.2	1.6	100	17.4	976	0.492	2,155	2,214
Adv	15.2	1.6	90	16.5	950	0.465	2,082	2,140
Adv	15.5	1.7	100	17.1	976	0.478	2,129	2,187
Adv	15.5	1.7	90	16.3	954	0.455	2,064	2,121

NO_x emissions rise sharply at adiabatic flame temperatures above a certain flame temperature. This "inflection point" flame temperature varies with combustor design but is often near 1,800 to 1,900 K.

Gray symbols show second- and third-generation SV–LDI configurations as well as GE Aviation Twin Annular Premixing Swirler (TAPS) and United Technologies Research Center (UTRC) Pilot-in-Can Swirler (PICS) configurations developed for the Fundamental Aeronautics program circa 2010. For these configurations, NO_x is very low at the lower flame temperatures and rises sharply above temperatures about 1,800 K. These configurations would produce very low NO_x emissions for high-power ICAO and subsonic cruise points for the AATT small-core cycle and would be close to the CST supersonic cruise goal of 10 EI for the derivative supersonic cycle if the combustor liner cooling could be kept to 15 percent. However, the NO_x emissions at supersonic cruise are very high—above 25 to 30 EI—for the derivative cycle with 20-percent liner cooling and for the advanced cycle.

Comparing the nine-point UEET configurations (blue and purple symbols) based on swirler vane angle, the 45° swirler configurations would be better for the AATT cycle. For supersonic cruise conditions for which data is available, NO_x emissions are similar for the UEET designs; however, the 60° swirler configurations have a flatter NO_x versus flame temperature curve and so might be expected to have lower NO_x at the highest flame temperatures, for which no data are available. The HSR designs (dark green symbols) appear to have the flattest NO_x curve of the SV–LDI designs and so the lowest NO_x at the supersonic cruise conditions. However, this is due in part to HSR data being taken at a lower combustor inlet pressure and higher pressure drop. For the UEET SV–LDI configurations, NO_x emissions are roughly proportional to the square root of inlet pressure and one over the square root of combustor pressure drop. When the combustor inlet conditions are closer, NO_x emissions are comparable, for example, compare the star symbols, especially slightly above 1,900 K. The remaining colors (brown, green, yellow, red, and pink) show the MPIM and discrete-jet configurations. Although the discrete-jet configuration would have higher NO_x than many other configurations for the AATT engine cycle, it is the best configuration for NO_x emissions at the supersonic cruise conditions.

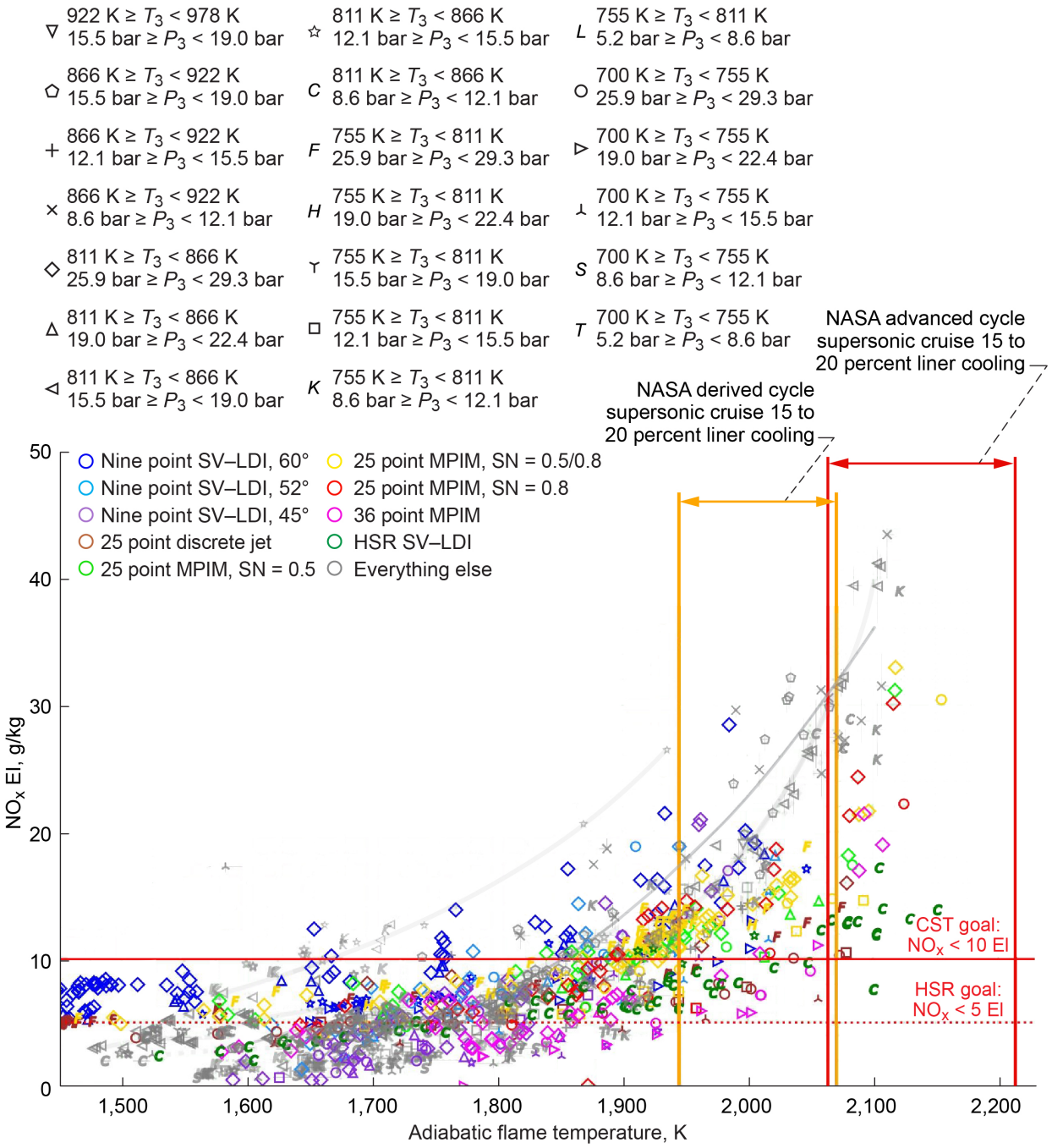

Figure 46.—Emissions index (EI) NO_x as function of adiabatic flame temperature compared to supersonic emissions goals. Plots are color-coded by combustor injector configuration. Symbols represent various ranges of inlet temperature T_3 and pressure P_3. Derived cycle conditions: T_3 785 to 805 K and P_3 7.5 to 8.1 bar. Advanced cycle conditions: T_3 950 to 976 K and P_3 16.3 to 17.4 bar. Swirl number (SN). Swirl-venturi lean direct injection (SV–LDI). Macrolaminate LDI (MPIM). High-Speed Research (HSR). Commercial Supersonic Technology (CST).

Appendix D.—Additional Considerations of Interactions Between Adjacent Swirlers

Four examples from other work that examined the effects of interactions between adjacent swirlers used linear arrays (Kao et al., 2013; Dolan, Villalva Gomez, and Gutmark, 2017) or annular arrays (Fanaca et al., 2010; Durox et al., 2016). Some arrays use mixers that are larger than the baseline swirl-venturi lean direct injection (SV–LDI), which is on the order of 25 mm in diameter. However, others are comparable in size to the baseline SV–LDI. These groups reported changes to adjacent identical fuel-air mixers that changed the strength and/or size of the recirculation zones that also affected flame stability, heat release, and pattern factor. For example, under certain situations, every other swirler was stronger or weaker than its neighbor, with one generating a "V" flame and its neighbor an "M" flame. These flame types are best described in Samarasinghe et al. (2016) and Rajasegar et al. (2019). More details of the four array studies are provided in the references at the beginning of this section. A brief synopsis of their findings is provided here. This references nondimensionalized systems by diameter (D) and the space between adjacent swirlers (S). For systems that varied the space between swirlers, S is given in terms of the number of D or by the ratio S/D.

The references cited here feature several types of fuel-air mixers, two for Jet-A and two for gas burners:

- Counterswirling radial-radial mixer, swirl number (SN) = 1
- United Technologies Aerospace Systems (UTAS), radial slotted diffuser, SN = 0.55
- Premixing, dual stage, Alstom EV–5 burner, SN = 1
- Premixed radial swirler, effective SN = 0.7

The counterswirling radial-radial mixer (Kao et al., 2013) is similar in design to what might be found in a jet-fueled General Electric Aviation combustor. The UTAS diffuser (Dolan, Villalva Gomez, and Gutmark, 2017) follows from an LDI discrete-jet (MPX LDI) concept developed under the Environmentally Responsible Aviation (ERA) program. These are non-premixed, liquid-fueled devices. Both were used in linear arrays, so endwall effects might present some effect on the flow field.

The two premixing fuel-air mixers used full annular combustors, so endwall effects are eliminated. These are the Alstom industrial combustor, investigated as both single-cup and 12-cup full annular burners (Fanaca et al., 2010) and the 16-cup methane-air annular combustor used by Durox et al. (2016).

In addition to confinement studies discussed in Section 4.0, Kao considered the effect of interactions of swirlers compared to the single swirler flow field in arrays of three or five elements, all with confinement ratio (CFR) of 5.1, and constant airflow per swirl cup. They saw that when three swirlers were used, the center swirler central recirculation zone (CRZ) was larger than the outer CRZs, which were more compact and had higher reverse velocity, so in terms of physical size, there was a small-large-small (S-L-S) pattern. However, when five elements were used, the pattern changed to L-S-L-S-L. Radial profiles of axial velocities also showed that the swirling jet from the center element and the swirling jet from the neighboring element merged together. These are locations where peak turbulent kinetic energy was highest (where mixing interactions take place). Additionally, the change from three to five elements increased the mean overall turbulent kinetic energy.

Kao et al. (2013) also considered the spacing between five swirlers, keeping the endwall distance the same. Using spacings of 1.5 D, 2 D, 2.5 D, and 2.75 D, an alternating pattern of L-S-L-S-L developed for 1.5 D and 2 D, but the pattern flipped to S-L-S-L-S for the larger swirler spacings. All large CRZs could be characterized as having wall jets and the small CRZs as having free jets bounding them.

Fanaca et al. (2010) compared the flow field behind a single Alstom EV–5 premixed gas burner (referred to as "SCC") to one of 12 burners in an annular array (ACC). The SN of each EV–5 burner was one. The two had similar confinements, but the ACC CFR was slightly larger (8 percent) than the SCC. A key difference between the flow fields is that the SCC issued a jet with a half-angle of about 50° compared to 30° for the ACC, rendering a larger CRZ than for the ACC. This very large difference the authors attribute to the swirling jets being in different regimes. The wider angle SCC was in the wall-jet regime, while the ACC was in the free-jet regime. They posited that there is a critical CFR that refers to a transitional regime between wall- and free-jet behavior. The swirlers act as free jets above the critical ratio and act as wall jets below the ratio.

This change of regime they attribute to a change in effective SN for the array swirler. Because the swirlers are all coswirling, the tangential velocity is reduced substantially due to the fluid between them moving in an opposed fashion, thus rendering a smaller effective SN. They went on to develop a model and operating map based on the effective SN versus CFR. Details can be found in the Fanaca et al. (2010) report.

Durox et al. (2016) conducted a study to consider the alternating structure between adjacent swirlers in an array, looking at the flare angle of the diffuser and the effect it had on a single annular combustor array. The array consisted of 16 individual fuel injectors that had SN = 0.71 in a propane-air combustor that used quartz walls. Four flare angles were considered: 0° (no flare), 70°, 90°, and 105°. They also considered the effect of bulk velocity and equivalence ratio. Without the flare, the flames exhibited a V shape and fell into the free-jet regime, as did the cups with 70° flares. However, visually, the 90° and 105° flares exhibited an alternating light-dark pattern around the combustor. The darker flames were M flames. These M flames expanded laterally, along the walls, rather than axially downstream and were present at all equivalence ratios tested, from 0.64 to 0.94. The V flames stabilized in the inner shear layer and anchored to a centerbody, whereas M flames stabilized in both the inner and outer shear layers and anchored to both the centerbody and outer edge of the swirl cup.

Durox et al. (2016) determined the M flames were cooler than the V flames by about 150 °C, with a lower volumetric heat release rate, and demonstrated the heat release pattern and profile factors that developed would not be beneficial in a gas turbine combustor. With respect to bulk velocity, the only change to the V flames when using the 70° flare was that the flame thickened as bulk velocity increased; however, the larger flare angles consistently showed an alternating flame pattern where the M flames became less luminous as bulk velocity increased. With respect to equivalence ratio, at low equivalence ratio, the 90° cups switched modes, that is, they changed from M to V (and vice versa) and back at a measurable frequency. As the equivalence ratio approached unity, the flame shapes became harder to distinguish.

Based on the cup SN and CFRs, Durox et al. (2016) considered the Fanaca et al. (2010) operating map and determined that their observations were fairly consistent with the map. The 70° flare cup was near the critical CFR, and the 90° and 105° flares lay deeper in the wall-jet regime portion of the map. Given that the 90° flares switched modes depending on equivalence ratio, another factor appears to be heat release rate, or perhaps jet momentum, which did not factor into the operating map.

Dolan, Villalva Gomez, and Gutmark (2017) also compared a swirler array to a canonical flow. However, instead of using the analogy of free jets versus wall jets, Dolan, Villalva Gomez, and Gutmark compared their results to opposed jets. In this study, Dolan, Villalva Gomez, and Gutmark changed the element spacing between two swirlers of a two-swirler linear array but did not change the confinement (i.e., the outer boundaries of the box surrounding the array remained constant). Element spacings were 1.1 *D*, 1.36 *D*, 1.89 *D*, and 2.72 *D*. Using particle image velocimetry (PIV), they looked at noncombusting and combusting flow structures in propane-air flames and compared with methane-air for

1.89 *D* spacing. In this study, all element spacings resulted in some outer recirculation areas at the dome face or the sidewall. The CFR was 14.7, which is different from all other studies that used more than one element; those other studies used a CFR about five or less. Under nonreacting conditions at the smallest spacing, they saw a familiar pattern of a CRZ behind each swirler with high downstream velocity between them. On either side of the CRZ, the bounding jets (which are the left and right bounds of the conical gas spray generated by the swirler) exited at an angle that would classify it as a free jet. These bounding jets had similar angles with respect to the swirler centerline. For the spacings of 1.36 *D* and 1.89 *D*, a small recirculation bubble appeared at the dome between the swirlers and the CRZs increased in size. At the widest spacing, the two elements were almost far enough apart to be independent of each other. In all cases, though, the angle of both wings of each downstream-going jets through the swirler were at roughly the same angle and can be characterized as free jets.

For all burning cases, the jets widened, and all but the smallest spacing might be called wall jets. Only the smallest spacing, 1.1 *D*, displayed a similar velocity field to the nonreacting case, in that there were two distinct CRZs within the field of view and that field was fairly symmetric. Volume expansion and heat release due to combustion cause the centers of the CRZs to be pushed outward from the injector centerlines.

For the wider injector spacings, jet wings have a shallower angle, possibly forced wider by the reverse flow. Larger spacings (S/D = 1.89 and 2.72) display highly asymmetric flow fields, although there is a sense of repeating pattern. For instance, the left jet of both injectors is short and does not penetrate much into the flow; mostly running parallel to the dome face, resembling the M flame of Durox et al. (2016). The big difference is on the right-hand wing of each: for the left injector, the right wing penetrates deeply downstream, mainly because the left-wing flow mixes and becomes entrained with that stream. Meanwhile, the right wing of the right injector does not penetrate but flows along the dome face.

Dolan, Villalva Gomez, and Gutmark (2017) posited an explanation for the interaction, based on considering turbulent opposed jet studies, which indicate that two jets can be deflected in an oscillating pattern that switches flow direction.

The Dolan, Villalva Gomez, and Gutmark (2017) experiment does not quite conform to the map by Fanaca et al. (2010). The CFR is large, so unless the SN is quite high, all injector spacings should result in free jets; however, the reported SN is just 0.55. The confinement used was also quite large, compared to the other studies, and is not realistic for use in an annular combustor. Another difference is that the wall distance changes every time there is an injector spacing change. Although the Dolan, Villalava Gomez, and Gutmark study does not report the diffuser flare angle, assuming the cross section shown is to scale, the diffuser angle is on the order of 110, so following Durox et al. (2016) the Dolan, Villalva Gomez, and Gutmark system will experience M flames. Thus, the Dolan, Villalva Gomez, and Gutmark work seems something of a hybrid and indicates an area for further study.

References

Ajmani, Kumud; Mongia, Hukam C.; and Lee, Phil (2013a): Evaluation of CFD Best Practices for Combustor Design: Part I—Non-Reacting Flows. AIAA 2013–1144.

Ajmani, Kumud; Mongia, Hukam C.; and Lee, Phil (2013b): Evaluation of CFD Best Practices for Combustor Design: Part II—Reacting Flows. AIAA 2013–1143.

Ajmani, Kumud; Mongia, Hukam C.; and Lee, Phil (2013c): Evaluation of a Time-Filtered Navier Stokes (TFNS) CFD Approach for LDI Combustor Analysis. AIAA 2013–3688.

Ajmani, Kumud; Kundu, Krishna P.; and Yungser, Shaye J. (2014): Assessment of Reduced-Kinetics Mechanisms for Combustion of Jet Fuel in CFD Applications. AIAA 2014–3662.

Ajmani, Kumud; Mongia, Hukam C.; and Lee, Phil (2014a): Assessment of CFD Approaches for Next-Generation Combustor Design. ASME GTINDIA2014–8361.

Ajmani, Kumud; Mongia, Hukam; and Lee, Phil (2014b): CFD Computations of Emissions for LDI–2 Combustors With Simplex and Airblast Injectors. AIAA 2014–3529.

Ajmani, Kumud; Mongia, Hukam; and Lee, Phil (2015): Parametric Design of Injectors for LDI–3 Combustors. AIAA 2015–3785.

Ajmani, Kumud; Mongia, Hukam C.; and Lee, Phil (2016): CFD Based Design of a Filming Injector for N+3 Combustors. AIAA 2016–4783.

Ajmani, Kumud; Mongia, Hukam; and Lee, Phil (2017): CFD Evaluation of a 3rd Generation LDI Combustor. AIAA 2017–5017.

Ajmani, Kumud, et al. (2018a): CFD-Led Designs of Pre-Filming Injectors for Gas-Turbine Combustors. ASME GT2018–75329.

Ajmani, Kumud, et al. (2018b): CFD Predictions of N+3 Cycle Emissions for a Three-Cup Gas-Turbine Combustor. AIAA 2018–4957.

Ajmani, K., et al. (2019a): CFD Evaluation of a Lean-Direct Injection Combustor for Commercial Supersonics Technology. AIAA 2019–4199.

Ajmani, Kumud, et al. (2019b): Pilot Injector Redesign to Reduce N+3 Cycle Emissions for a Gas-Turbine Combustor. AIAA 2019–4371.

Alekseenko, S.V.; Kuibin, P.A.; and Okulov, V.L. (2007): Theory of Concentrated Vortices. Springer, Berlin, Germany.

Banaszuk, A., et al. (2002): Active Control of Engine Dynamics. NATO RTO–EN–020.

Beer, J.M.; and Chigier, N.A. (1972): Combustion Aerodynamics. First ed., Wiley & Sons, New York, NY.

Cai, J.; Jeng, S.-M.; and Tacina, R. (2002): Multi-Swirler Aerodynamics: Comparison of Different Configurations. ASME GT2002–30464.

Chang, Clarence T., et al. (2013): NASA Environmentally Responsible Aviation Project Develops Next-Generation Low-Emissions Combustor Technologies (Phase I). J. Aeronaut Aerospace Eng., vol. 2, no. 4.

Chigier, N.A.; and Beer, J.M. (1964): Velocity and Static-Pressure Distributionsin Swirling Air Jets Issuing From Annular and Divergent Nozzles. J. Basic Eng., vol. 86, no. 4, pp. 788–796.

Chigier, N.A.; and Chervinsky, A. (1967): Experimental Investigation of Swirling Vortex Motion in Jets. J. Appl. Mech., vol. 34, no. 2, pp. 443–451.

Chin, J.S.; Rizk, N.K.; and Razdan, M.K. (2000): Effect of Inner and Outer Airflow Characteristics on High Liquid Pressure Prefilming Airblast Atomization. J. Propuls. Power, vol. 16, no. 2.

Del Rosario, Ruben (2014): An Overview of Low-Emission Combustion Research. Presented at the CAEP Review of Advanced Aero-Engine Combustor Designs, Munich, DE.

Dewanji, D. (2012): Flow Characteristics in Lean Direct Injection Combustors. Master's Thesis, Birla Institute of Technology, Calcutta, India.
Dolan, B.; Villalva Gomez, Rodrigo; and Gutmark, E. (2017): Measurements and Analysis of Alternating Flow Patterns in a Multinozzle Combustor. AIAA J., vol. 55, no. 1, pp. 161–171.
Durox, Daniel, et al. (2013): Flame Dynamics of a Variable Swirl Number System and Instability Control. Combust. Flame, vol. 160, no. 9, pp. 1729–1742.
Durox, Daniel, et al. (2016): Different Flame Patterns Linked With Swirling Injector Interactions in an Annular Combustor. J. Eng. Gas Turbine Power, vol. 138, no. 10.
El-Asrag, Hossam A.; Iannetti, Anthony C.; and Apte, Sourabh V. (2014): Large Eddy Simulations for Radiation-Spray Coupling for a Lean Direct Injector Combustor. Combust. Flame, vol. 161, no. 2, pp. 510–524.
Ercegovic, David B. (1979): Effect of Swirler-Mounted Mixing Venturi on Emissions of Flame-Tube Combustor Using Jet A Fuel. NASA TP–1393 (AVRADCOM Technical Report 78–41). https://ntrs.nasa.gov
Fanaca, D., et al. (2010): Comparison of the Flow Field of a Swirl Stabilized Premixed Burner in an Annular and a Single Burner Combustion Chamber. J. Eng. Gas Turbine Power, vol. 132, no. 7.
Fu, Yongqiang, et al. (2005): Confinement Effects on the Swirling Flow of a Counter-Rotating Swirl Cup. ASME GT2005–68622.
Fu, Yongqiang; Jeng, San-Mou; and Tacina, Robert (2006): Confinement Effects on the Swirling Flow Generated by a Helical Axial Swirler. AIAA 2006–0545.
Goeke, Jerry, et al. (2014): Multi-Point Combustion System Final Report. NASA/CR—2014-218112. https://ntrs.nasa.gov
Gupta, A.K.; Lilley, D.G.; and Syred, N. (1984): Swirl Flows. Abacus Press, Kent, England.
Heath, Christopher M. (2014): Characterization of Swirl-Venturi Lean Direct Injection Designs for Aviation Gas Turbine Combustion. J. Propuls. Power, vol. 30, no. 5.
Heath, Christopher M. (2016): Parametric Modeling Investigation of a Radially-Staged Low-Emission Aviation Combustor. AIAA 2016–1394.
Heath, Christopher M., et al. (2010): Optical Characterization of a Multipoint Lean Direct Injector for Gas Turbine Combustors: Velocity and Fuel Drop Size Measurements. ASME GT2010–22960.
Hicks, Yolanda R.; Anderson, Robert C.; and Locke, Randy J. (2007): Optical Measurements in a Combustor Using a 9-Point Swirl-Venturi Fuel Injector. ISABE 2007–1280.
Hicks, Yolanda R., et al. (2011): Investigations of a Combustor Using a 9-Point Swirl-Venturi Fuel Injector: Recent Experimental Results. NASA/TM—2012-217245 (ISABE 2011–11062011). https://ntrs.nasa.gov
Hicks, Yolanda R., et al. (2014): Fundamental Study of a Single Point Lean Direct Injector. Part II: A Comparison of Cold Flow and Burning Measurements. CCSCI 087IC–0008.
Hicks, Yolanda R. (2015): CFD Analysis of Emissions for a Candidate N+3 Combustor. ISABE 2015–20245.
Hicks, Yolanda R., et al. (2016): A Comparison of Flow Fields Generated by Varying Air Swirler Configurations in a 7-Point Lean Direct Injector Array. CSSCI 145IC–0035.
Hicks, Yolanda R.; Tedder, Sarah A.; and Anderson, Robert C. (2016): Alternative Bio-Derived JP–8 Class Fuel and JP–8 Fuel: Flame Tube Combustor Test Results Compared Using a GE TAPS Injector Configuration. AIAA 2016–4890.
Hicks, Yolanda R.; and Tacina, Kathleen M. (2017): Flow Structure Comparison for Two 7-Point LDI Configurations. Presented at the 10th U.S. National Combustion Meeting, College Park, MD.

Hicks, Yolanda R., et al. (2019): Combustion and Emissions Study Using a 7-Point Lean Direct Injector Array: Focus on Flame Stability. ISABE 2019–24404.
Iannetti, Anthony C.; Liu, Nan-Suey; and Davoudzadeh, Farhad (2008): Effect of Spray Initial Conditions on Heat Release and Emissions in LDI CFD Calculations. NASA/TM—2008-215422. https://ntrs.nasa.gov
Ingebo, R. (1983): Aerodynamic-Wave Breakup of Liquid Sheets in Swirling Airflows and Combustor Modules. NASA TM–83353. https://ntrs.nasa.gov
Johnson, Susan M. (1982): Venturi Nozzle Effects on Fuel Drop Size and Nitrogen Oxide Emissions. NASA TP–2028. https://ntrs.nasa.gov
Kao, Yi-Huan; Tambe, Samir B.; and Jeng, San-Mou (2013): Aerodynamics of Linearly Arranged Rad-Rad Swirlers, Effect of Number of Swirlers and Alignment. ASME GT2013–94280.
Kao, Yi-Huan (2014): Experimental Investigation of Aerodynamics and Combustion Properties of a Multiple-Swirler Array. Ph.D. Thesis, Univ. of Cincinnati.
Kim, Sayop; Menon, Suresh; and Darin, Joel B. (2014): Large-Eddy Simulation of a High-Pressure, Single-Element Lean Direct-Injected Gas-Turbine Combustor. AIAA 2014–0131.
Kirtas, Mehmet, et al. (2006): Large-Eddy Simulation of a Swirl-Stabilized, Leand Direct Injection Spray Combustor. ASME GT2006–91310.
Knudsen, E.; and Pitsch, H. (2010): Large Eddy Simulation of a Spray Combustor Using a Multi-Regime Flamelet Approach. Center for Turbulence Research Annual Research Briefs, pp. 337–350.
Lefebvre, A.H. (1999): Gas Turbine Combustion. 2nd ed., Taylor and Francis, Philadelphia, PA.
Lefebvre, Arthur; and McDonell, Vincent G. (2017): Atomization and Sprays. Second ed., CRC Press, Boca Raton, FL.
Li, Guoqiang (2004): Emissions, Combustion Dynamics, and Control of a Multiple Swirl Combustor. Ph.D. Dissertation, Univ. of Cincinnati.
Lieuwen, Timothy C.; and Yang, Vigor (2005): Combustion Instabilities in Gas Turbine Engines: Operational Experience, Fundamental Mechanisms, and Modeling. American Institute of Aeronautics and Astronautics, Reston, VA.
Liu, Nan-Suey; Shih, Tsan-Hsing; and Wey, C. Thomas (2011): Numerical Simulations of Two-Phase Reacting Flow in a Single-Element Lean Direct Injection (LDI) Combustor Using NCC. NASA/TM—2011-217031. https://ntrs.nasa.gov
Mansour, Adel (2015): Development of Advanced Low Emission Injectors and High-Bandwidth Fuel Flow Modulation Valves. NASA/CR—2015-218899. https://ntrs.nasa.gov
Patel, Nayan, et al. (2007): Simulation of Spray Combustion in a Lean-Direct Injection Combustor. Proc. Combust. Inst., vol. 31, no. 2, pp. 2327–2334.
Patel, Nayan; and Menon, Suresh (2008): Simulation of Spray–Turbulence–Flame Interactions in a Lean Direct Injection Combustor. Combust. Flame, vol. 153, nos. 1–2, pp. 228–257.
Rajasegar, Rajavasanth, et al. (2019): Mesoscale Burner Array Performance Analysis. Combust. Flame, vol. 199, pp. 324–337.
Ren, Xiao, et al. (2016): The Impact of Venturi Geometry on Reacting Flows in a Swirl-Venturi Lean Direct Injection Airblast Injector. AIAA 2016–4650.
Ren, Xiao, et al. (2018): Fundamental Investigations for Lowering Emissions and Improving Operability. J. Propuls. Power Res., vol. 7, no. 3, pp. 197–204.
Ren, Xiao, et al. (2019): The Impact of Swirling Flow Strength on Lean-Dome LDI Pilot Mixers' Operability and Emissions. Exp. Therm. Fluid Sci., vol. 109, no. 109840.
Ren, Xiao, et al. (2020): Experimental Investigation of Lean-Dome High-Airflow Airblast Pilot Mixers' Operability, Emissions, and Dynamics. Aerosp. Sci. Technol., vol. 100, no. 105737.

Richards, Geo; Straub, Doug; and Robey, Ed (2003): Control of Combustion Dynamics Using Fuel System Impedance. ASME GT2003–38521.
Samarasinghe, Janith, et al. (2016): The Three-Dimensional Structure of Swirl-Stabilized Flames in a Lean Premixed Multinozzle Can Combustor. J. Eng. Gas Turbine Power, vol. 138, no. 3.
Schuller, T.; Durox, D.; and Candel, S.: Self-Induced Combustion Oscillations of Laminar Premixed Flames Stabilized on Annular Burners. Combust. Flame, vol. 135, no. 4, 2003, pp. 525–537.
Syred, N.; and Beer, J.M.: Combustion in Swirling Flows: A Review. Combust. Flame, vol. 23, 1974, pp. 143–201.
Tacina, Kathleen M., et al. (2014): A Second Generation Swirl-Venturi Lean Direct Injection Combustion Concept. AIAA 2014–3434.
Tacina, K.M., et al. (2015): An Assessment of Combustion Dynamics in a Low-NOx Second-Generation Swirl-Venturi Lean Direct Injection Combustion Concept. ISABE 2015–20249.
Tacina, Kathleen M., et al. (2016): A Comparison of Three Second-Generation Swirl-Venturi Lean Direct Injection Combustor Concepts. AIAA 2016–4891.
Tacina, K., et al. (2017): Gaseous Emissions Results From a Three-Cup Flametube Test of a Third-Generation Swirl-Venturi Lean Direct Injection Combustion Concept. ISABE 2017–22606. https://ntrs.nasa.gov/citations/20170009090
Tacina, Kathleen M. (2018): Swirl-Venturi Lean Direct Injection Combustion Technology for Low-NOx Aero Gas Turbine Engines. Presented at the Spring Technical Meeting of the Central States Section of the Combustion Institute, Minneapolis, MN.
Tacina, K.M. (2019): A Third-Generation Swirl-Venturi Lean Direct Injection Combustor With a Prefilming Pilot Injector. ASME GT2019–90484.
Tacina, Robert, et al. (2002): A Low-NOx Lean-Direct Injection, Multipoint Integrated Module Combustor Concept for Advanced Aircraft Gas Turbines. NASA/TM—2002-211347. https://ntrs.nasa.gov
Tacina, Robert; Mao, Chien-Pei; and Wey, C. (2003): Experimental Investigation of a Multiplex Fuel Injector Module for Low Emission Combustors. AIAA 2003–0827.
Tacina, Robert; Mao, Chein-Pei; and Wey, Changlie (2004): Experimental Investigation of a Multiplex Fuel Injector Module With Discrete Jet Swirlers for Low Emission Combustors. NASA/TM—2004-212918 (AIAA 2004–0135). https://ntrs.nasa.gov
Tacina, R.R.; Lee, P.; and Wey, C. (2005): A Lean-Direct-Injection Combustor Using a 9 Point Swirl-Venturi Fuel Injector. ISABE 2005–1106.
Tedder, Sarah A., et al. (2014): Fundamental Study of a Single Point Lean Direct Injector. Part I: Effect of Air Swirler Angle and Injector Tip Location on Spray Characteristics. AIAA 2014–3435.
Villalva, Rodrigo, et al. (2015): Experimental Study of a Multinozzle Combustor at Elevated Pressures. AIAA J., vol. 53, no. 4.
Zink, Gregory A., et al. (2014): Intermediate Pressure Combustion Research of a Multipoint Low NOx Combustion System. AIAA 2014–3629.